

APPROVAL SHEET

Title of Dissertation: Developing a Quantitative Framework for Designing Responsive
RNA Electrochemical Aptamer-Based Sensors and Applications

Name of Candidate: Lauren R. Schoukroun-Barnes
Ph.D in Chemistry, 2015

Dissertation and Abstract Approved: _____

Dr. Ryan J. White
Assistant Professor
Department of Chemistry and Biochemistry

Date Approved: _____

Abstract

Title of Document: Developing a Quantitative Framework for Designing Responsive RNA Electrochemical Aptamer-Based Sensors and Applications

Lauren R. Schoukroun-Barnes, Doctor of Philosophy, 2015

Directed By: Dr. Ryan J. White, Professor
Department of Chemistry and Biochemistry

Electrochemical aptamer-based sensors utilizing structure-switching aptamers are specific, selective, sensitive, and widely applicable to the detection of a variety of targets. The specificity is achieved by the binding properties of an electrode-bound RNA or DNA aptamer biorecognition element that is a single-strand of DNA or RNA selected for *in vitro* to bind to a specific target molecule. Signaling in this class of sensors arises from changes in electron transfer efficiency upon target-induced changes in the conformation/flexibility of the aptamer probe. The changes in aptamer flexibility can be readily monitored electrochemically. The signaling mechanism enables several approaches to maximize the analytical attributes (i.e., sensitivity, limit of detection, and observed binding affinity) of the aptamer sensor. The work in this dissertation describes the quantitative effects of two different approaches to control sensor signaling in order to rationally tune sensor performance.

The first part of this dissertation describes the effects of nucleic acid sequence and structure on the signaling of a representative small molecule aptamer-based sensor for the detection of aminoglycoside antibiotics. Modifying aptamer sequences to undergo large conformation changes upon target addition improves and maximizes E-AB sensor

signaling because the collisional frequency and electron transfer rate of the 3'-attached redox molecule exhibits strong distance dependence. This dissertation also discusses the effects of stabilizing a folded structure of the aptamer to conserve the signal change, but reduce the binding affinity in order to shift the functional region of the sensor towards the therapeutic window of aminoglycoside antibiotics. Finally, with a newly developed family of aptamer sequences, tunable and predictable sensor responses achieved by employing different ratios of two aptamers with different affinities for the same target molecule on one sensor surface. The studies here were performed on a test bed aminoglycoside E-AB sensor, however the design criteria and framework established to tune sensor responses are generally applicable to any aptamer-based sensor.

The second part of this dissertation explains the use of hydrogels to protect RNA E-AB sensors to enable use in complex media, such as whole blood, serum, plasma, etc.. The motivation is to bring the promising attributes of E-AB sensors to the clinic or bedside for real-time therapeutic drug monitoring. However, RNA E-AB sensor application has been limited as a result of degradation of the RNA sensing element in biological samples. To improve E-AB sensor function in complex samples, this work describes the development of a biocompatible hydrogel material to protect the oligonucleotides from degradation and inhibit non-specific absorption of proteins to the sensor surface – both of which impede sensor function. Specifically, RNA sensors for aminoglycoside antibiotics were coated with a polyacrylamide hydrogel and tested in serum. Coating the RNA sensors with the hydrogel enabled sensor stability for a period of 3h in serum, which is a significant improvement from the uncoated sensors. The hydrogel coating also did not significantly affect E-AB sensor function based on the

comparable titration curves of the uncoated and coated E-AB sensors. While sensor function and stability were tested specifically with aminoglycoside targets the technique employed to coat sensors with a hydrogel should be generally applicable to any small molecule E-AB sensor.

Developing a Quantitative Framework for Designing Responsive RNA Electrochemical
Aptamer-Based Sensors and Applications

By

Lauren R. Schoukroun-Barnes

Dissertation Submitted to the Faculty of the
Graduate School of the University of Maryland, Baltimore County,
in partial fulfillment of the requirements for the degree of
Doctor of Philosophy
2015

©Copyright by
Lauren R. Schoukroun-Barnes
2015

Dedication

I dedicate my dissertation to my husband, Eric.

Acknowledgments

I greatly appreciate Dr. Ryan J. White for being an outstanding advisor and mentor. You pushed me, enabling me to broaden my scientific scope and to publish as many papers as humanly possible. For everything you have done for me and being supportive when I needed it most you have my utmost thanks and admiration.

I must thank my committee members: Professors Bradley Arnold, Jennie Leach, Brian Cullum, and Elsa Garcin for their thorough grilling during my oral examinations, which I believe, made me a better scientist.

I also appreciate the White Lab group members. Specifically Florika Macazo, who always supported me when I needed it most and for your scientific input into my Ph.D project. I would like to thank two undergraduates who worked on some of my project Mr. Ethan Glaser and Mr. Sam Wagan.

Lastly, I would like to thank all the graduate students that went to various practice examinations and edited my documents, I will always be grateful.

Table of Contents

Dedication	ii
Acknowledgements	iii
Table of Contents	iv
List of Tables	vi
List of Figures	vii
List of Schemes	viii
List of Abbreviations	ix
Chapter 1: Reagentless Structure-Switching Electrochemical Aptamer-Based Sensors	1
Introduction	1
Electrochemical, Aptamer-Based Sensor Fabrication Parameters	3
Fundamentals of Sensor Signaling	10
Illustrative Examples of Aptamer-Based Sensing	20
Alternative Strategies	22
Perspectives	23
Conclusion	26
Chapter 2: Enhancing Analytical Performance of RNA E-AB Sensors for the Detection of Aminoglycoside Antibiotics	28
Introduction	28
Experimental	30
Results and Discussion	32
Conclusions	45
Chapter 3: Rationally Designing Aptamer Sequences with Reduced Affinity for Controlled Sensor Performance	47
Introduction	47
Experimental	50
Results and Discussion	53
Conclusions	63
Chapter 4: Heterogeneous E-AB Sensor Surfaces for Controlled Sensor Responses	65
Introduction	65
Experimental	67
Results and Discussion	69
Conclusions	79

Chapter 5: Biocompatible Hydrogel Membranes for the Protection of RNA E-AB Sensors	81
Introduction.....	81
Experimental	83
Results and Discussion	85
Conclusions.....	92
Chapter 6: Conclusions and Future Directions	93
Quantitative Sensor Performance Conclusions and Future Directions.....	93
Membrane Coated Sensor Conclusions and Future Directions	94
References.....	96

List of Tables

Table 1: Parent and Modified Aptamer Sequences.....	30
Table 2: E-AB Sensor Analytical Performance	42
Table 3: Mutated Aminoglycoside Aptamer Sequences.....	51
Table 4: ATP Aptamer Sequences.....	68
Table 5: Aminoglycoside Aptamer Sequences	68
Table 6: K_m Values for Heterogeneous Sensor Surfaces	76
Table 7: Dynamic Ranges and Sensitivities of the Heterogeneous Sensors.....	79

List of Figures

Figure 1: Structure-Switching Aptamer Architecture.....	2
Figure 2: Structure of an Aptamer Sequence for E-AB Sensing	5
Figure 3: Detection of Two Molecules Using a Single E-AB Sensor	9
Figure 4: Heterogeneously Coated E-AB Sensor Responses	14
Figure 5: Sensor Responses Based on SW Interrogation Frequency	17
Figure 6: High and Low Gain E-AB Sensor Architectures	29
Figure 7: Peak Current Normalized by Frequency	35
Figure 8: Signal Polarity of the Parent Aminoglycoside Sensor	36
Figure 9: Secondary Structures of the Mutated Aptamer Sequences	37
Figure 10: Newly Engineered Aptamer Sequence Sensor Responses.....	40
Figure 11: Signal Change Dependence on Frequency	42
Figure 12: Structural Comparison of Tobramycin to Glucosamine.....	43
Figure 13: Specificity of Mutated Aptamer Sensors.....	44
Figure 14: Function of a Mutated Aptamer Sensor in Filtered Serum	45
Figure 15: Sensors Fabricated with the High Gain Aptamer	53
Figure 16: Secondary Structure Prediction for the High Gain Aptamer.....	56
Figure 17: Aptamer-Tobramycin Interaction Proposed Mutation Site.....	58
Figure 18: Secondary Structure Prediction for the Mutated Aptamers.....	58
Figure 19: Site-Mutated Aptamer Sensor Responses.....	59
Figure 20: Stabilized Aptamer Sequence Structures	60
Figure 21: Stabilized Aptamer Sensors Responses.....	62
Figure 22: Comparison of E-AB Sensors Responses	63
Figure 23: Heterogeneously Coated E-AB Sensor Responses	70
Figure 24: Absolute Signals of Different E-AB Sensors	73
Figure 25: Current Signal Difference with and without Aptamer	73
Figure 26: Heterogeneously Coated RNA E-AB Sensors and Responses.....	75
Figure 27: Heterogeneously Coated DNA E-AB Sensors and Responses	76
Figure 28: Regeneration of E-AB DNA and RNA Sensors.....	86
Figure 29: DNA and RNA Aminoglycoside Aptamer-Based Sensor Responses	87
Figure 30: Comparison of DNA and RNA Sensor Stability in Serum	88
Figure 31: Regeneration of Hydrogel Coated DNA and RNA E-AB Sensors	90
Figure 32: Stability of Hydrogel Coated RNA Sensors in Serum	91

List of Schemes

Scheme 1: Conformation Change of Structure Switching Aptamers	50
---	----

List of Abbreviations

E-AB	Electrochemical Aptamer-Based
RNA	Ribonucleic Acid
DNA	Deoxyribonucleic Acid
MFOLD	Molecular Free Energy for Folding
ATP	Adenosine Triphosphate
SWV	Square Wave Voltammetry
CV	Cyclic Voltammetry
ACV	Alternating Current Voltammetry
DPV	Differential Pulse Voltammetry
SAM	Self-Assembled Monolayer
TOB	Tobramycin

Chapter 1: Reagentless Structure-Switching Electrochemical Aptamer-Based Sensors

Introduction

Electrochemical, aptamer-based (E-AB) sensors that utilize structure-switching nucleic acid aptamers have garnered the attention of researchers as a result of the specific, reagentless, and reversible analyte detection abilities of the sensor platform (for example, see refs ¹⁻¹⁰). Coupling the sensitivity of electrochemical methods with the specificity afforded by aptamer-based recognition opens electrochemical detection to a wide expanse of previously unattainable targets. There are a myriad of electrochemical detection schemes that utilize aptamers as a biorecognition element.¹¹⁻¹³ In this introduction the focus is on reagentless sensors that rely on structure-switching aptamers first introduced by Plaxco and coworkers ¹⁴ and the advantages provided by this detection scheme. This class of structure-switching sensors couples a target-induced change in aptamer conformation with a change in electron transfer ability between a distal-appended redox marker and an electrode surface (Fig. 1). These sensors can be viewed as the electrochemical equivalent to aptamer beacons ¹⁵.

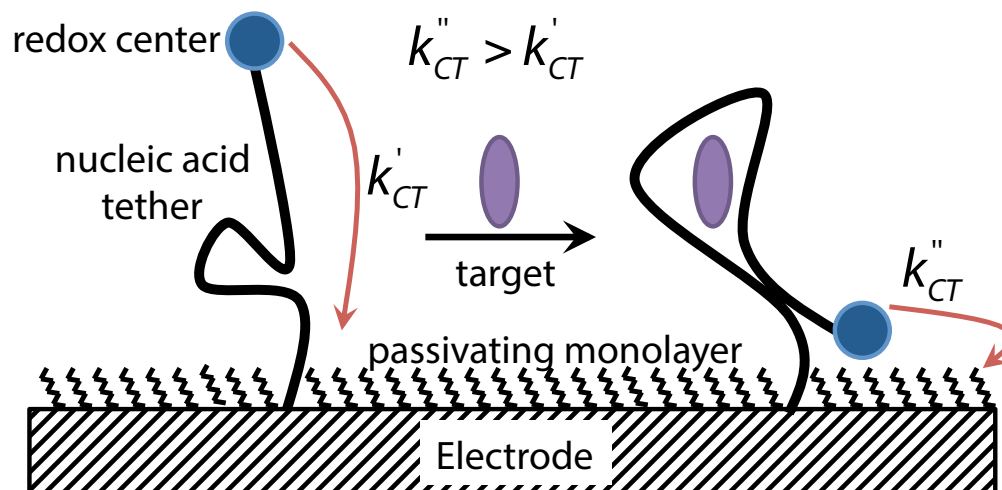


Figure 1. Reagentless structure-switching, aptamer-based employ DNA or RNA aptamers for the specific detection of analytes. To support reagentless sensing, the redox-labeled aptamer undergoes a flexibility and/or conformation change upon target binding that alters the charge transfer rate (k_{ct}) between a redox reporter and electrode surface. This change in charge transfer rate can be readily measured using a variety of different voltammetric methods.

Coupling electrochemical signaling to a change in aptamer conformation affords several advantages in analytical sensing. First, because the redox-active molecule is covalently linked to the nucleic acid aptamer, the change in electrochemical signal results solely from the target-induced conformation change of the aptamer. This signaling mechanism is thus less prone to signals arising from nonspecific interactions between matrix elements and the electrode surface.^{1,4,7,8,10,16,17} It is often typical to see some signal degradation due to nonspecific adsorption of proteins or other contaminants when a sensor is employed in a complex matrix, however, this signal typically equilibrates after ~1 h allowing for specific target measurements to be made.^{1,5,8} Furthermore, with the covalently linked redox-active reporter, the sensor is reagentless and reversible.^{5,7,14,18} This allows the sensor to function without the addition of exogenous reagents, which

enables real-time detection of changes in analyte concentration. These attributes render this class of sensor amenable to the development of field deployable devices.

Here the focus is on the fabrication and design of electrochemical, aptamer-based sensors (E-AB) and the parameters employed during these processes that can affect analytical performance. In addition, several works are emphasized that discuss the fundamentals of the electrochemical signaling observed with this class of sensors and provide a quantitative framework for evaluating sensor performance. Several illustrative examples and recent advances that take advantage of the unique attributes of structure-switching sensors, including some promising alternative strategies using structure-switching aptamers, are highlighted. Finally, some of the challenges that are impeding the progress of E-AB type sensors are discussed. Even with these challenges, this class of reagentless and reversible detection shows great analytical promise in the fields of chemical, clinical, and environmental sensors.

Electrochemical, Aptamer-Based Sensor Fabrication Parameters

Sensing Self-Assembled Monolayer Chemistry

The fabrication of E-AB sensors is a relatively straightforward process; however, there are a variety of parameters that can affect the signaling and analytical performance of the resulting sensor. A typical gold electrode surface comprises a mixed monolayer of a thiol-modified nucleic acid and a diluent thiol spacer (Fig. 2). The most often used spacer is an alcohol-terminated, six-carbon alkane thiol (6-mercapto-1-hexanol). Early studies by Herne and Tarlov demonstrated that the deposition of thiolated DNA followed

by 6-mercapto-1-hexanol as a spacer lifted any nonspecifically bound DNA and enabled reproducible control over the surface density of the DNA.¹⁹ Using this “backfill” method, Herne and Tarlov established that the packing density of the DNA on the surface affects the hybridization efficiency of complementary DNA, indicating this as an important aspect of sensor performance.¹⁹ This observation holds true for aptamer-based sensors as discussed in detail below. More recently, Josephs and Ye published a study on mixed monolayer formatting using an “*insertion*” method in which the passivating monolayer is deposited first followed by the deposition of thiolated DNA.²⁰ Using atomic force microscopy, Josephs and Ye showed that the insertion method created reproducibly dispersed monolayer surfaces in contrast to the clusters of DNA found using the backfill method. Needless to say, the nature of the sensing monolayer used to fabricate structure-switching aptamer sensors have proven to be important aspects to consider when fabricating sensors.²¹

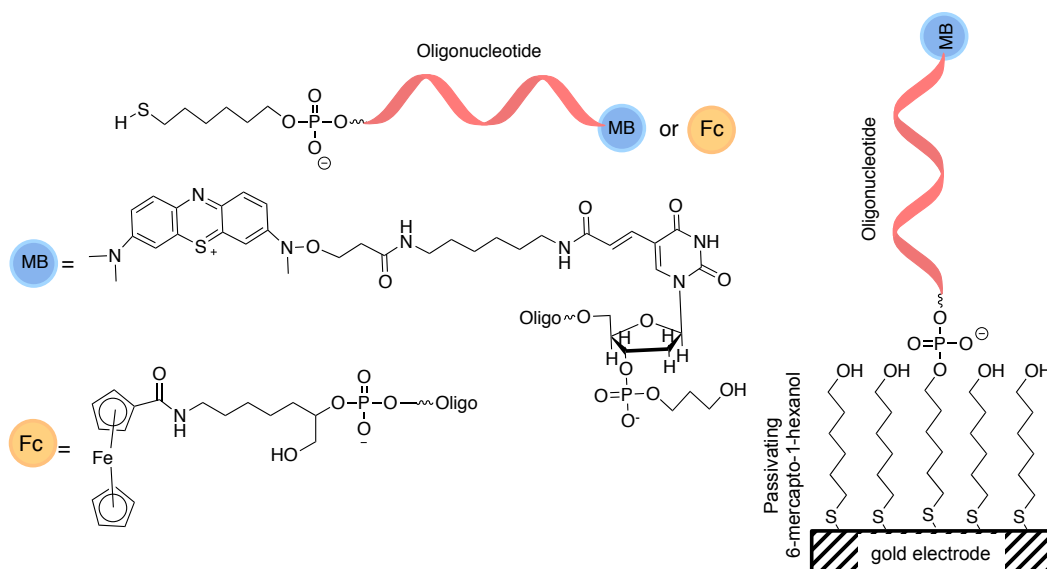


Figure 2. Typical E-AB sensors comprise mixed monolayers on gold of both a sensing aptamer, labeled at the distal end with a redox-active molecule, and of a diluent or spacer thiol. The predominant surface chemistries in the literature include a six-carbon thiol linker at the 5'-phosphate group. The most widespread used spacer thiol is 6-mercapto-1-hexanol. The most commonly used redox molecules include methylene blue (MB) and ferrocene (Fc).

The chemistry of the passivating monolayer represents a compromise between sensor signaling and stability.^{2,22} Increasing the number of carbons in an alkane thiol chain results in improved packing of this monolayer as a result of increased van der Waals interactions between neighboring thiols.²³ Consequently, the resulting thicker monolayer increases the plane of closest approach of the redox molecule, which increases the tunneling barrier.²³ The thicker monolayer compromises the magnitude of faradaic current that can be measured. Lai *et al.* published a study exploring the difference in stability and signaling of an electrochemical, DNA-based sensor employing either a six-carbon or eleven-carbon passivating thiol. Lai *et al.* demonstrated that the eleven-carbon sensor exhibited improved sensor lifetimes while maintaining an appreciable single-to-noise ratio.²² While these studies do not employ aptamer sequences, they do use

structure-switching nucleic acids for the detection of complementary nucleic acids and serve as a reasonable analogue to E-AB sensors. It should also be noted that in these studies, the number of carbons in the alkane thiol linker at the 5'-end of the DNA matched that of the passivating layer.

In addition to thiol length, the charge on the exposed terminus of the passivating monolayer also affects the signaling abilities of structure-switching nucleic acid sensors. For example, Ricci *et al.* demonstrated the sensor performance improved for both positively (amine-terminated thiols) and negatively charged (sulfonic acid-terminated thiols) monolayers.²⁴ Specifically, both monolayers improved the maximum signal (sensor signal observed at saturating target concentrations) for E-DNA sensors when compared to the typical mercaptohexanol monolayer sensors. The origin of these signal improvements is unclear, and mercaptohexanol still remains the most widely used passivating thiol.

Aptamer Packing Density

As suggested in the initial Herne and Tarlov study, the packing density of the nucleic acid aptamer (aptamers/cm²) on an E-AB sensor surface is a controllable parameter to optimize sensor performance. Aptamer packing density is typically controlled by the concentration of thiolated aptamer, incubation time, and temperature employed during monolayer formation. Values reported for aptamer packing density range from $\sim 10^{11}$ - 10^{13} aptamers/cm².^{2,25} These values represent $\leq 10\%$ of the maximum packing density of $\sim 9 \times 10^{13}$ molecules/cm² assuming a 0.7 nm cross-sectional radius for fully extended, single-stranded DNA.²⁶ The optimal packing density for a given aptamer sequence, as determined by sensor performance, is dependent on the aptamer geometry,

or tertiary structure, as well as the size and structure of the target analyte.² In general, steric interactions between neighboring aptamers can inhibit target accessibility and aptamer folding at high aptamer packing densities. The latter can alter the observed binding affinity (K_d) of the sensor.^{2,25} When aptamer packing densities become too low, the number of aptamers on the surface may not produce appreciable faradaic signal above background.

Covalently-Attached Redox Molecule

The majority of E-AB sensors employ MB^{1,10,27,28} or Fc^{9,10,16} as the redox-active tag and each molecule offers different advantages and disadvantages.^{10,16} The covalent coupling of methylene blue is typically achieved by reacting a 3'-amine-terminated nucleic acid with n-hydroxysuccinimide ester-activated methylene blue.²⁹ Ferrocene can be coupled using similar chemistry with a ferrocene carboxylic acid n-hydroxysuccinimide ester and has been coupled both pre- and post monolayer formation. Ferapontova *et al.* demonstrated that the post coupling procedure provides better coupling efficiency of the redox marker.¹⁶

The convenience of reversible electrochemical behavior and standard conjugation chemistry makes MB and Fc molecules candidates to use as signaling moieties. Methylene blue undergoes a reversible two-electron, one-proton reduction²⁹ and has seen the most widespread use. However, the redox reaction of MB is sensitive to changes in pH and thus, care must be taken when working in conditions where pH is unknown or varies. Conversely, ferrocene undergoes a reversible, one-electron oxidation to form ferrocenium. However, ferrocenium is prone to nucleophilic attack even by mild nucleophiles like chloride, which ultimately can displace the molecule from the nucleic

acid.³⁰ Ferroceniums susceptibility to nucleophilic attack limits its utility in physiologically-relevant solutions. The reaction of ferrocenium with nucleophiles can be avoided by using buffers that do not contain strong nucleophiles.^{16,31,32} Further studies by Ferapontova *et al.* demonstrate that the use of ferrocene as a redox label in physiological matrices is problematic.²⁹ Specifically, their study demonstrated that the positive potential at which ferrocene is oxidized induces nonspecific protein adhesion.^{10,29}

The use of these reversible redox couples offers the advantage of reagentless and reusable or reversible sensor signaling. Aptamer-target binding is reversible and the electrochemistry of the redox tags is reversible, which enables E-AB sensors to have the ability to report on “*real-time*” changes in the solution concentration of target analyte. Monitoring real-time changes in concentration, however, is limited by the aptamer binding kinetics. Reports indicate that association rate constants range from $\sim 10^3$ - 10^5 M⁻¹s⁻¹ and dissociation rates range between $\sim 10^{-2}$ - 10^{-3} s⁻¹ for small molecule binding.^{33,34} The downside to these common redox markers is the finite amount of charge available for measurement. Given that there is a finite number of molecules on the surface and each molecule only provides 1 or 2 electrons worth of charge limits the sensitivity and limit of detection of the E-AB sensor. As discussed below, the ability to introduce an amplification strategy that maintains the reagentless nature of the sensor could prove to be a major step forward in the development of E-AB sensors.

Several other oligonucleotide-bound redox molecules have been employed, such as iron oxide particles³² and anthraquinones,³⁵ but these are rarely used. Introduction of new redox reporters with different standard reduction potentials enables the ability to perform multiplexed detection. For example, Revzin and coworkers developed sensors

with a mixed monolayer of methylene blue-modified tumor necrosis factor (TNF)- α aptamers and anthraquinone-modified interferon- γ aptamers to simultaneously detect both targets using the same electrode surface (Fig. 3).³⁵ Their study demonstrates several compelling features of E-AB sensors, including the selective detection abilities of electrochemical detection, the specificity of aptamer-target interactions, and the ability to function in complex media (cell culture media).

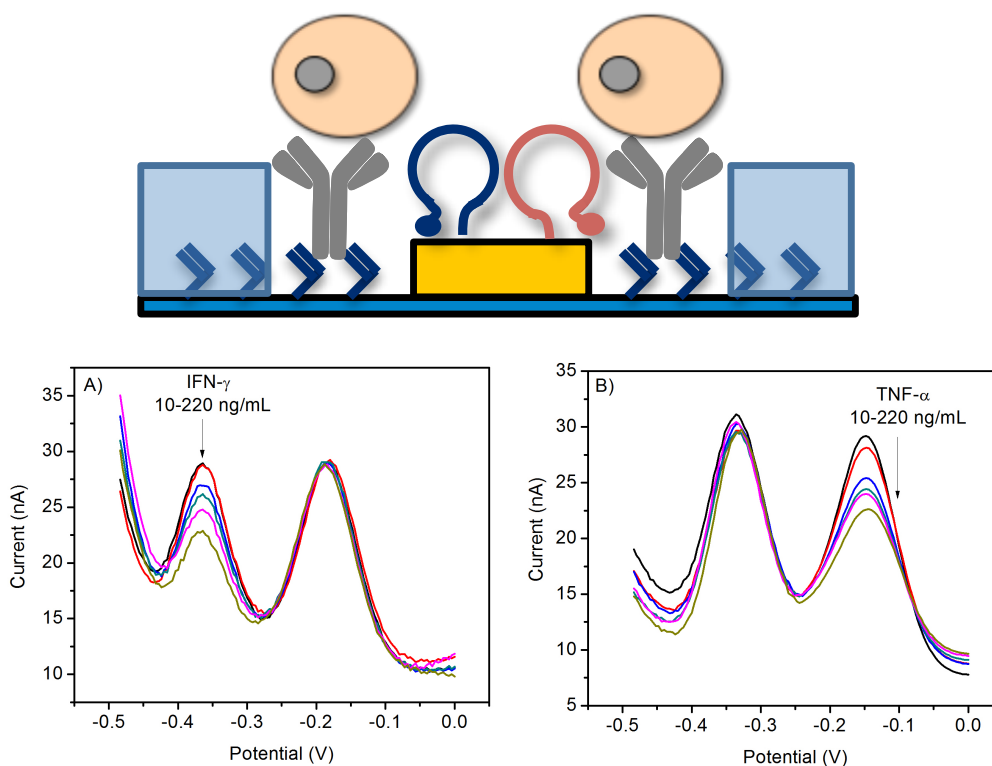


Figure 3. The use of multiple aptamers and redox reporters enables the detection of multiple analytes simultaneously highlighting the specificity of aptamer recognition and the selectivity of electrochemical detection. The difference in standard reduction potential of methylene blue (-0.15 V vs. Ag/AgCl) and anthraquinone (-0.37 V vs. Ag/AgCl) is used for simultaneous multiplexed detection of specific cytokines released from numerous cell types using the same electrode. Figure adapted from reference 35.

Fundamentals of Sensor Signaling

The Electrochemistry of E-AB Sensors

The relative coverage of nucleic acid on a typical E-AB sensor surface is such that the dynamic motion of the biopolymer chain becomes important in determining the charge transfer rate between the redox molecule and the electrode surface. This dependence is the basis for signaling in structure-switching, electrochemical aptamer-based sensors. Signaling is linked to changes in the conformation and dynamics of the grafted redox-labeled nucleic acid.

There have been several reports of quantitative models to describe the dynamic motion of end-grafted DNA on an electrode surface.³⁶⁻⁴¹ Several of these use the electrochemical response of the tethered redox molecules to estimate an apparent diffusion coefficient for the tethered redox marker as a proxy for the motion of short nucleic acid strands, including a recently reported model.³⁸⁻⁴¹ This measure is achieved by comparing the faradaic current as a function of the voltammetric scan rate for cyclic voltammetry, which defines the experimental time scale. Moiroux and coworkers reported at slow scan rates the electrochemical reaction exhibits Nernstian behavior as indicated by symmetrical cathodic and anodic peaks and little peak separation. This observation suggests that at slow scan rates, the experimental time scale is such that all of the attached redox molecules can reach the electrode surface and transfer electrons. Anne *et al.* use the area under the cathodic/anodic peak in this voltammetric regime to quantify the number of nucleic acid molecules on the surface. This measurement represents a direct, quantitative method for characterizing aptamer surface coverage.⁴⁰ It was unclear to Anne *et al.* why this method was not used more commonly in this field. The indirect

method of measuring the charge consumed relating to nucleic acid associated $\text{Ru}(\text{NH}_3)_6^{3+}$ has been the method of choice first described by Tarlov and coworkers to quantify unlabeled DNA on a surface.⁴² This method, however, was originally used on electrode-grafted nucleic acids without covalently attached redox molecules.

Much like a thin layer electrochemical cell, as the experimental timescale is shortened via the increase of voltammetric scan rate, the observation of a diffusion-dependent electrochemical response emerges for nucleic acid tethered redox molecules like those used in E-AB sensors.³⁸⁻⁴¹ Coupling this experimental observation with random walk simulations, recently reported a quantitative metric for estimating an apparent diffusion coefficient of a flexibly-tethered redox molecule at the distal end of a surface-bound nucleic acid. Typically, in thin layer electrochemistry, the electrochemical reaction follows Nernstian behavior when the cell thickness (L – analogous to nucleic acid tether length) is much less than the diffusion layer thickness ($(2Dt)^{1/2}$) determined by the scan rate (n – V/s) and diffusion coefficient (D – cm^2/s) of the molecule. This criterion is met when the diffusion layer thickness is less than 10 times the tether length ($10L \leq (2Dt)^{1/2}$). Using this criteria, diffusion coefficients of $\sim 7 \times 10^{-11} \text{ cm}^2/s$ for redox molecules tethered to unstructured poly-thymine linkers, as a model nucleic acid, are estimated. These estimated diffusion coefficients are similar to those reported by Anne *et al.*⁴⁰ and Ferapontova and co-workers.³⁹

The dependence of sensor signaling on the voltammetric scan rate leads to interrogation methodology optimization. E-AB sensors work based on changes to the charge transfer rate as a result of target-induced conformation changes that alter the structure and ultimately apparent diffusion coefficient of the appended redox molecule.

Each state – target-bound and unbound – has different charge transfer rates, which allows for quantitative determination of the presence of target (Fig. 1). This observation can be used to further optimize sensor signaling as discussed in detail below.

Quantitative Binding Curves and Analytical Figures of Merit

Quantifying the analytical response of E-AB sensors is necessary for benchmark comparison with existing sensing techniques and strategies. As mentioned above and explored in more detail below, there are several factors in the fabrication and analysis of E-AB sensors that can affect sensor performance. There are several core analytical parameters that can be used to describe the performance of these sensors, including sensitivity, limit of detection, binding affinity, specificity, and selectivity. Herein, specificity is defined as the degree to which the biorecognition element is free from interference by other species, which is an intrinsic property of the aptamer sequence. Selectivity is defined by the degree to which the method (*i.e.*, electrochemical detection) is free from interference by other species in a complex sample matrix.

E-AB sensor responses follow a Langmuir-like binding isotherm. For a given electrode surface, there is a finite number of binding sites (aptamers) and as such, there is a target concentration at which all binding sites are occupied. This type of binding follows the Langmuir isotherm model with several assumptions, including that target binding to one aptamer does not affect target binding to a neighboring aptamer, or the binding sites are non-interacting. The stipulations of the Langmuir isotherm may not hold true at high packing densities. Moreover, the assumption is made that target binding does not appreciably alter the free target concentration in bulk solution. While free target concentration generally true, when working with low concentration and small volumes,

this can become problematic.⁴³ Starting with an equilibrium expression for target (L) binding a receptor aptamer (R), and using the aforementioned assumptions, the fraction of occupied sites (β) can be written as

$$\beta = \frac{K_a[L]}{1+K_a[L]} \quad (1)$$

where K_a and $[L]$ are the association constant and target concentration, respectively. Rewriting eq.1 in terms of K_d (the dissociation constant or binding affinity), the expression for sensor signaling becomes:

$$\frac{S}{S_{\max}} = \frac{[L]}{K_d+[L]} \quad \text{and} \quad \frac{S}{S_{\max}} = \beta \quad (2)$$

where S and S_{\max} (*i.e.*, peak current) are the sensor signal at a given concentration and sensor signal at saturating concentrations respectively. It should be noted that when the model is fit to the data the binding affinity is only an apparent affinity (affinity of the E-AB sensor determined by the Langmuir Isotherm) and does not necessarily represent the intrinsic binding affinity (affinity of the aptamer to a target molecule in solution). This apparent affinity can change based on the sensitivity of the sensor device, which can be significantly altered by changing the voltammetric interrogation frequency or scan rate, or the aptamer geometry as discussed below in more detail.

The Langmuir-type isotherm described above can be modified to account for two different binding sites. The isotherm can then be utilized for multiple aptamers on a sensor surface for the same target but with different affinities. A recent report demonstrated that a bi-Langmuir isotherm accurately predicts E-AB sensor response based on the ratio of the aptamers employed on the sensor surface, the individual observed binding affinities, and S and S_{\max} (Fig. 4).⁴⁴ Creating heterogeneously-coated sensor surfaces with multiple aptamers represents a method to rationally tune the

sensitivity and dynamic range of the resulting sensor. Employing heterogeneously coated sensors is only one of the many methods that enable tuning sensor response.

Tuning Analytical Figures of Merit

A compelling aspect of E-AB sensors is the ability to tune the analytical figures of merit. Sensor fabrication parameters can affect the analytical performance of the resulting aptamer sensor. The control over the sensor performance, by modifying the fabrication parameters is minimal. There are a variety of other methods that can be utilized that have larger effects on the analytical performance than modifying sensor fabrication parameters.

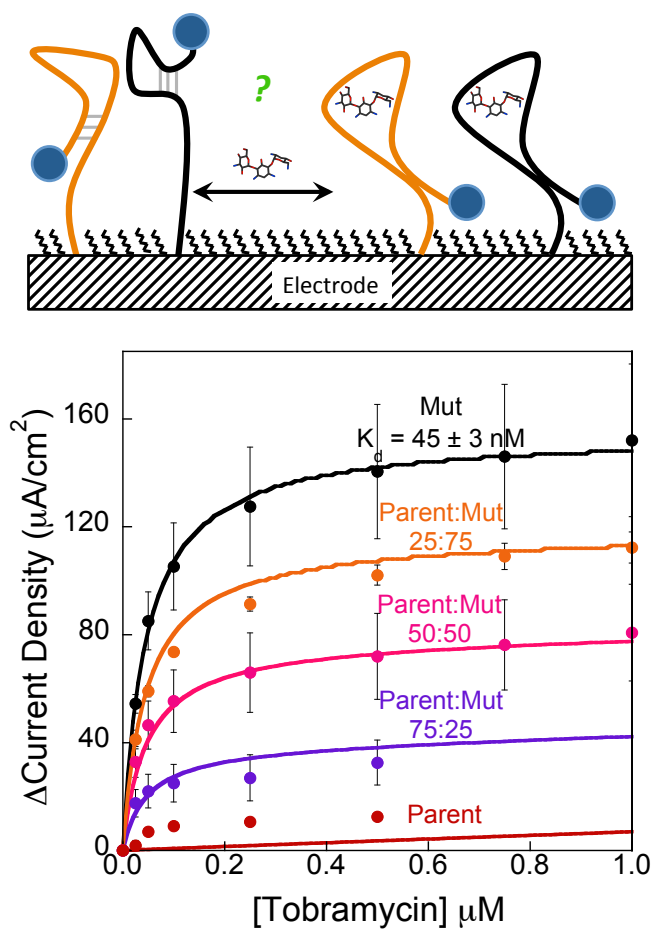


Figure 4. The use of multiple aptamers with different binding affinities on the same surface enables tunable sensor responses with respect to the ratio used. The ratio used of

the aptamers dictates the sensor responses and alters the maximum signal change observed at saturating target concentrations.

Voltammetric Methods of Interrogation

Given that the motional dynamics, and change in these dynamics, of the sensing aptamer is an important factor, it is not surprising that the time scale of the voltammetric interrogation is an important parameter in sensor function. Cyclic (CV), alternating current (ACV), squarewave (SWV), and differential pulse (DPV) voltammetry are all suitable methods for monitoring aptamer conformation change and the resulting change in charge transfer rates. The latter three are particularly well suited for monitoring surface-confined reactions as they reduce non-faradaic background charging currents. The experimental time scale is dictated by the scan rate or frequency of each technique and can have profound effects on signaling – especially in the differential technique of SWV.

The frequency of the excitation potential waveform employed in ACV, SWV, and DPV affects sensor sensitivity, signal change magnitude, polarity, and observed binding affinity.^{2,28,45,46} Signal polarity refers to either the increase (signal on) or decrease (signal off) in current upon target addition. In the specific case of SWV, the magnitude of signal change at saturating conditions, and the signal polarity of a given sensor can be dramatically altered.^{2,28,45,46} The dependence of sensor performance on the squarewave frequency employed is attributed to the time scale of the voltammetric measurement (frequency) with respect to differences in apparent rate between the target-bound and unbound states (Fig. 5).^{28,46} Current is sampled near the end of each squarewave pulse, and thus the magnitude of current measured is related to the apparent rate of the charge

transfer reaction. Because the target- bound and unbound states have different charge transfer rates, the magnitude of current measured for a fixed pulse width (frequency) is different. For example, as an approximation, a sensor in the unbound state with a charge transfer rate of 100 s^{-1} gives a higher measurable current using a frequency of 100 Hz than that of the bound state with a charge transfer rate of 6 s^{-1} .⁴⁵ Conversely, if using a squarewave frequency of 5 Hz, the sensor in the bound state gives a larger measurable current than that of the unbound state. Utilizing different frequencies when testing E-AB sensors can lead to a signaling polarity switch between a signal-on and a signal off-sensor. The interrogation frequency can be optimized for a given aptamer geometry. The frequency dependence of sensor signaling abilities has also been shown for E-AB sensors employing ACV by White *et al.*² and E-DNA sensors employing ACV by Ricci *et al.*⁴⁶.

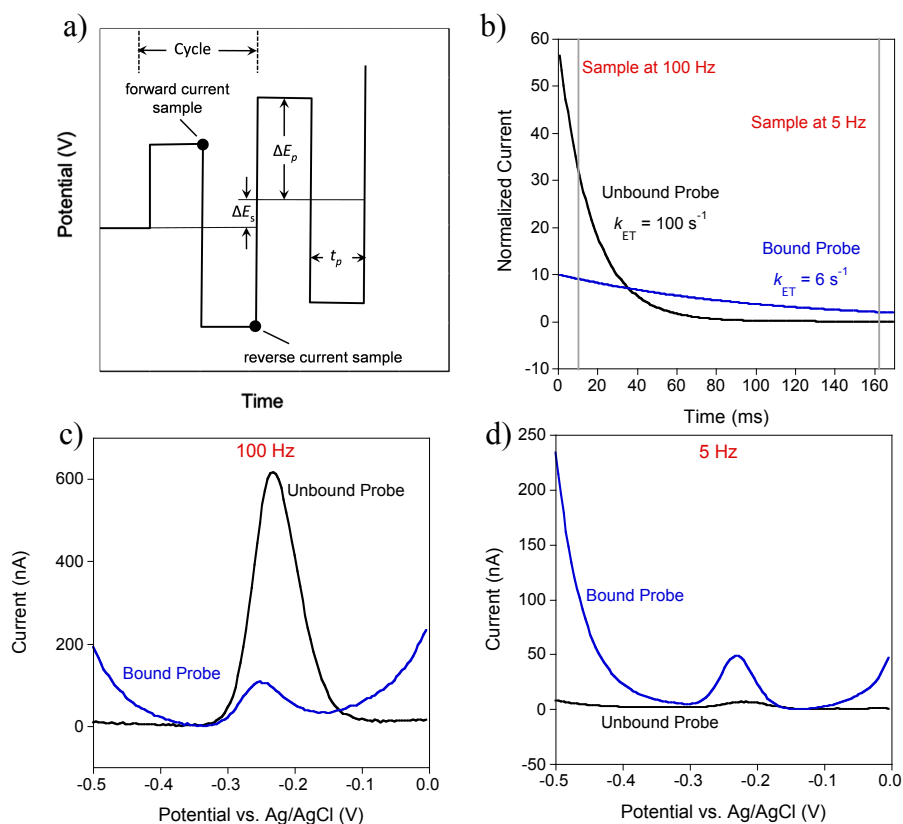


Figure 5. The voltammetric parameters when utilizing squarewave voltammetry (SWV) to interrogate sensor surfaces can alter the current observed. (a) SWV utilizes a square potential wave that incrementally rises to a set potential and the current is sampled at the end of each squarewave pulse. (b) The magnitude of the current measured is thus related to the apparent electron transfer reaction rate. The bound and unbound probes have different apparent rates, therefore the current magnitude for a fixed pulse width (frequency) is different. (c) For example, at 100 Hz the peak current is larger for the unbound probe with respect to the bound probe because the apparent electron transfer rate is faster for the unbound probe. (d) If the frequency is altered to 5 Hz the bound probe gives a larger measurable current because the apparent reaction rate is slower for the bound probe. Figure adapted from reference 45.

Designing Aptamer Conformation for Sensor Signaling

Structure-switching, aptamer-based sensors rely on a target-induced conformation change in the electrode-bound aptamer. It is clear that the difference in apparent charge transfer rate between the target-free state and the target-bound state is important in determining the signaling abilities of E-AB sensors. Unfortunately, current aptamer selection strategies do not select for functionality beyond target binding (*i.e.*, there is no

selection pressure for structure-switching aptamer). Fortunately, the base-pair programming language of nucleic acids and the aid of secondary structure prediction software (MFOLD)^{47,48} enable the design of altered aptamer sequences to support reagentless, electrochemical signaling.^{3,18,28,45,49–52}

Beyond creating aptamer sequences to support reagentless signaling, altering the aptamer sequence to modify the magnitude of the conformation change can have dramatic effects on the analytical performance of E-AB sensors. There are several strategies for creating alternative aptamer structures. Typical strategies include destabilization, alternative folds, and the introduction of the aptamer into a scaffold.^{3,28,45,49,52} Solution-phase 3-dimensional structures of aptamer-target complexes can assist in the modification of aptamer sequences.

A recent report utilized a combination of secondary structure predictions and the NMR structure of the aminoglycoside-binding RNA aptamer⁵³ to rationally design sequences to undergo larger conformation changes in the presence of tobramycin, in comparison to the published parent aptamer sequence.^{28,54} The NMR structure of the aptamer enabled careful conservation of nucleotides and portions of the RNA backbone hypothesized to bind with tobramycin to maintain specific binding ability.²⁸ The aptamer sequence was altered outside of the binding site by removing base pairs to destabilize the secondary structure in the unbound state. Disrupting the stem-loop secondary structure of the parent aptamer forces the aptamer to undergo a larger conformational change upon target addition, significantly improving E-AB sensor sensitivity.²⁸ Interestingly, given the similarities between the target-bound structure and the predicted secondary structure, it was surprising to observe an improvement in the observed binding affinity of the new

aptamer constructs. This observation indicates that the reported affinity for E-AB sensors is convoluted by the sensitivity and signal change magnitude and not necessarily a direct indication of the intrinsic binding affinity. Finally, care should be taken when altering aptamer sequences as alterations to the sequence can detrimentally affect target binding ability.³ Furthermore, Bonham and coworkers published a universal approach to creating reagentless, structure-switching E-AB sensors by incorporating an aptamer sequence into a DNA scaffold.⁵² This approach divides the aptamer into sections and incorporates into a structure-switching DNA scaffold and was universally applied to a ricin-binding and botulism toxin-binding aptamer for E-AB signaling.

Function in Complex Media

One of the most compelling attributes of E-AB sensors is their ability to function in complex media. This attribute is a result of specific aptamer-target interactions and selective electrochemical detection of specific redox markers. To date, aptamer-based sensors have been tested in a variety of complex media, including foodstuffs,⁵⁵ undiluted serum,^{1,4,7} saliva,^{18,55} whole blood,^{8,50} and real-time in the circulating blood of living animals¹⁷. While detection can be performed, there can still be complications from non-specific binding as seen by Ferguson *et al.*,¹⁷ where the sensing device is coupled with a microfluidic filter (discussed in more detail below). Conversely, E-AB sensors fabricated with RNA aptamers are less able to function in complex media as a result of the inherent instability of RNA and susceptibility to nuclease degradation. RNA-based sensors will function in serum only after the serum has been filtered (using the filtrate of a solution that is filtered through a 3000 molecular weight cutoff filter) or treated with an RNase inhibitor. For example, Ferapontova *et al.* compared RNA E-AB sensor function in buffer

and RNase inhibitor-treated serum, while RNA sensors did not function at all in untreated serum¹⁶ further indicating nucleases are the main cause of RNA sensor instability.^{7,16}

Illustrative Examples of Aptamer-Based Sensing

The growing analytical detection capabilities of E-AB sensors are a direct consequence of their sensitive signaling mechanism, as well as the specific recognition abilities of aptamers. Recent advances in the field have shown utility of these unique attributes of structure-switching E-AB sensors in real-world applications. While not all-encompassing, the reports discussed below highlight some of the major breakthroughs achieved thus far in the field, which attest to the great analytical promise of this class of sensors in the fields of chemical, clinical, and environmental sensing.

Ion and Small Molecule Detection

One advantage of conformation-switching aptamers is realized in the detection of low molecular weight targets, including inorganic ions and small molecules. Radi and O'Sullivan first demonstrated a conformation-switching aptamer sensor for the detection of potassium (K^+) ions via the use of guanine-rich (G-rich) DNA aptamers appended to a gold electrode surface. The G-quartet structure is particularly well suited to recognize monovalent cations, specifically K^+ ions.⁵⁶ The G-rich aptamers undergo recognition-induced conformational changes that promote conversion of loose random coil sequences into a more compact G-quadruplex form. The method was shown to be highly selective for K^+ ions when tested against other mono- or divalent cations (e.g. Na^+ , Mg^{2+} , Ca^{2+}) and achieved an limit of detect (LOD) of about 0.015 mM.⁵⁶ This study not only validates the potential of these structure-switching E-AB sensors in the field of chemical sensing

with good sensitivity and selectivity, but also highlights an issue that may plague E-AB sensors – structural sensitivity to ion composition, since several DNA and RNA structure motifs rely on specific ion composition. Aptamer dependence on ion composition include the reliance of the G-quadruplex motif on K^+ ions,⁵¹ as well as the K-turn (kink turn) motif on Mg^{2+} ions⁵⁷.

E-AB sensors have made excellent progress in the detection of small molecules beyond the benchtop. Notable publications from Baker, *et al.*, Zayats, *et al.*, Wu, *et al.*, and Zhang, *et al.* demonstrate the utility of these sensors in the detection of small molecules, such as purine nucleosides^{58–60} and small drugs¹⁸. As mentioned earlier, work by the groups of Plaxco and Soh, introduced a rapid, reusable, and label-free electrochemical detection of circulating therapeutic agents directly in the flowing blood of a living animal.¹⁷ The microfluidic-based electrochemical sensing platform, termed as MEDIC (microfluidic electrochemical detector for *in vivo* continuous monitoring), detected therapeutic *in vivo* concentrations of doxorubicin and kanamycin in live rats and in human whole blood with high sensitivity and sub-minute temporal resolution.¹⁷

Protein Detection

Proteins are yet another type of target molecules that have been successfully studied employing structure-switching E-AB sensors. For example, Plaxco's, Heeger's, and Revzin's groups reported a general electrochemical sensing platform for the detection of the proteins thrombin,¹⁴ PDGF (platelet-derived growth factor),¹ interferon gamma (INF- γ),⁶¹ and botulism toxin⁵² in buffer and in serum, which does not require analyte modification or labeling, and is highly sensitive, selective and reusable. In the presence of the target proteins, the methylene blue (MB)-tagged DNA aptamers undergo

target-induced conformational changes from partially unfolded states to more rigid folded states or vice versa, which alter the efficiency of the electron transfer between the MB redox molecule and the gold surface, and thus, result in either a decrease (i.e. thrombin- and INF- γ binding aptamers) or an increase (i.e. PDGF-binding aptamer) in the observed current signal. Interestingly, Revzin's group introduced a way to carry out simultaneous, multiplexed detection of cytokines (tumor necrosis factor (TNF)- α , INF- γ , transforming growth factor (TGF)- β 1) via fabrication of micropatterned gold electrode arrays functionalized with redox-active DNA aptamers specific for their respective targets and integration with a microfluidic device.^{35,62,63} This emerging microfluidic-based sensing approach that utilizes the specific recognition mechanism of structure-switching E-AB sensors offers advantages of rapid, simultaneous, sensitive and highly specific detection of immune cell-secreted cytokines, which shows its great potential in the fields of immunology and cancer research.

These studies demonstrate the tunability and highly flexible sensing capabilities of structure-switching E-AB sensors that make these sensors adaptable to the development of transportable sensing devices. These reports also demonstrate the powerful sensing abilities of this class of sensor, and thus, may very well present a means to detect a broader range of targets *in vitro* and particularly *in vivo*.

Alternative Strategies

Nanopore-Based Sensing

Integration of specific aptamers with single-molecule detection techniques, particularly *stochastic nanopore-based sensing*, is being explored as an alternative strategy to further improve its sensitivity and detection limit, potentially down to the

single molecule level. Stochastic nanopore sensing has emerged as a powerful resistive-pulse, single-molecule detection technology that measures the electrical current carried by ions flowing through a resistive nanopore, where a single binding event causes a fluctuation in the ionic current flow that can be measured and used to identify and quantify target analytes.⁶⁴⁻⁶⁶ Coined as *aptamer-based nanopores*, a few studies to date have already been reported in the literature showing the potential of these sensors in stochastic nanopore sensing of various targets, such as proteins⁶⁷ and biomarkers^{68,69}. For example, Rotem *et al.* demonstrated nanomolar (nM) sensitivity of an aptamer-based nanopore sensor via the utility of staphylococcal α -hemolysin (α HL) modified with a 15-mer DNA aptamer that specifically bound thrombin.⁶⁷ In this approach, binding of thrombin to the aptamer hybridized to the α HL pore produced a cation-stabilized quadruplex that resulted in a modulation in the ionic current flowing through the pore, allowing sensitive and specific quantification of thrombin in the nM concentration range (20 - 350 nM).⁶⁷

Thus far, this new class of aptamer-based nanopores shows promise in the detection of target analytes, offering advantages of tremendous sensitivity, excellent specificity and reproducibility.

Perspectives

Challenges of E-AB Sensors

While it is clear that structure-switching, electrochemical aptamer-based sensors hold promise as a detection strategy, there are several challenges that need to be kept in mind when designing and employing new sensors.

Conformation Change Dependence on Environmental Factors

An inherent limitation to using biomolecules, such as nucleic acids, as a recognition element, is that structure and function depend on environmental factors such as pH, temperature, and ionic strength. In the body, environmental conditions are regulated homeostatically, however, on the bench or in the field, sensor response can be altered based on changes in environmental conditions. Cho *et al.* cite that buffer conditions and temperature are important factors that need to be considered when working with aptamer sequences.⁷⁰ A clear example of matrix effects is seen with an E-AB sensor fabricated with the thrombin binding aptamer.¹⁴ The thrombin binding aptamer forms a G-quadruplex structure, which requires potassium ions to fold, in order to bind an exo binding site on human α -thrombin. Xiao *et al.* investigated the dependence of signal change of thrombin E-AB sensors based on the ionic strength and composition. They determined that at a high ionic strength (300 mM Tris base, 420 mM NaCl, 60 mM KCl, and 60 mM MgCl₂) the apparent binding affinity of an E-AB sensor for thrombin is 50 nM. Conversely, at a low ionic strength, without the presence of potassium (100 mM Tris Base) the sensor exhibits an apparent binding affinity of 21 nM with an increase in sensitivity. The improvement in sensor function appears to relate to aptamer folding and not directly ionic strength.⁷¹ Without potassium, the aptamer is unfolded and likely exhibits a larger conformation change in the presence of thrombin, which leads to better sensitivity. Other instances where pH and temperature can affect sensor responses specifically for E-DNA and aptamer molecular beacon sensors have been shown.^{72,73} Because matrix effects can affect the performance of a sensor it is prudent to calibrate sensors in the sample matrix.

Improving Aptamer Selection

The performance of E-AB sensors is ultimately linked to the aptamer that is used to fabricate the sensor. While protein-binding aptamers can be specific, aptamers selected for small molecule binding targets, with only a few exceptions, often lack specificity. For example, protein-binding aptamers, including thrombin, INF- γ , and TNF- α exemplify target specificity in complex media and when challenged by similar proteins.^{8,14,62} In contrast, the aminoglycoside RNA aptamer will bind several aminoglycoside antibiotics, including tobramycin, kanamycin, neomycin B, gentamycin C, erythromycin, and tobramycin analogs.⁵⁴ In addition, the cocaine aptamer will bind cocaine, ecgonine methyl ester, lidocaine, and procaine.⁷⁴ There are counter examples, like the RNA theophylline aptamer that will bind theophylline with a 500-fold better affinity than caffeine even though the targets differ by a single methyl group.¹⁶ Needless to say, as selection procedures improve, the field will benefit from increased specificity and affinity, particularly for low molecular weight targets. In addition, current selection methodologies do not search for structure-switching aptamers needed for E-AB signaling.

Signal Amplification

The signaling of E-AB sensors is limited to only a handful of demonstrated redox markers that can only provide ~1-2 electrons of current. Because of the finite number of redox-labeled aptamers on the surface, only a finite charge is measured. The limited charge measured ultimately restricts the sensitivity and detection limit of structure-switching, aptamer-based sensors. The charge measured can dramatically improve by employing a signal amplification technique that bio- or electrocatalytically regenerates the redox molecule for amplified currents. There are a myriad of examples of such amplification coupled with aptamer recognition.⁷⁵⁻⁷⁸ However, these examples eliminate

one of the most compelling attributes of E-AB sensors – their reagentless nature. The introduction of signal amplification that retains the reagentless nature of E-AB sensors would be a major breakthrough in this class of promising biosensors.

Electrode Miniaturization

Coupling E-AB sensors to micro- and nanoelectrodes has the ability to bring the promising attributes of small electrodes - low ohmic (IR) drop, small background capacitive charging current, rapid steady-state equilibration, high current density and minimal sample requirement⁷⁹ – with aptamer recognition to further the expanse of applications these sensors can impact. These advantages open up E-AB sensor applications to biological and chemical sensing,^{5,80} but also to Scanning Electrochemical Microscopy (SECM)⁸¹. Furthermore, miniaturization of electrodes allows their integration with devices for non-invasive *in vivo* measurement and point-of-care diagnosis. This transition, however, has met many challenges, including limited current signal resulting from the small size and low number of aptamers on the sensor surface. Liu *et al.* reported the first reversible and reproducible use of microelectrodes for E-AB sensing for the detection of ATP and tobramycin quantification directly in 100% undiluted serum.⁵ This report used deposition of gold nanoparticles to overcome the inherent low signal to noise. The introduction of an amplification technique would greatly facilitate the transition to small electrodes.

Conclusion

Advances in the field of structure-switching electrochemical aptamer-based sensors have continued to expand in the past 10 years. Due to the versatility of this class

of sensor, they can be applied to a wide variety of applications for any aptamer-target pair. Here, widely applicable techniques employed to fabricate, tune, and optimize E-AB sensor responses were reviewed. This class of sensor has been applied to direct detection of target molecules in a variety of complex biological samples, including *in vivo* measurements, due to their reagentless, reusable, and specific nature. On the other hand, the sensor signaling can vary depending on the ionic strength, pH, and temperature, which can inhibit broader use. In addition, regenerative amplification techniques have not yet been applied to E-AB sensors, which limit sensitivity. Thus, the future of E-AB sensors relies on aptamer selection protocols, specifically for small molecule targets, and reagentless signal amplification of sensor responses. All of the aforementioned parameters are necessary to consider when designing aptamer-based sensors.

In conclusion, aptamer-based sensors coupled to an electrochemical platform have been a major role in bioanalytical sensors and applications. This class of sensor has the attributes to become the new basis for real-time patient diagnostics. The potential of these sensors for therapeutic drug monitoring will improve upon the novel development of aptamer selection strategies and regenerative amplification techniques coupled to the E-AB sensor platform. As novel amplification and application platforms emerge for E-AB sensors, others are encouraged to enable their sensing mechanism for widespread impact above and beyond their own laboratory.

Chapter 2: Enhancing Analytical Performance of RNA E-AB Sensors for the Detection of Aminoglycoside Antibiotics

Introduction

Electrochemical, aptamer-based (E-AB) sensors employing structure-switching aptamers represent a promising platform for the rapid and sensitive quantification of target analytes. To date, E-AB sensors have been reported against a wide variety of targets including ions,⁵⁶ proteins,^{14,62,82–85} small molecules,^{7,10,16,50,86} and bacterial^{87,88} and mammalian cells⁸⁸. Target detection is achieved through the utilization of single-stranded DNA or RNA aptamer sequences that have been selected *in vitro* to bind to a specific target of interest.^{54,89–91} The principal signaling mechanism in this class of sensors is a result of conformation and flexibility changes in the electrode bound aptamer.^{1,2,4,14,18,45,71} Typically, the aptamer is modified at the 5'-end for electrode attachment (e.g., thiolated) and at the distal, 3'- end, with a redox reporter molecule (typically methylene blue or ferrocene). The electron transfer efficiency is a function of the distance and collision frequency between the redox reporter and the electrode surface, thus changes in faradaic current upon target binding is readily measured electrochemically. Target quantification is performed by measuring changes in voltammetric peak current, typically defined as percent signal change. Using this sensing strategy, E- AB sensors have been reported to exhibit typical limits of detection from micromolar down to subnanomolar levels when detecting, for example, proteins or small molecules. In addition, sensors are able to perform such detection in complex sample matrixes, like serum or whole blood.^{1,14,16,50,56,61}

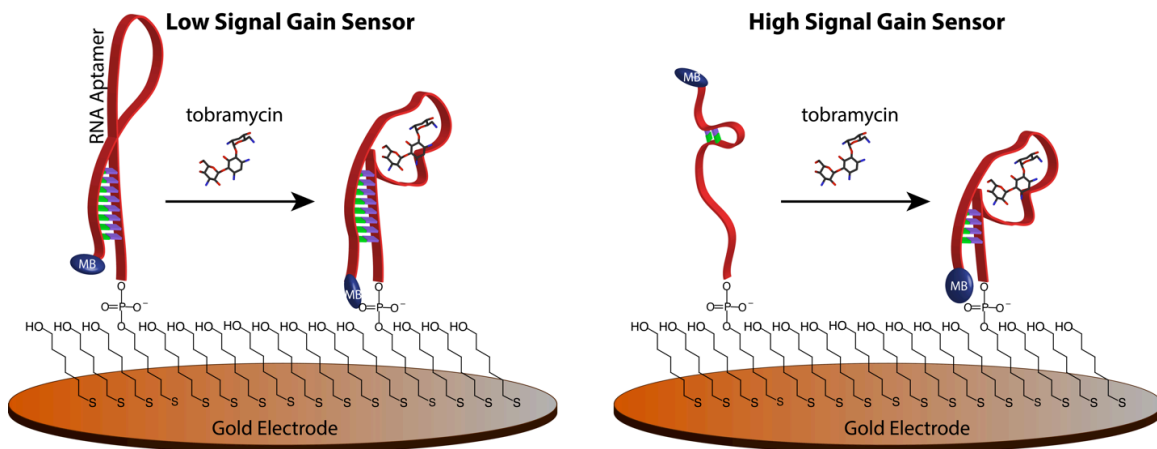


Figure 6. Electrochemical, aptamer-based sensors employing structure-switching aptamers rely on specific target-induced changes in the conformation and/or flexibility of the aptamer. All sensor architectures investigated in this study appear to demonstrate changes in conformation and flexibility upon target binding (Fig. 7). However, the magnitude of these changes ultimately affects the magnitude of the signal gain achieved by the respective sensors. Below is a schematic illustration of two E-AB sensor architectures: a low signal gain sensor and a high signal gain sensor. The latter illustration shows a larger change in conformation upon target binding thus leading to a high signal change.

In this report two strategies were utilized to greatly improve the analytical performance of a representative electrochemical RNA aptamer-based sensor directed against aminoglycoside antibiotics. Specifically, electrochemical strategies were explored to better exploit the target binding-induced changes in aptamer conformation and flexibility (i.e., voltammetric interrogation frequency). Rationally designed mutant aptamer sequences to support larger conformation changes were employed, which caused larger changes in sensor signaling in the presence of target analyte (Fig. 6). As a result, analytical parameters (binding affinity, sensitivity, and limit of detection) for previously reported E-AB sensors employing the parent RNA aptamer sequence were improved.⁷ The strategies highlighted here provide a general approach to developing E-AB sensors

with improved sensitivity, without compromising the attractive characteristics of this class of sensors in that they are relatively simple, reagentless, rapid, and reusable.

Experimental

Materials

6-Mercapto-1-hexanol (99%), tobramycin, sodium chloride, Trizma base (2-amino-2-(hydroxymethyl)-1,3-propanediol, referred to as Tris), magnesium chloride, and tris-2-carboxyethyl-phosphine (TCEP) (Sigma Aldrich) were all used as received. All buffer solutions were prepared using autoclaved, ultrapure water (Mili-Q Ultrapure Water Purification, Millipore, Billerica, MA). RNA probe sequences (Table 1) were synthesized and purified using dual-HPLC (Biosearch Technologies, Inc. Novato CA). The probes were aliquoted at 0.2 μ M in autoclaved 0.01 M EDTA aqueous solution, pH 8.0 (Sigma Aldrich) and stored at -20 °C until use. Fetal bovine serum (Fisher Scientific) was centrifuged using 10 kDa and 3 kDa centrifuge columns (Millipore) in a Legend X1R Centrifuge (Thermo Scientific) for 1 h in each filter.

Table 1. Parent and Modified Aptamer Sequences

Sequence Name	Sequence
Parent Aptamer	5'-HSC ₆ - GGGACU <u>UGGUUUAGGAAAUGAGU</u> CCC - MB - 3'
Probe D1	5'-HSC ₆ - ACU <u>UGGUUUAGGAAAUGAGU</u> - MB - 3'
Probe D2	5'-HSC ₆ - CU <u>UGGUUUAGGAAAUGAGU</u> - MB - 3'
Probe D3	5'-HSC ₆ - GGGACU <u>UGGUUUAGGAAAUGAGU</u> - MB - 3'

Electrochemical Aptamer-Based (E-AB) Sensor Fabrication

All E-AB sensors were fabricated on 2 mm diameter polycrystalline gold electrodes (CH Instruments, Austin, TX). Electrode modification was performed as

previously described ⁷. To briefly summarize, these electrodes were first hand polished in a circular fashion on a microcloth (Buehler) in a 1 μm diameter diamond particle suspension (Buehler), followed by polishing in an alumina oxide slurry (Buehler). The electrodes were then rinsed with and sonicated in ultrapure water for 5 min. Following the hand polishing steps, electrodes were electrochemically cleaned via a series of voltammetric scans in dilute sodium hydroxide and sulfuric acid solutions as previously described ². After cleaning, each electrode was incubated in a 200 nM RNA probe solution in autoclaved 20 mM Tris buffer with 100 mM sodium chloride and 5 mM magnesium chloride at pH 7.4 for 1 h. Prior to RNA immobilization, the RNA probes reacted with 4 μL of 10 mM TCEP for 1 h to reduce the 5'-disulfide bond resulting from oligonucleotide synthesis. After the RNA layer is formed, the electrodes were dipped into an autoclaved buffer solution to remove excess and nonspecifically adsorbed RNA, followed by incubation in a 3 mM solution of 6-mercapto-1-hexanol in 20 mM Tris buffer with 100 mM sodium chloride and 5 mM magnesium chloride for 1 h. These electrodes were dipped into autoclaved buffer solution to remove traces of 6-merapto-1-hexanol and stored in autoclaved Tris buffer for \sim 1 h prior to use to enable a stable sensor signal.

Electrochemical Measurements

Electrochemical measurements were performed using CH Instruments 620D Electrochemical Workstation (CH Instruments, Austin, TX). These measurements were performed in a three-electrode cell using an Ag/AgCl (3 M NaCl) reference and a platinum wire counter electrode. Square wave voltammetry parameters were as follows: a pulse amplitude of 25 mV, frequency was varied, and a step width of 1 mV.

Measurements were performed in a glass cell with 6 or 3 mL of Tris buffer. For measurements performed in filtered fetal bovine serum, the sensors were allowed to equilibrate in 1.5 mL of serum for 1 h prior to use.

Results and Discussion

The sensors in these studies utilized the 26-nucleotide aminoglycoside-binding RNA aptamer containing the same core sequence first reported by Wang and Rando.^{54,91} The aptamer binds tobramycin with an intrinsic binding affinity of 12 ± 5 nM determined via a solution-phase fluorescence assay.⁵⁴ The 26-nucleotide aptamer was shortened by 4 nucleotides to be incorporated into an E-AB sensor by Rowe *et al.*^{7,54,91} The sensor described by Rowe *et al.* is a signal-off sensor, signaling the presence of aminoglycosides by a decrease in measured current. The signal change is attributed to a target-induced change in conformation of the sensing aptamer.^{7,92}

In this work, several strategies were utilized to enhance the signaling and analytical figures of merit of aptamer-folding based sensors to improve the detection abilities of an RNA-based electrochemical sensor. Specifically, the signaling of the parent aptamer was optimized through the use of numerous electrochemical interrogation frequencies, a known parameter to improve signaling.⁴⁵ Then a biomolecular engineering strategy was executed to create larger target-induced conformation changes in the aptamer structure, thus larger signal changes upon target addition (Fig. 6). Consequently, these changes lead up to ~100 fold improvements, in observed binding affinity, sensitivity, and limit of detection.

Optimization of E-AB Sensor Employing the Parent RNA Aptamer

E-AB sensors employing the aminoglycoside parent RNA aptamer responds quantitatively to the amount of tobramycin in solution.⁴⁵ Specifically, using squarewave voltammetry with a 60 Hz interrogation frequency, the sensors respond to tobramycin with a decrease in voltammetric peak current within seconds (Fig. 8a).⁷ To quantify the change in signal upon target addition, percent signal change was utilized (eq. 3). The percent signal change is calculated using the following formula:

$$100 \times [(i_p(\text{target}) - i_p(\text{baseline})) / i_p(\text{baseline})] \quad (\text{eq. 3})$$

where $i_p(\text{target})$ is the voltammetric peak current at a specific target concentration and $i_p(\text{baseline})$ is the voltammetric peak current in the absence of target. By using Equation (3) the aminoglycoside E-AB sensor exhibited a percent signal change of $-48 \pm 3\%$ upon the addition of excess (2 mM) tobramycin (Fig. 8d). Unlike previous reports, however, the sensor exhibited an improved binding affinity (K_d) of $42 \pm 2 \mu\text{M}$ compared to $319 \mu\text{M}$.⁷ The different observed affinities between the sensors presented here and those fabricated by Rowe *et al.*⁷ could be due the fact that sensor signaling and performance is intimately linked to the nature of the sensing monolayer,^{2,93,94} which causes differences in probe packing densities as a function of electrode surface (hand polished polycrystalline gold electrodes versus electrodeposited gold)⁹⁵.

The signal polarity and magnitude of the aminoglycoside sensor are controlled by the frequency of the potential waveform employed during squarewave voltammetry. Specifically, the sensor can be converted from a signal-off type sensor to a signal-on type sensor. A signal-off response was observed at frequencies ≤ 200 Hz (Fig. 8a), while at frequencies ≥ 300 Hz, the sensor behaved as a signal-on type sensor. Control over signal polarity is typical of this class of folding-based sensors, as previously described.⁴⁵ The

change in polarity was a consequence of the time scale of the voltammetric experiment with respect to the differences in apparent rate between the target-bound and unbound states. Qualitatively, by evaluation of the current response as a function of frequency, the unbound state exhibits a lower apparent rate than the target-bound state (Fig. 7).^{45,96} While, quantitative conclusions cannot be made about electron transfer rates using these observations because the rate-limiting step is not known,^{97,98} the best frequency to exploit the difference between the unbound and target-bound states can be qualitatively determined.⁴⁵ In addition to controlling the polarity of signaling, the magnitude of signal change is controlled by varying the squarewave frequency. At saturating target conditions (2 mM), a maximum signal change of $+66 \pm 5\%$ was achieved using a frequency of 900 Hz (Fig. 8d).

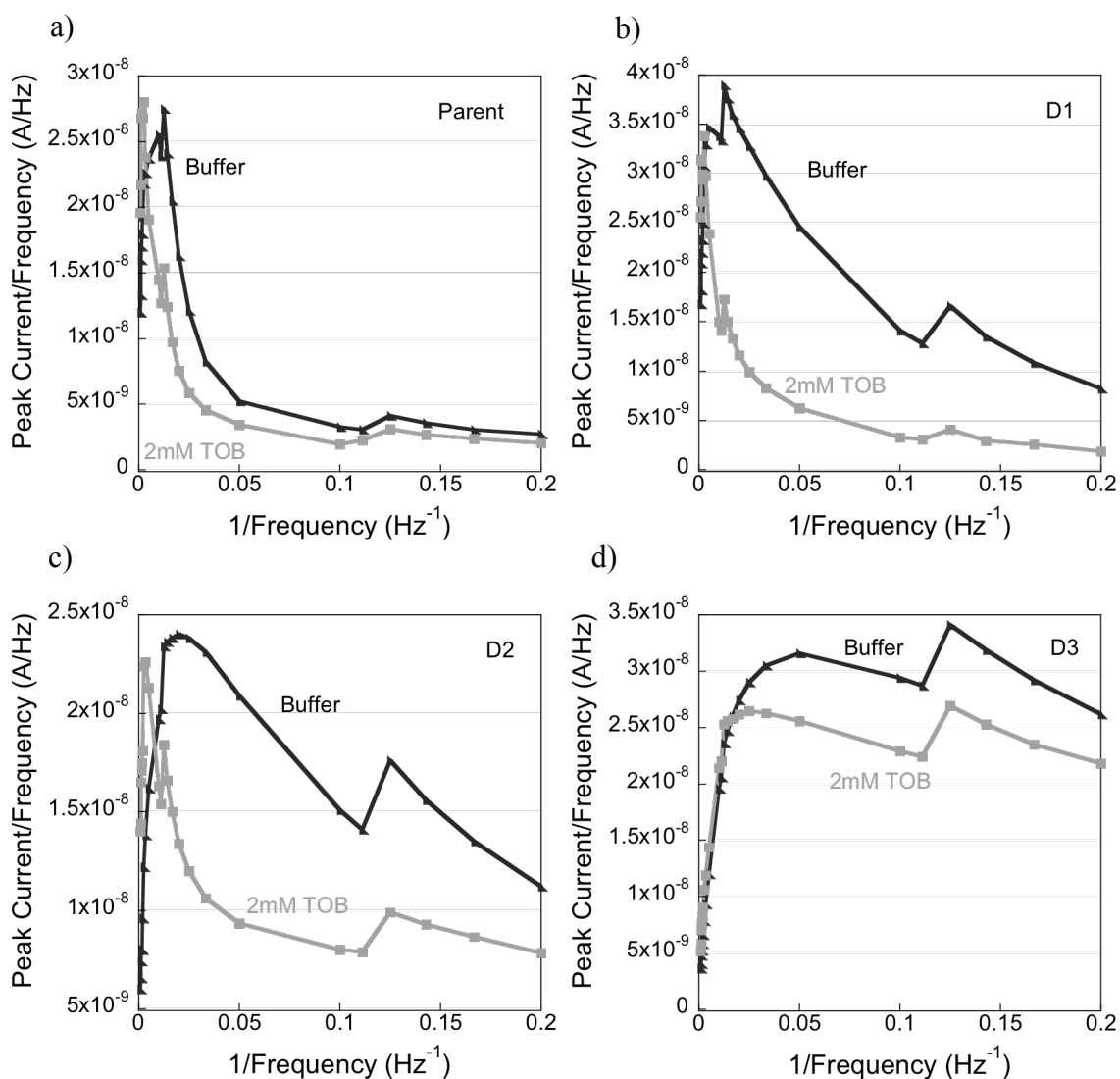


Figure 7. Comparing net peak current normalized by frequency as a function of 1/frequency provided information about the apparent rate of the surface reaction.^{45,99,100} While quantitative conclusions cannot be made about the rates, as that would require knowing the rate limiting step is the electron transfer,^{97,98} the differences can be exploited to optimize sensor signaling. In all aptamer sensors tested here, including the parent sequence, the apparent rate was faster when tobramycin target is present as indicated in the shift in maximum signal. These differences in rate enable polarity switching of the sensor signaling.

Finally, using the newly discovered optimal interrogation frequency of 900 Hz, the aminoglycoside sensor exhibited enhanced sensitivity and observed binding affinity. At 900 Hz, the sensors exhibited a $16 \pm 3 \mu\text{M}$ binding affinity in contrast to the $42 \pm 2 \mu\text{M}$ observed using 60 Hz. A $\sim 20\%$ increase in absolute percent signal change was

observed at saturating tobramycin concentrations (Fig. 8d). Unfortunately, even with the improved analytical performance of the aptamer sensor using 900 Hz as the interrogation frequency, the performance of the sensor at therapeutic tobramycin concentrations (4–10 $\mu\text{g}/\text{mL}$ or 7–18 μM) was poor as described in more detail below.¹⁰¹ Thus, other strategies were explored for improving signaling.

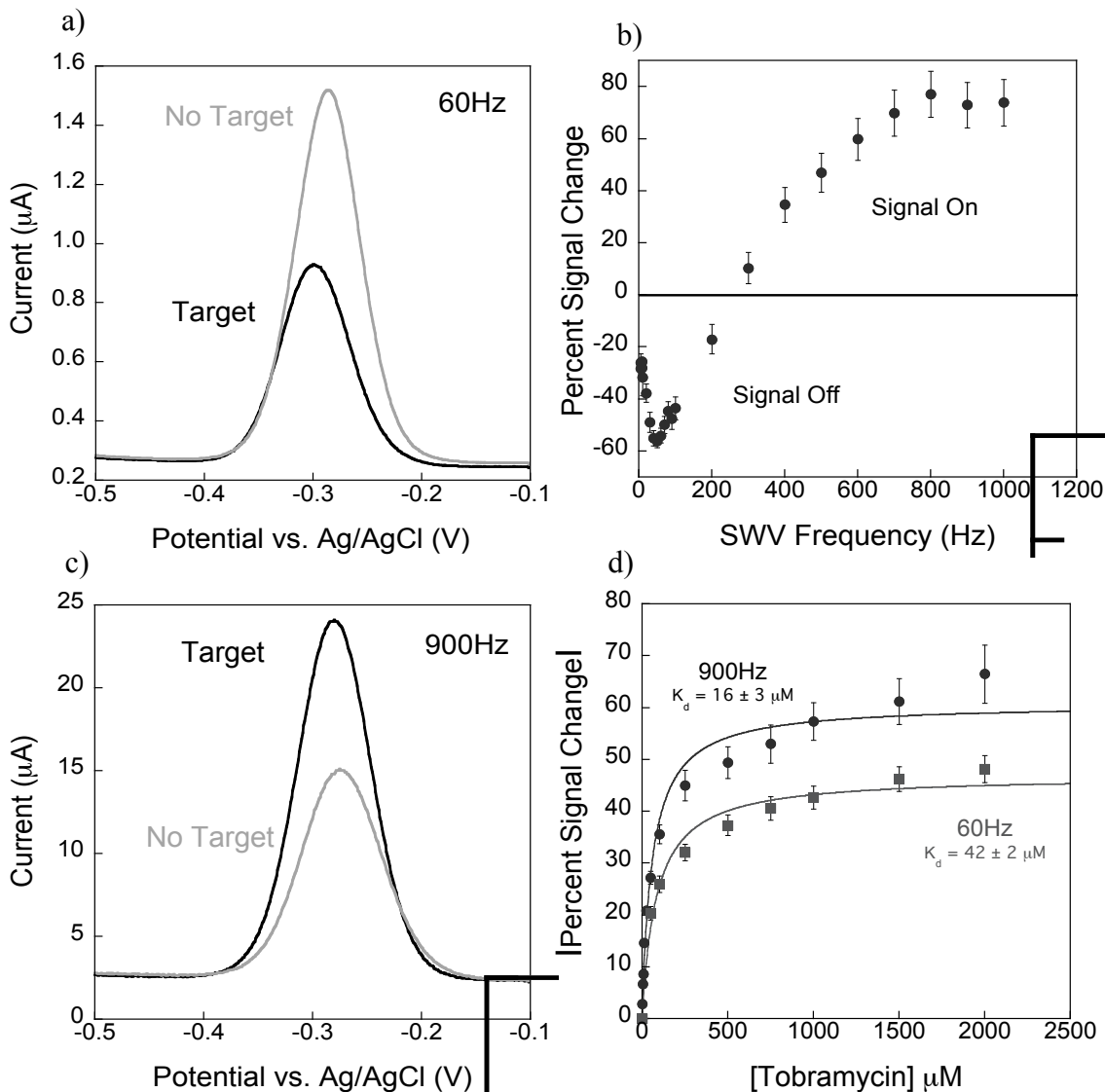
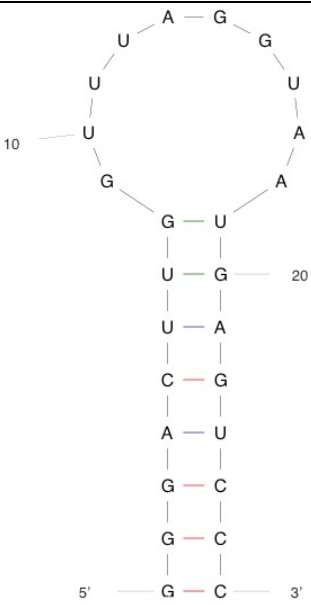


Figure 8. Using different square voltammetric interrogation frequencies enhanced signal polarity, sensitivity, and affinity of the aminoglycoside sensor. Using a square wave interrogation frequency of 60 Hz (a) yielded an aminoglycoside sensor that behaved as a signal-off sensor compared to a (c) signal-on sensor when using 900 Hz. (b) The magnitude of signal and polarity changes upon addition of 2 mM tobramycin as a

function of squarewave frequency exhibiting optimal signal on performance at 900 Hz. As a consequence of the increased signal change, (d) the observed binding affinity improved from $42 \pm 2 \mu\text{M}$ to $16 \pm 3 \mu\text{M}$, when evaluating binding curves generated using 60 Hz compared to 900 Hz.

Engineering Modified Aptamer Sequences for Improved Detection

A set of modified aptamer sequences was designed with the goal of generating larger signal changes in the presence of target analyte. Using the solved NMR structure of the RNA aptamer-target complex,⁹² and MFOLD secondary structure predictions,^{47,48} three new aptamer sequences were rationally designed. These aptamers were developed with the hypothesis that the aptamers would undergo a larger conformation change upon target binding, and consequently enable more sensitive detection.

Sequence	MFOLD Predicted Structure	MFOLD Predicted ΔG at 25°C (kcal/mol)
Parent Aptamer		-11.67

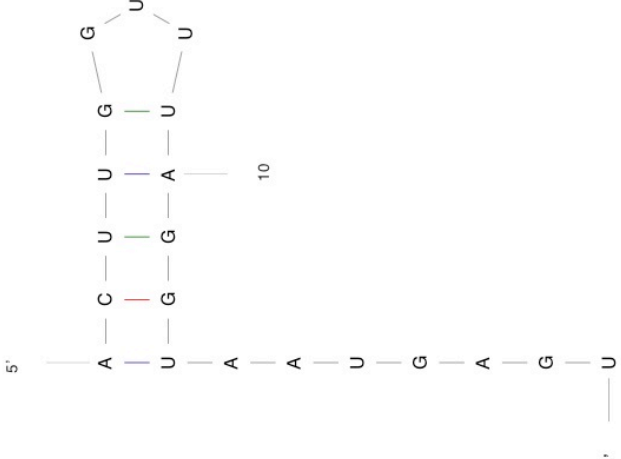
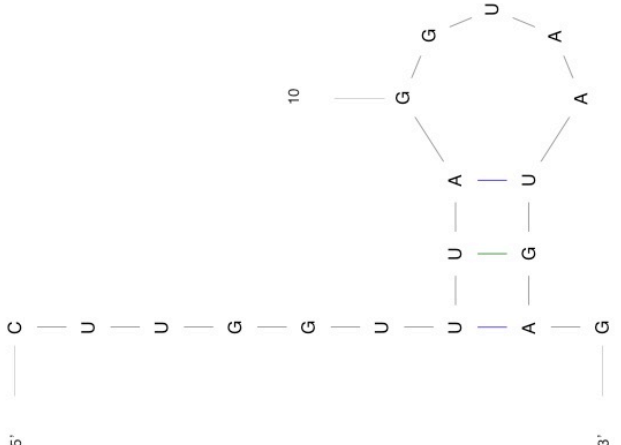
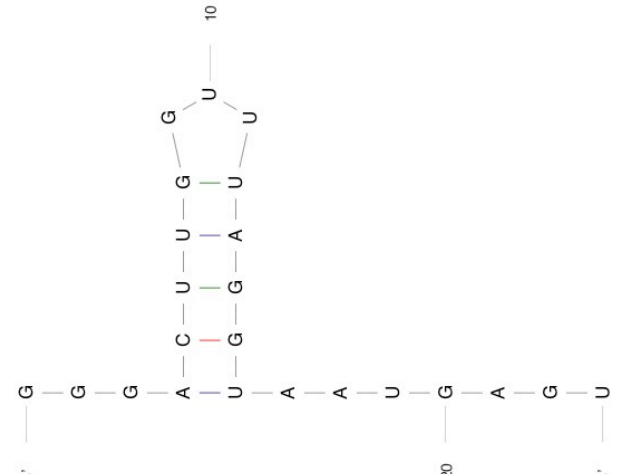
D1		-3.22
D2		-0.66
D3		-3.58

Figure 9. Lowest energy secondary structure predictions of the aptamer sequences employed in this study. Predictions were made using MFOLD at 25°C and 1 M Na⁺.

To rationally design modified aptamer sequences, two criteria that must be met with each new mutant sequence were established. First, bases participating in binding with tobramycin were conserved. To conserve bases, the 3D NMR structure was utilized to visualize which bases are involved in binding⁹². Upon analysis of the structure, 15 polar contacts exist (potential hydrogen bonding sites) between tobramycin and 10 nucleotides in the aptamer sequence were found. Of these 15 contacts, 7 appeared to be between a base and tobramycin, while 8 are between tobramycin and the RNA backbone. As such, the following bases were conserved in the binding pocket: 5'-UGGUUUAGGUAUG-3'. The second criterion was that the modified sequence should exhibit minimal secondary structure as predicted by MFOLD software.^{47,48} Secondary structure predictions using MFOLD for the parent aptamer sequence suggested that the lowest energy structure is a stem-loop anchored with 8 base pairs, including 3 guanine-cytosine (G-C) base pairs at the base (Fig. 9). The solution-phase structure indicates that 5 of these base pairs exist when bound to tobramycin. Of note, 3 of the G-C base pairs are not shown in the NMR structure,⁹² thus they do not appear to participate in target binding. The evidence suggests that the aptamer structure, even in the absence of target, will be folded into a stem-loop structure. As such, target binding will only cause a small change in the aptamer structure. Given these observations, destabilization of this stem should disrupt the secondary structure of the sensing aptamer, allowing it to undergo a larger conformation change upon target binding. The large change in conformation will produce a larger percent signal change in the presence of target. Therefore, three modified sequences were designed (shown in Table 1). First, a sequence was designed in which the three G-C base pairs were deleted (probe D1).^{47,48} Other deletions were

attempted in order to achieve destabilization of the parent aptamer, including deletion of the 5'-terminal bases GGGGA and 3'-terminal bases UCCC (probe D2) and the deletion of the three C residues at the 3'-terminus (probe D3). All mutant sequences were evaluated using MFOLD to determine the predicted secondary structure and free energy. All probes were predicted to possess more positive free energies for folding and thus minimal secondary as compared to the parent sequence (Fig. 9).

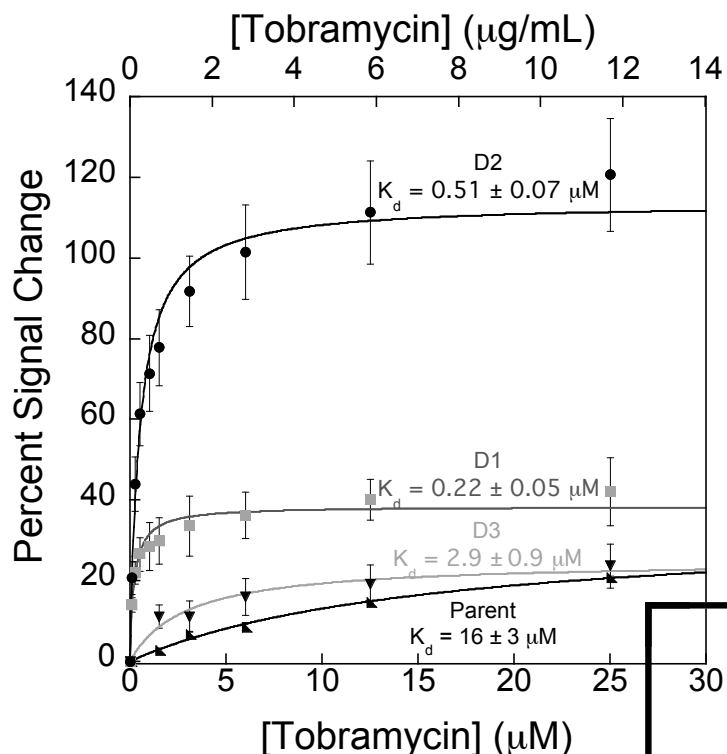


Figure 10. Newly engineered sequences provided dramatically improved sensitivity and binding affinity for the aminoglycoside tobramycin. While the parent aptamer- and D3-based sensors only exhibited ~20 % signal change at 25 μM tobramycin, D1- and D2-based sensors exhibited ~90 % and ~120 % signal changes, respectively. In addition, the newly designed sensors exhibited better binding affinities as denoted by the dissociation constants. Sensors using D3, D1, and D2 exhibited K_d values of $2.9 \pm 0.9 \mu\text{M}$, $0.22 \pm 0.05 \mu\text{M}$, and $0.51 \pm 0.07 \mu\text{M}$ respectively, representing improvements over the of $16 \pm 3 \mu\text{M}$ K_d of sensors using the parent aptamer.

The modified aptamer sequences exhibited enhanced detection abilities compared to sensors built with the parent aptamer sequence (Fig. 10). All sensors were

characterized for optimal squarewave frequency, yielding an optimal, signal-on frequency of 900 Hz (Fig. 11). The optimal frequency for each aptamer sensor depends on the individual aptamer and the sensor must be tested at various frequencies to determine which gives the largest difference in signal between the target-unbound and – bound state. As such, sensors fabricated with the D2 probe and tested at 900 Hz exhibited an observed binding affinity (K_D) of 510 ± 7 nM and a maximum signal change of $120 \pm 14\%$ at $25 \mu\text{M}$ tobramycin. The change represents a 30-fold improvement in binding affinity and a 2-fold increase in percent signal change (Fig. 10). Furthermore, the improved binding affinity is approaching the 12 ± 5 nM intrinsic affinity reported for the solution-phase aptamer.⁵⁴ Sensors fabricated with D1 and D3 also exhibited improved binding affinities and improved or similar signal changes compared to the parent aptamer. Sensors based on D1 and D3 exhibited affinities of 220 ± 5 nM and $2.9 \pm 0.9 \mu\text{M}$, respectively, and percent signal changes of $42 \pm 8\%$ and $23 \pm 5.4\%$ at $25 \mu\text{M}$ tobramycin, respectively. Finally, with improved sensitivities and affinities, the newly modified aptamer sequences exhibited improved detection abilities of tobramycin concentrations. Using the slope of the linear portion of the response curves, sensors fabricated with D2 were found to be the most sensitive in the range of $\sim 0.02\text{--}0.5 \mu\text{M}$ with a slope of $\sim 136\%$ signal change/ μM tobramycin. Linear ranges were calculated using the limit of detection and upper limit as determined by the maximum concentration that could be measured before deviation from linearity.¹⁰² The sensors fabricated with probes D1, D3, and the parent aptamer had slopes of 95, 0.5, and 1.3, respectively (Table 2).

Table 2. E-AB Sensor Analytical Performance

Sequence Name	K_d (μM)	Linear Range (μM)	Sensitivity*
Parent Aptamer	16 ± 3	2.6-12.5	1.3
Probe D1	0.22 ± 0.05	0.01-0.25	95.3
Probe D2	0.51 ± 0.07	0.02-0.5	135.9
Probe D3	2.9 ± 0.9	12-25	0.52

*Sensitivity is reported as the slope of the response curve in the linear range (% signal change/ μM tobramycin)

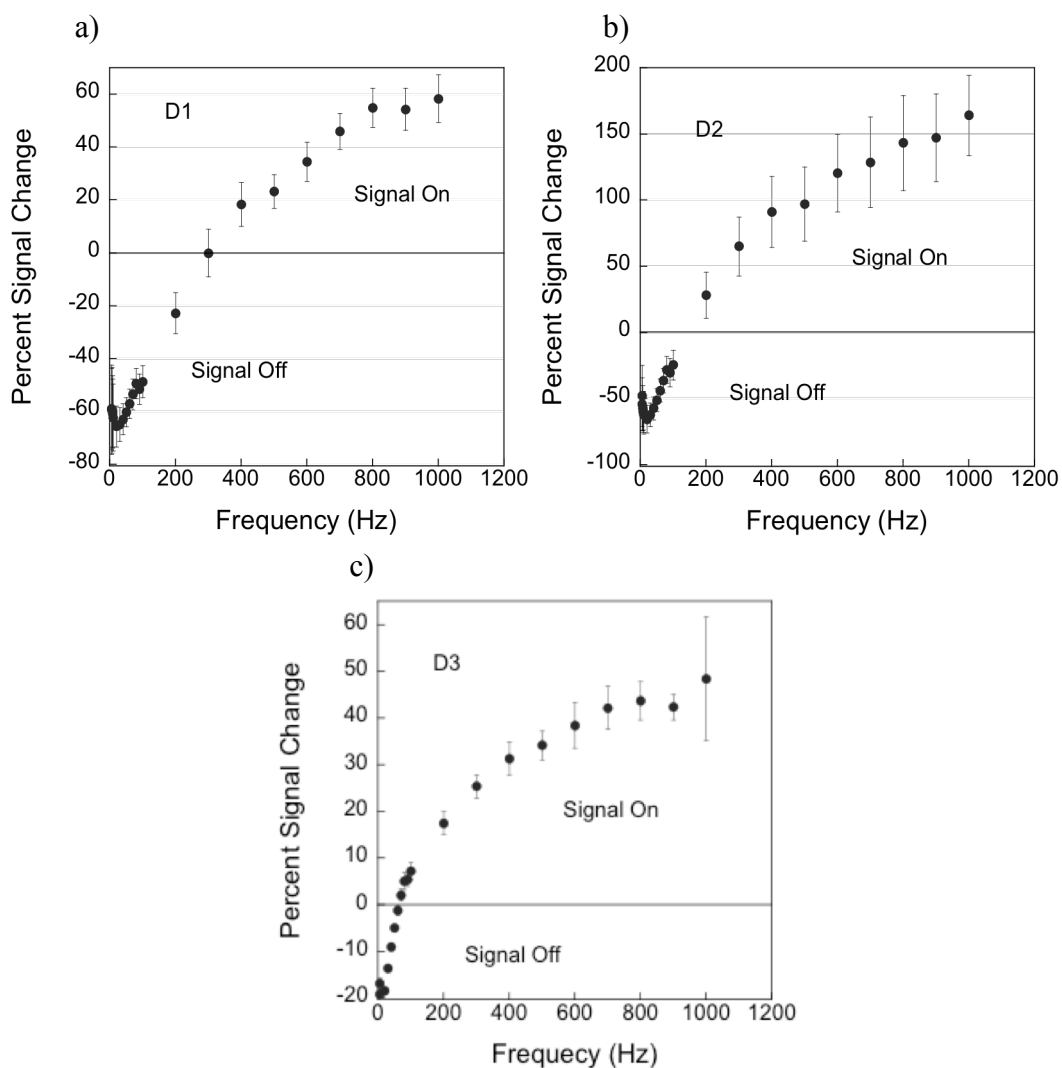


Figure 11. Percent signal change as a function of squarewave interrogation frequency for sensors fabricated with D1 (a), D2 (b), and D3 (c). The percent difference was calculated based on the buffer runs and upon addition of 2mM tobramycin. The polarity of the signaling can be observed on each graph. All of the scans indicated that the best signaling occurs at about 900 Hz in all cases, which was the chosen frequency.

Aminoglycoside Sensors Are Specific

E-AB sensors fabricated with all four sequences specifically bind to aminoglycoside targets. To test specificity, each sensor architecture was challenged in a buffer solution containing excess amounts of glucosamine (Fig. 12, 13). Glucosamine was selected because it is positively charged and has a sugar moiety similar to the target molecule, tobramycin (Fig. 12). It should be noted, this aptamer sequence will bind other aminoglycoside antibiotics, including kanamycin and gentamycin.⁷ To challenge the specificity, the sensors were tested against 10-fold excess of glucosamine (2.5 mM), no appreciable signal change was observed in comparison to signal changes observed for each sequence tested with tobramycin. A small, but noticeable, decrease in signal was observed with the addition of glucosamine. The origin of the decrease in signal negligible, but reproducible, observation is unknown at this time.

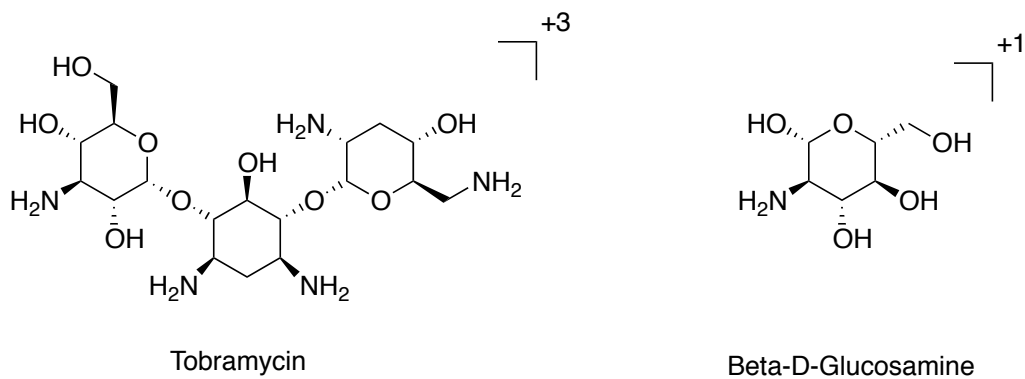


Figure 12: Molecular structure of the target molecule, tobramycin, and the molecule utilized to test the specificity of the sensors, glucosamine. Glucosamine is similar in structure to tobramycin with a similar charge.

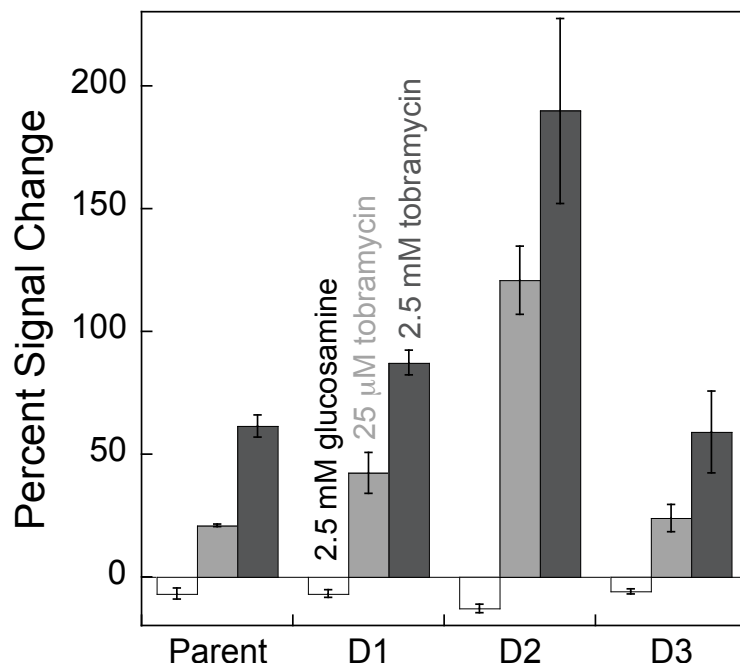


Figure 13. Aptamer sensors responded specifically to the aminoglycoside target. When challenged with 2.5 mM glucosamine, sensors utilizing all four aptamer sequences tested displayed negligible changes in signal, as compared to signal changes observed with 25 μ M and 1.5 mM tobramycin.

Detecting Tobramycin in Serum

Finally, using the optimal sequence, probe D2, we demonstrated that the E-AB sensor detected target in filtered serum. E-AB sensors utilizing RNA aptamers are typically unstable in unfiltered, unadulterated serum. However, several studies demonstrate that this type of sensor functions when challenged in serum that is filtered with a 3000 molecular weight cutoff without additional pretreatments.^{7,10,16} After \sim 1 h equilibration time in filtered serum, the sensors were challenged with increasing concentrations of tobramycin. The sensor exhibited a reduced observed binding affinity ($148 \pm 4 \mu\text{M}$) when compared to buffer, with a similar maximum signal change of $139 \pm 24\%$ signal at saturating tobramycin. (Fig. 14a). Ferapontova and Gothelf reported similar decreases in sensor performance upon testing RNA-based sensors for theophylline in

filtered serum.²⁹ While the binding affinity was reduced in serum, the sensor was able to quantitatively signal the presence of tobramycin within the therapeutic window (Fig. 14b).

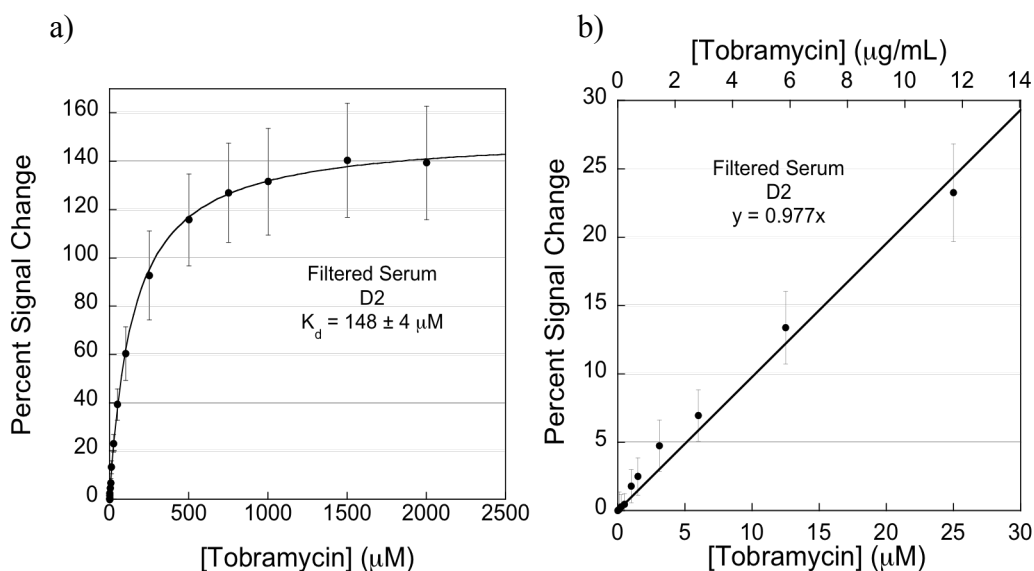


Figure 14. Newly designed E-AB sensors for tobramycin are selective. (a) Specifically, sensors utilizing the D2 sequence respond specifically to tobramycin in filtered serum, albeit with a lower binding affinity and sensitivity as compared to sensor performance in buffer ($K_d = 148 \pm 4 \mu\text{M}$). (b) Nonetheless, the sensor using D2 is still able to perform sensitive detection in the therapeutic concentration window of tobramycin.

Conclusions

Here, several strategies were demonstrated for improving the analytical figures of merit of an electrochemical, aptamer-based sensor capable of detecting the aminoglycoside antibiotic, tobramycin, at physiologically relevant concentrations. Exploiting binding-induced changes in probe aptamer flexibility and conformation by choosing the optimal squarewave frequency to employ when measuring E-AB sensor signaling of the aminoglycoside sensor optimized sensor performance. In addition, several new mutant aptamer constructs were constructed in an attempt to develop

sequences that would undergo a larger conformation change and, thus, create a larger signal change. Aptamers that are hypothesized to undergo a larger conformation change do indeed result in sensors with improved sensitivities and overall performance. Using these optimization parameters, a new E-AB sensor for tobramycin was designed, which employs a modified aptamer sequence (D2) and an optimal interrogation frequency of 900 Hz to detect tobramycin, with improved sensitivity without compromising sensor specificity and selectivity.

The set of parameters employed to improve the performance of electrochemical, aptamer-based sensors utilizing structure-switching aptamers should be applicable to improving the performance of sensors employing any aptamer. Optimization of the magnitude and polarity of signal changes via the use of different squarewave frequencies has been shown to be a general methodology,⁴⁹ and here it was shown that significant improvements in the observed binding affinity of the sensor is achieved. In addition, the solution-phase NMR structure of the parent aptamer binding target molecule assisted in aptamer sequence design, as well as the secondary structure predictions. The 3D structure only provided a guideline for identifying which bases needed to be conserved. As such, these simple sensor optimization guidelines represent a straightforward method for optimizing the analytical performance of E-AB sensors.

Chapter 3: Rationally Designing Aptamer Sequences with Reduced Affinity for Controlled Sensor Performance

Introduction

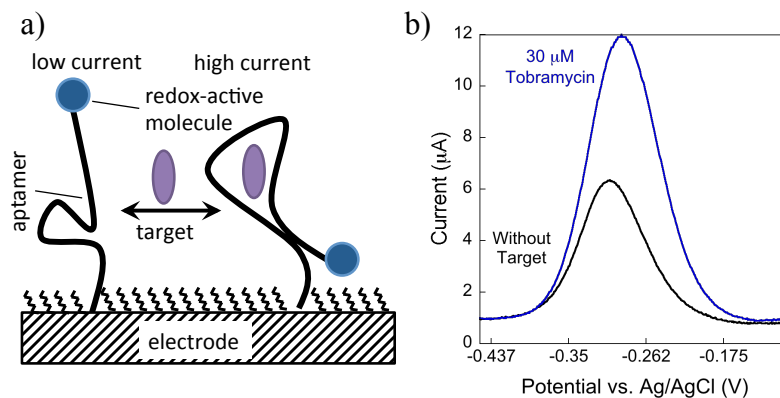
Bioaffinity electrochemical sensors typically rely on the coupling of an affinity agent (protein, enzyme, nucleic acid) to an electrode surface.^{103–106} Specific target recognition between the electrode-immobilized affinity agent is transduced into an electrochemical readout that is correlated to the concentration of analyte. The analytical performance (e.g., limit of detection, dynamic range, sensitivity, response time) of electrochemical biosensors is a topic of intense research when considering the real-world applications of the sensing device.^{7,13,28} While methods such as introducing catalytic signal amplification,¹⁰⁷ nanostructured electrode surfaces,⁵ and changing/altering the electrode material^{108,109} can be used to improve the performance of electrochemical biosensors, ultimately sensor performance is dictated by the nature and strength of the interaction between the bioaffinity agent and substrate. The interaction is intrinsic to the affinity-agent:substrate pair. Examples demonstrating site-directed mutagenesis of enzymes or various allosteric or binding site modifications^{110–114} that improve sensor performance, however, it is often difficult to mutate proteins in a way that rationally tunes sensor performance.

Biosensors that employ nucleic acids as the affinity agent have emerged as a powerful class of electrochemical biosensors as a result of the predictable control over nucleic acid architectures.^{13,28,115,116} A key example of nucleic acid, bioaffinity electrochemical biosensors is the electrochemical aptamer-based (E-AB) sensor

platform^{4,9,25,37} that utilize in vitro-selected DNA or RNA sequences^{9,10,16,24,29} as recognition elements. Target binding induces a conformation change in the electrode bound aptamer, which is coupled to an electrochemical readout mechanism (Scheme 1). Several reports describe in detail the mechanisms behind signaling in this class of sensor.^{28,45,49,50} As mentioned above, sensor performance is usually linked to the intrinsic binding interaction (affinity) between the aptamer (bioaffinity agent) and the analyte. However, due to the folding-based mechanism and the predictability of nucleic acid secondary structure, sequences can be altered to modify the nature of the binding interaction between the aptamer and target. In addition, the potential applied to the electrode surface to reduce/oxidize the signaling molecule (methylene blue or ferrocene)¹¹⁷ and the charge and length of the passivating monolayer can also affect the apparent affinity of the aptamer:target complex¹¹⁸ when employed in an electrochemical sensor. Alternatively, mutations to an aptamer sequence have been demonstrated to be an effective method for tuning the sensor performance of several E-AB sensors.^{28,49,50} Specifically, aptamer sequences designed to undergo a larger conformation changes result in an electrochemical sensor with improved signaling abilities in terms of sensitivity, limit of detection, and affinity.^{28,49,50} It has been demonstrated that altering the stability of a DNA probe sequence by modifying nucleotides outside the binding site alters the binding affinity of the respective sensor to its complementary DNA strand as described by a three-state binding model.^{115,116}

In this work, two different strategies were utilized to reduce the binding affinity of an RNA-based aminoglycoside sensor to shift the dynamic range and sensitivity towards the therapeutic window for the antibiotic tobramycin. Specifically, the predictable

secondary structure as well as the solved NMR structure⁹² were used to alter the described high-gain parent sequence²⁸ to create new aptamer sequences for use in electrochemical sensors that perform within the therapeutic window of tobramycin (7–18 μM)¹⁰¹. The overarching goal of the work described here was to develop new sequences that indeed exhibit a reduced affinity while maintaining the high sensitivity ($\Delta\text{signal}/\Delta[\text{tobramycin}]$) achieved from the high-gain sequence. The high-signal gain of the sequence is afforded by the magnitude of the target-induced conformation change.²⁸ Using secondary structure predictions, several new aptamer sequences were engineered with mutated binding sites as well as aptamer sequences with stabilized target-free states in attempts to reduce the intrinsic interaction between the aptamer-target pair. The motivation for this work was two-fold. (1) The strength of aptamer-target interactions is a product of the selection protocol, thus they are often not ideal for sensing purposes. In this case, the affinity of the tobramycin sensor is too high (nM), thus precluding measurements in the low micromolar therapeutic window for the drug; (2) While it is typical to report on modifications to increase the binding affinity and lower the limit of detection,^{7,28,49,50} on a fundamental level, general guidelines for sequence alterations that can produce reduced affinity sensors are provided.



Scheme 1. (a) E-AB sensors utilize structure-switching aptamer. The change in conformation results in changes in the electron transfer efficiency between a 3'-distal-end-appended redox-active molecule, which is readily measured voltammetrically using SWV (b). Signal is quantified using voltammetric peak current.

Experimental

Materials

Sodium chloride, Trizma[®] base (2-amino-2-(hydroxymethyl)-1,3-propanediol), and magnesium chloride (Sigma Aldrich, St. Louis, MO, USA) were all used as received. 6-mercapto-1-hexanol (99%) and tris-2-carboxyethyl-phosphine (TCEP) were also used as received (Sigma Aldrich). The buffer solutions were prepared using autoclaved, ultrapure water (Mili-Q Ultrapure Water Purification, Millipore, Billerica, MA, USA). The RNA sequences (Table 3) were synthesized and purified via dual HPLC (Biosearch Technologies, Inc., Novato, CA, USA). The oligonucleotides were modified at the 5'-terminus with a 6-carbon thiol to immobilize the aptamer on a gold electrode and at the 3'-terminus with a redox active methylene blue (MB) via a 7-carbon linker. The aptamer probe solutions were all aliquoted at a stock concentration of 0.2 μM in an autoclaved 0.01 M Tris-EDTA solution buffered at pH 8.0 (Sigma Aldrich) and stored at -20°C until used.

Table 3. Mutated Aminoglycoside Aptamer Sequences

Sequence Name	Sequence
High-Gain Parent	5'-HSC ₆ H ₁₂ -CUUGGUUUAGGAAAUGAG-MB-3'
7UG	5'-HSC ₆ H ₁₂ -CUUGGUGUAGGAAAUGAG-MB-3'
7UC	5'-HSC ₆ H ₁₂ -CUUGGUCUAGGAAAUGAG-MB-3'
16GU	5'-HSC ₆ H ₁₂ -CUUGGUUUAGGAAAUUAG-MB-3'
3-UAC	5'-HSC ₆ H ₁₂ -CUUGGUUUAGGAAAUGAGUAC-MB-3'

*The High-Gain Parent sequence displayed here is the same sequence as D2 in Chapter 2. The remaining sequences all differ from the previous Chapters.

Electrochemical Aptamer-Based (E-AB) Sensor Fabrication

The E-AB sensors were fabricated on 2 mm-diameter polycrystalline gold electrodes (CH Instruments, Austin, TX, USA). Sensors were fabricated as previously described.⁷ In short, the electrodes were hand polished circularly on microcloth in a 1 μ m diamond suspension followed by polishing in an alumina oxide water mixture (Buehler, Lake Bluff, IL, USA). The electrodes were then sonicated in water for 5 min. Afterwards, the electrodes were electrochemically cleaned via various voltammetric scans in dilute sodium hydroxide and sulfuric acid solutions as described previously.² Following the electrochemical cleaning, the electrodes were incubated in 200 nM RNA probe solution in autoclaved 20 mM Tris buffer, with 100 mM sodium chloride and 5 mM magnesium chloride, at pH 7.4 for 1 h. Before the immobilization of the RNA probes, the RNA was reacted with 4 μ L of either 10 mM or 50 mM TCEP for 1 h in order to reduce the 5'-disulfide bond, which was the result of the oligonucleotide synthesis. After the RNA immobilization, the sensors were dipped into an autoclaved Tris buffer solution to remove any nonspecifically absorbed RNA. The sensors were incubated in a 3 mM solution of 6-mercapto-1-hexanol in autoclaved Tris buffer for 1 h. The sensors were dipped into autoclaved Tris buffer solution to remove excess 6-mercapto-1-hexanol and

stored in 3 mL of autoclaved Tris buffer for 1 h prior to use.

Electrochemical Measurements

The electrochemical measurements were performed with a 620D Electrochemical Work Station (CH Instruments, Austin, TX, USA). All measurements were performed in a three-electrode cell using an Ag/AgCl (3 M NaCl) reference and platinum counter electrode. The square wave voltammetry (SWV) parameters were as follows: frequency was 900 Hz, a step width of 1 mV, and a pulse amplitude of 25 mV. The measurements were completed in a glass cell with 3 mL of Tris buffer. To generate calibration titrations, sensors were challenged with varying amounts of tobramycin and interrogated utilizing SWV. Upon target addition the aptamer undergoes a conformation change altering the electron transfer efficiency between the methylene blue and the electrode surface, which is observed as a change in peak current intensity (Fig. 15). Quantitation of a target concentration was based on the signal change observed (change in peak current) in the presence of target ($S_{[T]}$) with respect to baseline signal (or signal without target— $S_{[T]_0}$ — Fig. 15). The percent signal change (%SC) was calculated by normalizing to the peak current without target via the following equation:

$$\%SC = \frac{S_{[T]} - S_{[T]_0}}{S_{[T]_0}} \times 100 \quad (\text{eq. 4})$$

The concentration of target, tobramycin, versus percent signal changes were plotted to create calibration curves.

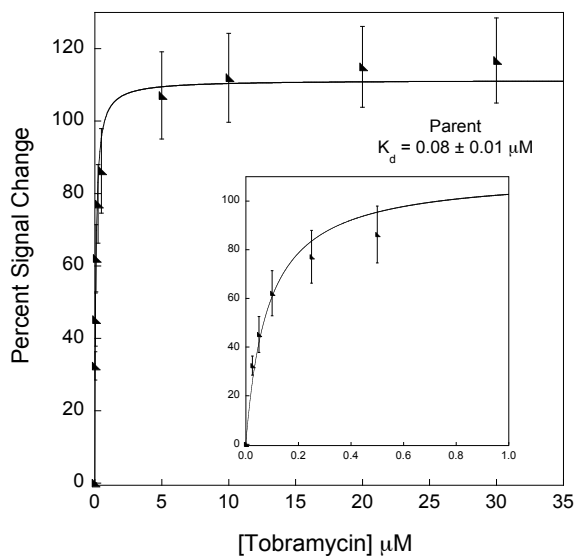


Figure 15. E-AB sensors for tobramycin fabricated with the high-gain parent sequence exhibited a dissociation constant of $0.08 \pm 0.01 \mu\text{M}$ and a $117 \pm 12\%$ signal change at saturating levels of tobramycin ($> \sim 5 \mu\text{M}$). While these sensors are sensitive, they saturate at concentrations much lower than the lowest anticipated concentration in the therapeutic window for the drug ($\sim 7\text{-}18 \mu\text{M}$)¹⁰¹. The inset illustrates the signal change at concentrations $\leq 1 \mu\text{M}$. All data shown is the percent signal change (explained in Experimental Measurements) plotted versus the concentration of target, tobramycin.

Results and Discussion

As a basis for sensor development, an 18-nucleotide mutated high-gain aptamer sequence (high-gain parent—Table 3) that specifically binds to aminoglycoside antibiotics was employed.²⁸ The high-gain modified sequence, adapted from the original aptamer sequence reported by Wang and Rando,⁵⁴ exhibited increased sensitivity and binding affinity when employed in electrochemical, aptamer-based (E-AB) sensors.^{28,54} The high signal gain is afforded by the large conformation change of the aptamer structure from the target-free to the target-bound state. Unfortunately, sensors using the high-gain parent aptamer exhibit a high affinity for tobramycin, such that the sensor saturates well before the therapeutic levels of the antibiotic tobramycin are needed in the 7–18 μM range¹⁰¹. The 18-nucleotide sequence exhibits a dissociation constant of 80 ± 10

nM and saturates at a tobramycin concentration of $\sim 5 \mu\text{M}$, precluding sensitive measurements in the therapeutic window (Fig. 15). Two strategies were explored to reduce the observed binding affinity of E-AB sensors while maintaining the magnitude of the signal change and thus sensitivity. While the motivation here was to shift sensor performance into the therapeutic window, the strategies outlined below should represent a general approach to reducing the observed binding affinity of E-AB sensors. Of note, in this report, “observed binding affinity” and “binding affinity” are used interchangeably; both terms refer to the binding affinity displayed by the fabricated sensors. The binding affinity is not to be confused with the intrinsic binding affinity, which is the affinity of the original RNA aptamer to tobramycin ($\sim 12 \text{ nM}$) in solution.⁵⁴

Two strategies are employed to engineer aptamers capable of supporting E-AB signaling with reduced affinity towards tobramycin. The first strategy was to mutate a nucleotide involved in binding interactions with tobramycin to reduce binding affinity while minimally perturbing the predicted secondary structure of the parent aptamer. Hypothetically, maintaining similar secondary structure to the high-gain parent sequence would ensure that the magnitude of the conformation change would be similar. The second approach was to modify the aptamer sequence in order to stabilize an alternatively-folded structure or target-free state, such that target binding would have to overcome a larger energy barrier to force the aptamer to the target-bound state. Altering aptamer sequences is similar to the three-state equilibrium model reported by Kang *et al.*^{115,116} in the development of electrochemical DNA hybridization sensors. The strategy again was to minimally perturb the predicted secondary structure in order to maintain similar sensor sensitivity.

To characterize the E-AB sensors developed in this manuscript, the sensor calibration curves were fit to a binding model adapted from the Langmuir isotherm.¹¹⁹ The calibration relies on the equilibrium reaction between the aptamer (A) and target (T) and form the aptamer:target complex A:T, where $A + T \leftrightarrow A:T$. The association constant (K_a) and the dissociation constant (K_d) is

$$K_a = \frac{[A:T]}{[A][T]} \text{ and } K_d = \frac{1}{K_a} \quad (5)$$

With the assumption that each non-interacting binding site (aptamer) binds one tobramycin and binding does not appreciably alter the concentration of free target ([T]) in solution. The binding isotherm is given by Equation (6):

$$S = S_{\max} \frac{[T]}{K_D + [T]} \quad (6)$$

where S and S_{\max} are the percent signal change at a given [T] and at saturating target concentration, respectively.

Disrupting the Aptamer–Target Interaction for Reduced Affinity Sensors

To design a mutated binding site aptamer sequence with a reduced affinity towards tobramycin, two design parameters were set to maintain sensitive signaling ability. The goal was to disrupt a polar contact (e.g., hydrogen bond) between the aptamer and tobramycin by mutating one of the nucleotides involved in binding (Figure 16). The first criterion was that the altered nucleotide should only have one polar contact with tobramycin in order to weaken the interaction rather than completely inhibit it. The second criterion was that the secondary structure of the new sequence must be similar to that of the 18-nucleotide parent sequence as predicted by MFOLD^{47,48} (Fig. 15). Similar secondary structures would ensure that, upon target binding, the signal change of the E-AB sensor (and thus sensitivity) would be similar to the original sensors.

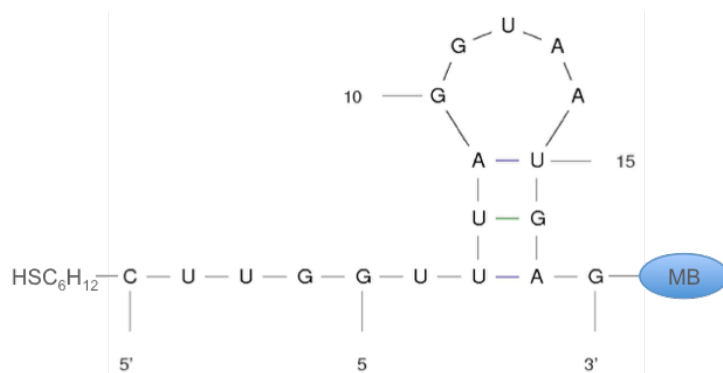


Figure 16. Secondary structure prediction for the parent sequence suggests an internal loop that can potentially keep the redox label (MB – methylene blue) distal from the electrode surface. The introduction of tobramycin forces the aptamer to fold bringing the methylene blue close to the 5'-terminus. The lowest energy secondary structure prediction is calculated using MFOLD^{47,48}. The MFOLD prediction was based on the parent aptamer in a 1 M NaCl solution at 25°C and has a folding energy of -0.66 kcal/mol.

The solved NMR structure of the aptamer-target complex was examined to determine possible polar contacts between the aptamer and tobramycin⁹² (Fig. 17). Upon analysis, 15 hydrogen bonds between 10 different nucleotides in the aptamer sequence and tobramycin were found. Of the 10 nucleotides, only eight have one polar interaction with the target of interest and only six of the nucleotide interactions involve the base (in contrast to interactions with the sugar or phosphate in the backbone). As a result, six possible sites for mutation were identified. The effects of iterative mutations were explored using MFOLD to ensure that the secondary structure of the mutant sequence was similar to that of the parent sequence.²⁸ Modifications to the uracil-7 site (5'-CUUGGUUUAGGUAAGAG-3') to adenine, guanine, or cytosine all exhibited similar structures (Fig. 18) and free energies for folding to the parent high-gain sequence. Two sequences in which the uracil-7 was changed to cytosine or guanine were selected (Fig. 18). The uracil was replaced with cytosine (sequence 7UC) with the prediction that the 4' nitrogen would inhibit the hydrogen bond interaction. Alternatively, the uracil was

replaced with a guanine (sequence 7UG) to sterically hinder the hydrogen bond between the aptamer and tobramycin (all sequences listed in Table 3).

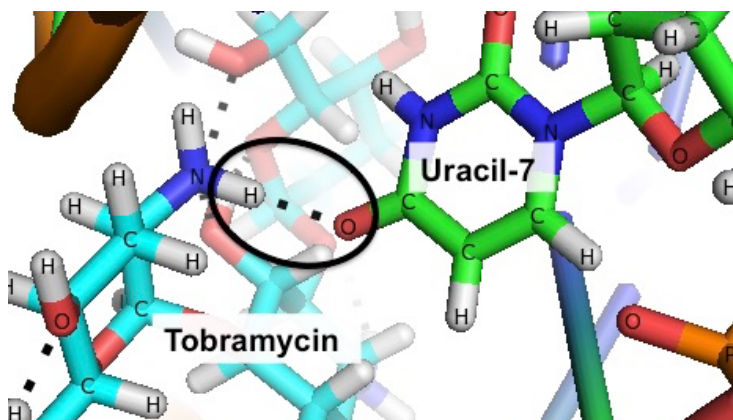


Figure 17. The uracil-7 site is a likely candidate for mutation to disrupt aptamer binding with target, thus reducing sensor affinity. Uracil-7 site was chosen based on the criteria described that it only has one polar contact (dashed lines) with tobramycin as determined via the NMR structure. The figure was generated from the previously reported NMR structure (PDB ID: 2TOB) by Jiang and Patel.⁹²

Sequence Name	Secondary Structure Prediction	Folding Energy (kcal/mol)
7UG		-0.64
7UC		-0.64

16GU		-2.13
3-UAC		-1.60

Figure 18: All of the lowest energy secondary structures for the novel aminoglycoside aptamer sequence. All of the structures were determined by using MFOLD and were done based on the aptamer in a 1 M NaCl solution at 25°C^{47,48}.

Unfortunately, the sensors employing both of the new sequences (7UC and 7UG) did not function as expected (Fig. 19). No appreciable or specific signal changes were observed with sensors fabricated using the 7UC and 7UG sequences. At 30 μM , tobramycin sensors employing 7UG displayed a $-9\% \pm 1\%$ signal change and 7UC exhibited a $3\% \pm 1\%$ percentage signal change. As such, these sensors exhibited no quantitative binding to tobramycin. It is likely that the alterations made to the aptamer sequence rendered the aptamer unable to bind tobramycin.

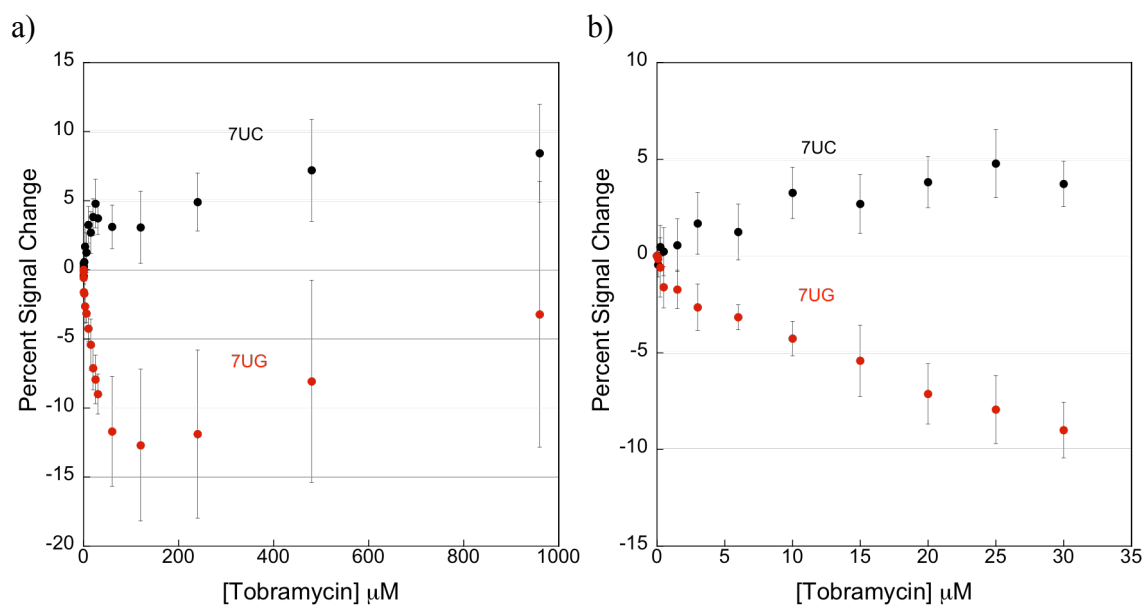


Figure 19. The aptamers with mutated binding sites, 7UG and 7UC, did not produce functioning electrochemical sensors. Unfortunately, both constructs exhibit largely variable signals with changing tobramycin concentrations suggesting that disrupting the interaction of uracil-7 abolished any specific interaction with the target molecule. (b) Illustrates the signal for sensors employing 7UG and 7UC at <35 mM tobramycin. These plots show titrations completed and plotted by utilizing percent signal change and the concentration of target.

Stabilizing an Alternative Fold for Reduced Affinity Sensors

As an alternative approach to design an aminoglycoside aptamer with a reduced binding affinity towards tobramycin, the goal was to stabilize an alternative aptamer fold by stabilizing a stem-loop structure internal to the aptamer sequence. Stabilization of the unbound structure will make it more difficult for the oligonucleotide to bind target and thus lower binding affinity.^{115,116} Stabilization of an oligonucleotide sequence was a technique that has been used before in the development of electrochemical DNA sensors in order to tune the linear range and sensitivity of the resulting sensors.¹¹⁶ Specifically, Kang *et al.* utilized a DNA sequence that forms a stem-loop structure when the oligonucleotide is not bound to its complementary target and altered the stability of the

DNA probe sequence by modifying nucleobases not involved in interacting with the target. The stability was improved by increasing the GC content in the stem, which is in the stem-loop of the unbound DNA probe, to reduce the affinity of the DNA sequence to its complementary target.¹¹⁶

Two approaches to stabilize the target-free aptamer structure as a stem-loop were explored. First, mutations were made at the 3'-end of the aptamer sequence to bases that are not involved in binding with tobramycin such that the 3'-terminus possessed internal complementarity. Alternatively, the sequence was extended at the 3'-end to self-fold into a stem-loop structure (Fig. 20). The secondary structures of the sequences were predicted by MFOLD to ensure that they formed a stem-loop structure where the 5' and 3' ends were distant from one another (Fig. 20) with a more favorable free energy for folding than the parent aptamer. It was necessary to ensure that the mutated aptamer sequences formed a stem-loop with distant 5' and 3' ends so that the probe will be forced to undergo large conformational changes upon target addition.

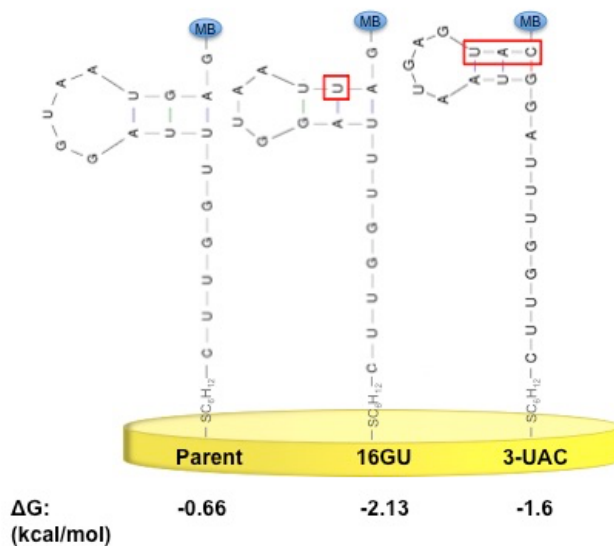


Figure 20. The goal was to alter the aptamer sequences to develop stabilized target-free states while maintaining similar secondary structure to the high-gain parent sequence.

The sequence mutations (highlighted in red boxes) attempted to stabilize the internal loop structure at the 3'-distal end. Free energies of each structure were calculated using MFOLD as described above.

In analyzing the parent aptamer structure, it was determined that there is a hydrogen bond interaction between uracil-8 and guanine-16 (Fig. 17). Mutating guanine-16 to uracil causes an interaction between adenine-9 and uracil-16, which stabilizes a stem-loop from -0.66 kcal/mol for parent, to -2.13 kcal/mol (Fig. 20). The new sequence is named 16GU. Extending the parent sequence with nucleotides UAC at the 3'-end results in predicted interactions between guanine-11 and cytosine-21, uracil-12 and adenine-20, and adenine-13 and uracil-19. The sequence, here named 3-UAC, also stabilizes a stem-loop structure with a free energy of -1.60 kcal/mol (Fig. 20).

The sensors fabricated with the new aptamers, 16GU and 3-UAC, were successful in creating reduced affinity sensors. For example, sensors prepared with the parent aptamer exhibited a dissociation constant of 0.08 ± 0.01 μM (Fig. 15), while sensors fabricated with the 16GU aptamer exhibited a dissociation constant of 3.0 ± 0.4 μM (Fig. 21) and sensors employing 3-UAC displayed a 0.17 ± 0.03 μM dissociation constant (Fig. 21). Consequently, the limits of detection (LOD) for each sensor were also affected. Specifically, the LODs increased as the dissociation constants for the aptamers increased. Sensors employing the parent, 3-UAC, and 16GU aptamers exhibited LODs of 1.99 nM, 14.8 nM, and 114 nM, respectively, calculated as three times the standard deviation of the blank. In addition, the E-AB sensors fabricated with the 16GU aptamer exhibited a maximum percent signal change at 30 μM of $112\% \pm 22\%$, which is comparable to that of the parent sensors ($117\% \pm 12\%$). The 3-UAC sensors, however, only exhibited a maximum percent signal change of $69\% \pm 8\%$, which is smaller than that exhibited by the 16GU sensors and the parent fabricated sensors (Fig. 22). It is still unclear as to why the

3-UAC sequence exhibits lower sensitivity, but is likely due to the difference in the secondary structure with respect to the high-gain and 16GU sequences.

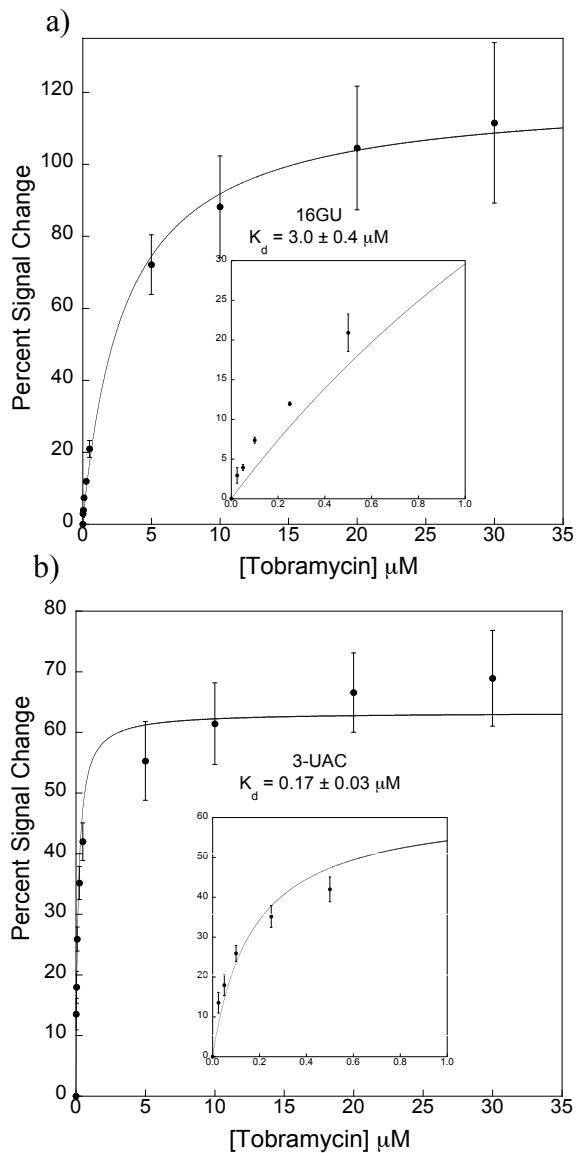


Figure 21. Sensors fabricated with mutated sequences stabilizing the target-free state exhibited reduced affinities (as indicated by the increase in dissociation constants – K_d). (a) For example, the sensors fabricated with the 16GU sequence exhibited a dissociation constant of $3.0 \pm 0.4 \mu\text{M}$ and a $112 \pm 22\%$ signal change at 30 μM tobramycin. (b) Similarly, the sensors fabricated with the 3-UAC sequence exhibited a K_d of $0.17 \pm 0.03 \mu\text{M}$, but with a lower overall signal change of $69 \pm 8\%$ at saturating conditions. In agreement with the predicted stabilities of the target-free structure, the more stable 16GU (-2.13 kcal/mol) exhibited the highest K_d , followed by 3-UAC (-1.6 kcal/mol), both of which are higher than the high-gain parent sequence (-0.66 kcal/mol) with a dissociation constant of 0.08 mM.

The initial goal was to design an aptamer sequence that would support sensing of tobramycin in the therapeutic window. Sensors utilizing the mutant aptamer 16GU provided better sensitivity towards tobramycin in the therapeutic window (Fig. 22). Specifically, 16GU sensors exhibited a $\sim 20\%$ signal change between 7 and 18 μM tobramycin, whereas the high-gain parent and 3-UAC (which both saturate before 7 μM) exhibited essentially no signal change in that window. The binding affinity of the E-AB sensors was successfully reduced and the sensitivity in the therapeutic window of tobramycin was significantly improved.

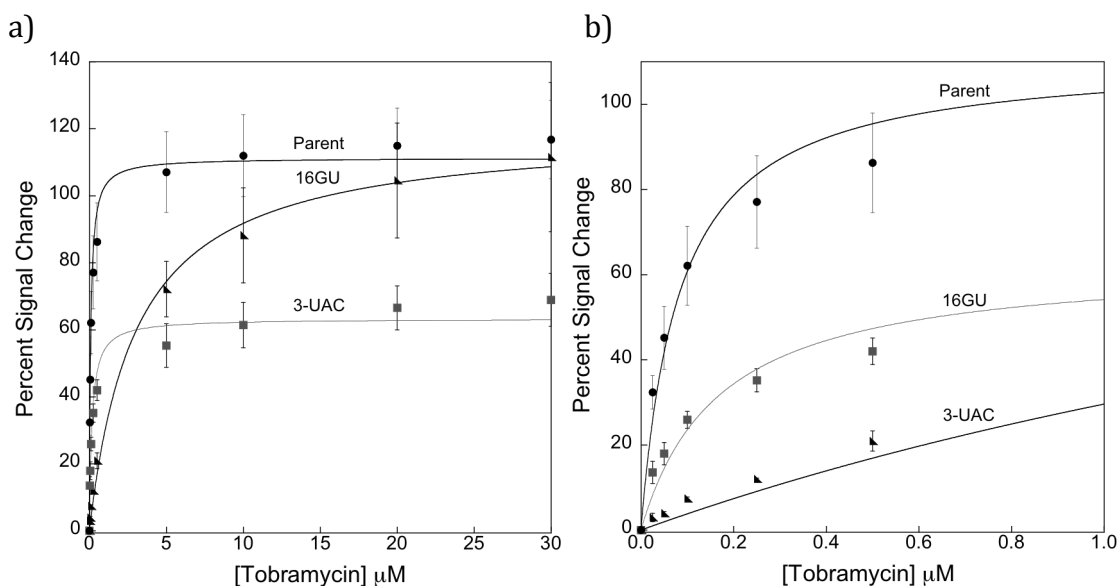


Figure 22: A comparison of the sensor responses when employing the parent, 16GU, and 3-UAC aptamers. (b) The sensor responses in the 0-1 μM window for the parent, 16GU and 3-UAC aptamer sequences in order to show the difference in sensor function.

Conclusions

In this work, an aminoglycoside aptamer sequence was successfully modified to reduce the binding affinity of an electrochemical, aptamer-based sensor. The motivation was to shift the functional region of the sensor to include the therapeutic window for the

aminoglycoside antibiotic tobramycin. Two methods for the rational design of sequences were proposed to achieve this goal. Unfortunately, the first method of altering bases involved in binding tobramycin was unsuccessful. The resulting sensors did not display appreciable signal, suggesting that we had eliminated any specific binding interactions. Alternatively, the secondary structure of the target-free state of the aptamer (i.e., stem-loop) was stabilized. Stabilizing the aptamer into a stabilized target-free state renders the interaction between the aptamer and the target less energetically favorable and thus reducing affinity. Stabilizing the aptamer sequence enabled the development of sensors that displayed better sensitivity in the therapeutic window for tobramycin. Using secondary structure predictions to design new aptamer sequences with alternative folds represents a potential universal method to tune the binding properties of an aptamer to its target. Typically, alterations to a bioaffinity agent are made in order to improve sensitivity and overall sensor performance.^{2,28,49,115,116} Here, a strategy is presented that, while reducing binding affinity, creates sensors that function in a desired concentration window dictated by the real-world application of the sensor—detecting drugs at a therapeutically relevant concentrations. Aptamers are typically selected to bind a target of interest without consideration of what is needed to develop a sensor (e.g., conformation switching). Methods to introduce sensing ability are thus of utility to scientists building biosensors. The strategies outlined in this work should be of relevance to a broad range of sensor development strategies employing aptamers.

Chapter 4: Heterogeneous E-AB Sensor Surfaces for Controlled Sensor Responses

Introduction

The use of nucleic acid aptamers in the development of chemical and biochemical sensors is a rapidly expanding field. While the list of sensing methods coupled with aptamers is long, electrochemical^{1,4,7,13,14,16,18,50,56,61,71,120} and optical methods^{74,85,121} dominate the literature. The specificity of aptamer-based sensors is afforded by the recognition abilities of the nucleic acid aptamer sequence to its binding target, which can range from ions, proteins, cells, and small molecules.^{1,4,10,16,56,62,122} The aptamer–target interaction typically involves a single binding site with a combination of shape complementarity, hydrogen bonding, and hydrophobic–hydrophobic, stacking, and electrostatic interactions.¹²³ The analytical figures of merit of the resulting sensors are a function of the signal transduction methodology, as well as the intrinsic binding abilities, or affinity, of the aptamer–target pair.^{4,28,49} When these aptamers are immobilized on a sensor surface (e.g., a sensing electrode), the resulting sensors exhibit single-site binding isotherms, similar to the Langmuir binding isotherm.^{2,61,71} Fitting data to this binding isotherm enables quantitative characterization and benchmarking of the analytical figures of merit, including the maximum signal, sensitivity, dynamic range, and observed binding affinity.

Electrochemical, aptamer-based (E-AB) sensors utilize surface immobilized aptamers to achieve sensitive, specific, and reusable analyte detection.^{1,4,10,14,16,18,29} The signaling abilities of an E-AB sensor is based on the target-induced conformation change of the electrode-bound aptamer.^{2,4,9,16,56,116} Target binding changes the conformation of

the aptamer and alters the electron transfer efficiency between a covalently altered redox reporter and the electrode surface.²⁸ As mentioned earlier, the sensor response typically follows a Langmuir binding isotherm. Using this sensing method, E-AB sensors have been reported to achieve dynamic ranges encompassing one to three orders of magnitude.^{14,28,124}

Numerous techniques exist to optimize the response and analytical figures of merit of E-AB sensors. Specifically, modifying the packing density of DNA or RNA on an electrode surface by changing the concentration of the nucleic acid probe used to fabricate sensors can affect the observed binding affinities, maximum signal change, and sensitivity.^{14,25,124} These parameters, however, have only modest effects. For example, White *et al.* utilized the cocaine aptamer at specific packing densities and obtained binding affinities ranging from 101 μM to 327.² Other methods have been utilized to tune the sensing abilities of E-AB sensors. For example, optimizing the potential waveforms used to voltammetrically interrogate the sensor surface can control the magnitude and polarity of the signal change upon target addition, as well as the observed binding affinity.^{25,28,49,125} A more radical technique to improve sensor response is to modify aptamer sequences to undergo larger conformation changes upon target binding, resulting in increased signaling with consequential changes in the observed affinity.^{28,50} In all of these examples, the sensing attributes are still limited by the employed aptamer sequence and its binding interactions. For the detection of complementary DNA with structure-switching sensors, Kang *et al.* introduced the concept of heterogeneous sensor surfaces with multiple DNA probes for the same complementary DNA strand, but with different binding affinities.¹¹⁶ They accomplished this goal by designing multiple stem-loop probes

for the same complementary target with stems of various stabilities. They then combined the DNA sequences on the electrode surface at selected ratios to control the dynamic range of the resulting sensors.¹¹⁶ This strategy of altering stem-loop DNA probes for tuned binding affinities is straightforward and has been reported for optical sensors as well.¹¹⁵

Here, for the first time, heterogeneous surfaces with rationally designed aptamer sequences to control the dynamic range and sensitivity of resulting E-AB sensors were designed. Two different representative E-AB sensors were designed employing DNA-based ATP aptamers⁴⁹ and RNA-based aminoglycoside aptamers^{7,28,54} to demonstrate that the technique is general. Using a combination of in-house-designed mutant aptamer sequences with different binding abilities to the same targets, mixed ratio sensor surfaces that exhibit predicted analytical responses were developed. Specifically, control over the dynamic range and sensitivity of the resulting sensors, as well as provide quantitative predictions of this performance are demonstrated. Finally, while control using electrochemical-based detection is confirmed, the aptamer design guidelines we present should be applicable to any type of structure-switching aptamer-based sensing strategy.

Experimental

Materials

Sodium chloride, Trizma base (2-amino-2-(hydroxymethyl)-1,3-propanediol-here called Tris), magnesium chloride, tris-2-carboxyethylphosphine (TCEP), and 6-mercapto-1-hexanol (99%) (Sigma-Aldrich) were used as received. Buffer solutions were prepared using ultrapure water (Mili-Q Ultrapure Water Purification, Milipore, Billerica, MA, USA). Buffer used for RNA-based sensor fabrication was autoclaved prior to use. RNA

and DNA sequences (Tables 4 and 5) were synthesized and purified using dual-HPLC (Biosearch Technologies, Inc., Novato, CA, USA). All of the probes were aliquoted at 0.2 mM in 0.01 M EDTA aqueous solution (autoclaved for the RNA sequences) at pH 8.0 (Sigma-Aldrich) and stored at $-20\text{ }^{\circ}\text{C}$ until use.

Table 4. ATP Aptamer Sequences

Sequence Name	Sequence
Full Length	5'-HSC ₆ H ₁₂ -ACCTGGGGGAGTATTGCGGAGGAAGGTT-MB-3'
Mut	5'-HSC ₆ H ₁₂ -CTGGGGGAGTATTGCGGAGGAAA-MB-3'
Parent	5'-HSC ₆ H ₁₂ -ACCT <u>GGGGGAGTATTGCGGAGGAAGGTTTTTTTCTTC</u> -MB-3'

*Underlined sequence was conserved in the mutant

Table 5. Aminoglycoside Aptamer Sequences

Sequence Name	Sequence
Parent	5'-HSC ₆ H ₁₂ -GGGACUUGGUUUAGGUA AUGAGUCCC-MB-3'
Mut	5'-HSC ₆ H ₁₂ -CUUGGUUUAGGUA AUGAG-MB-3'

*The Parent sequence shown here is the Parent sequence mentioned in Chapter 2 and the Mut sequence is the same as the D2 sequence in Chapter 2 and the High-Gain Parent in Chapter 3.

Fabrication of Electrochemical Aptamer-Based Sensors

All sensors were fabricated on 2 mm diameter polycrystalline gold electrodes (CH Instruments, Austin, TX, USA). Electrode modification was performed as previously described.²⁸ Briefly, the electrodes were hand polished in a circular fashion on microcloth (Buehler) in a 1 μm diamond suspension, and then they were polished in an alumina oxide slurry (Buehler). The electrodes were then rinsed and sonicated for 5 min. Sonication was followed by electrochemical cleaning of the electrodes via a series of voltammetric scans in sodium hydroxide and sulfuric acid solutions as previously described.²⁷ After cleaning the electrode surfaces, each electrode was incubated in a 200 nM probe solution for 1 h diluted in 20 mM Tris buffer with 100 mM sodium chloride and 5 mM magnesium chloride at pH 7.4, which was autoclaved for the RNA probe solutions. For the mixed monolayer sensors the total concentration of aptamer was kept

constant at a total oligonucleotide concentration of 200 nM to allow for constant aptamer packing density. Prior to probe modification, the aptamer was reacted with 4 μ L of 10 mM TCEP for 1 h to reduce the disulfide bond at the 5' end of the aptamer sequence, resulting from probe synthesis. The sensors were then incubated in 3 mM 6-mercapto-1-hexanol solution diluted with Tris buffer for 1 h.

Electrochemical Measurements

Electrochemical measurements were completed utilizing a CH Instruments 660D electrochemical workstation (CH Instruments, Austin, TX, USA). The measurements were performed in a three-electrode cell with an Ag/AgCl (3 M NaCl) reference electrode and a platinum auxiliary electrode. The square wave voltammetry conditions were as follows: pulse amplitude of 25 mV, frequency of 900 Hz for the RNA-based aminoglycoside sensors and 200 Hz for the DNA ATP-based sensors, and a step width of 1 mV.

Results and Discussion

In this work heterogeneous sensor surfaces employing several aptamer mutants, designed to bind the same target with different affinities, were used to tune the analytical response characteristics of the resulting sensor (Fig. 23). Previously reported rational modifications to an existing aptamer sequence can create larger target-induced conformation changes, which significantly enhances the observed binding affinity and sensitivity of the resulting sensor.²⁸ In this work, a new layer of control was added by utilizing multiple aptamers with different affinities for the same target molecule on a sensor surface for better control over the analytical figures of merit. Control over the analytical figures of merit was achieved by varying the ratio of the different aptamers

used during sensing monolayer formation. To demonstrate the generality of this approach, tunable sensors for two representative targets was successfully developed employing aptamer sequences for tobramycin and adenosine triphosphate. In addition, a general quantitative expression was presented to describe the analytical performance of the resulting aptamer-based sensors that took into account the variation in current densities of both the target-bound and -unbound state of each sensor, employing various aptamer architectures.

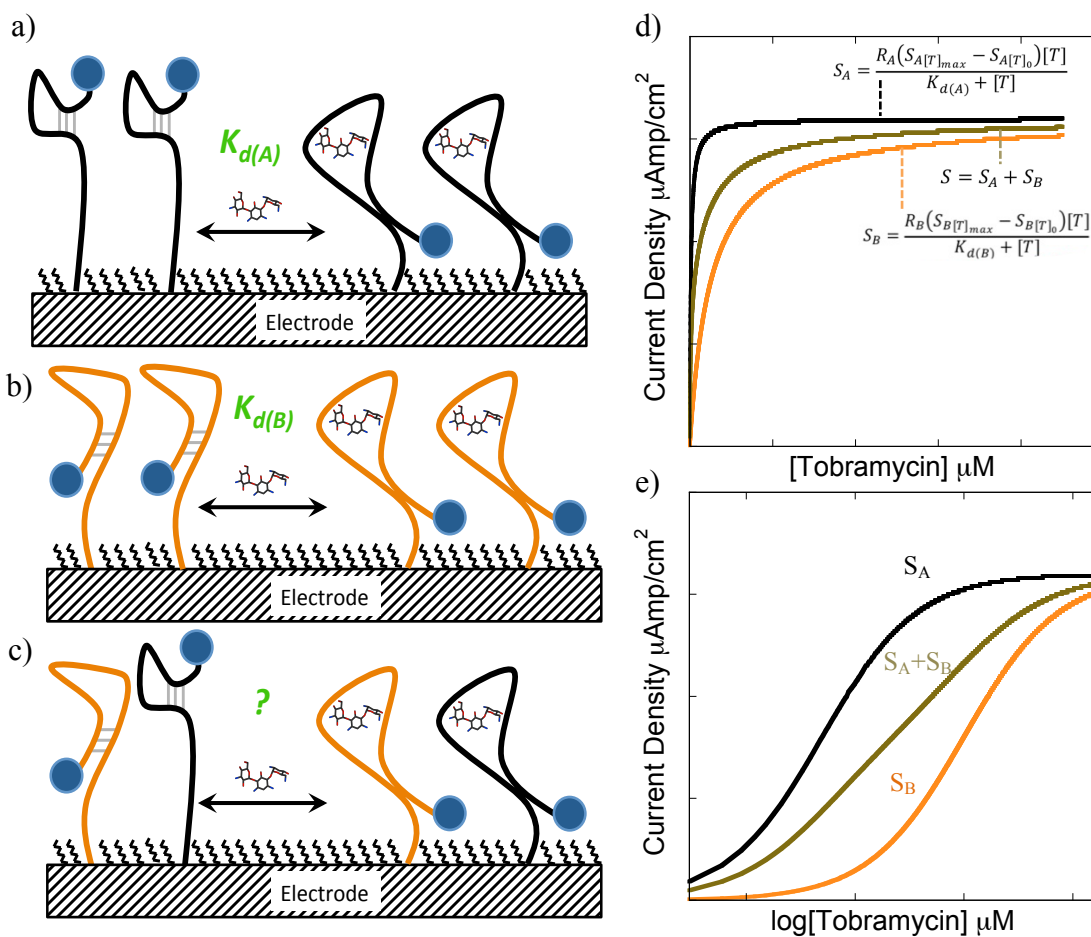


Figure 23. Aptamers engineered to undergo different conformation changes (a & b) in the presence of the same target resulted in different analytical figures of merit for the resulting sensor, including sensitivity and dissociation constants ($K_{d(A)}$ and $K_{d(B)}$). Sensors fabricated with mixtures of aptamers with different affinities for the same target (c) produced sensors with tunable analytical performance based on the ratio of the two aptamers. For example, the predicted sensor response of a sensor employing a 50:50

mixture of high- (black) and low-affinity (orange) aptamers fell between the responses of sensors fabricated with 100% high-affinity or low affinity aptamers (brown).

Quantitative Binding Isotherms for Heterogeneous Sensor Surfaces

A surface with two distinct noncooperative binding sites for the same target should exhibit a response that follows a combined binding isotherm or bi-Langmuir isotherm (Fig. 23).^{116,126} To quantitatively predict heterogeneous E-AB sensor response, a bi-Langmuir isotherm was derived written in terms of signal (S , absolute current density in units of A/cm^2) to provide a general expression for sensor response (eqs 7–9). To properly describe the heterogeneous sensors, the fact that the individual aptamer architectures exhibited different minimum current densities (S_{\min}) when no target is present and different maximum current densities (S_{\max}) at saturating target concentrations was taken into account. These values were a result of the apparent electron transfer rates given the different aptamer architectures. When a mixture of the two aptamers was on the surface, a weighted algebraic average of the signals was observed. Consistent with this, sensors employing either the parent or Mut tobramycin aptamers exhibited S_{\min} values for each architecture that are 306 ± 10 and $143 \pm 14 \mu A/cm^2$, respectively. When the mixing was at different ratios (R_i , where R is the fraction of aptamer i), the current density represents the weighted sum of the contributions of both aptamers. For example, a 50:50 mixture of parent and Mut give a S_{\min} of $226 \pm 40 \mu A/cm^2$ (see Fig. 24). Of note, no appreciable faradaic signal was observed when the aptamer was not present (Fig. 25). The quantitative binding isotherm for the mixed monolayer was thus described by the following:

$$S = R_A S_A + R_B S_B \quad (7)$$

$$S_A = \frac{(S_{max(A)} - S_{min(A)})[T]}{K_{d(A)} + [T]} + S_{min(A)} \quad (8)$$

$$S_B = \frac{(S_{max(B)} - S_{min(B)})[T]}{K_{d(B)} + [T]} + S_{min(B)} \quad (9)$$

In Equation 7 the heterogeneous sensor signal (S) is the sum of the contributions of the signal from aptamers A and B employed on the sensor surface. By definition, $R_A + R_B = 1$. Equations 8 and 9 represent the individual binding isotherms for sensors fabricated with aptamers A and B where [T] represents the concentration of free target in solution (M) and K is the dissociation constant of the sensor using the respective aptamer (Fig. 23). The preceding equations were used for constructing calibration curves for mixed aptamer coated sensor surfaces. Of note, when plotted as a calibration curve, all data were normalized to the initial current density (signal without target present). Normalization was done to better visualize the change in current density as a function of target concentration for the various mixtures, as the change is important in quantifying the target.

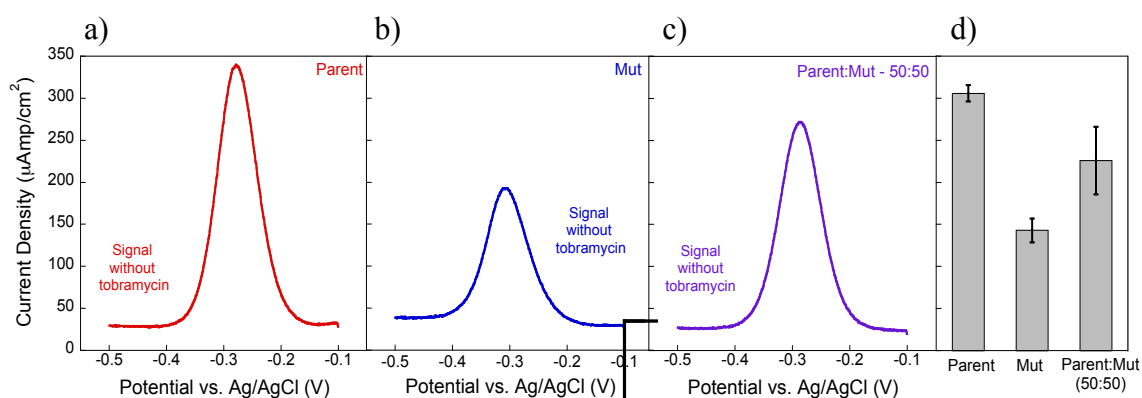


Figure 24. Absolute signal (current density) measured at a heterogeneous surface in the absence of target molecule representing the weighted algebraic sum of the contributions of each aptamer. At constant surface coverage this resulted in minimum current densities (signal without target) of 306 ± 10 and 143 ± 14 $\mu\text{A}/\text{cm}^2$ for the homogeneous parent and Mut sensors, respectively. When mixed at a 50:50 ratio, the current density with no target present was 226 ± 40 $\mu\text{A}/\text{cm}^2$. The voltammograms show representative data, and the bar graph and error bars represented the average of at least three independently fabricated sensors.

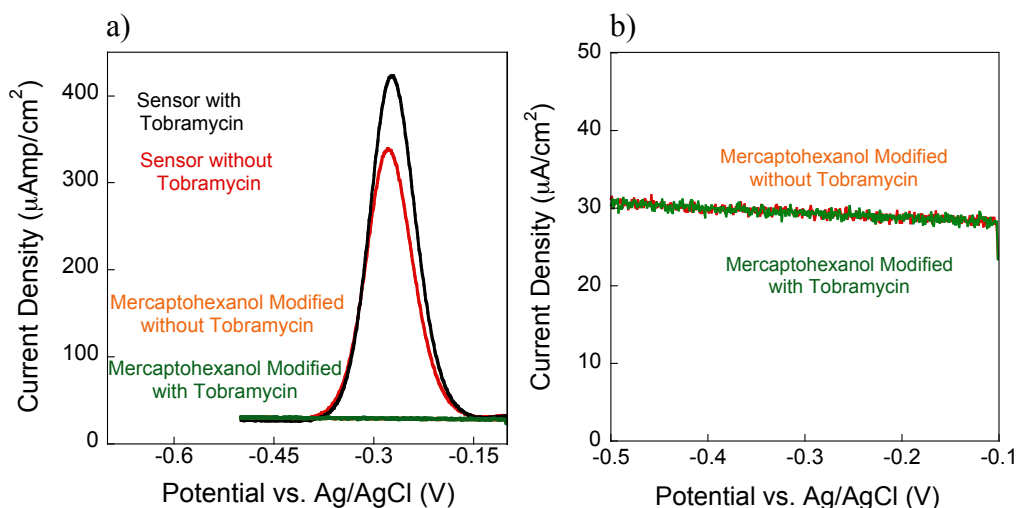


Figure 25. Electrochemical, aptamer-based sensors fabricated with parent aptamer responded (a) with an increase in voltammetric peak current resulting from the reversible reduction of methylene blue. (a & b) As a control, sensors fabricated without aptamers, and thus only the mercaptohexanol backfill monolayer, exhibited no appreciable faradaic current in the absence and presence of tobramycin.

Heterogeneous Sensor Surfaces That Allow Tunable Sensor Response

Heterogeneous, electrochemical, aptamer-based sensors with varying ratios of two different aptamers with different affinities for the same target quantitatively responded to the target as predicted by the bi-Langmuir isotherm model. Specifically, sensors for the detection of two representative small molecule targets tobramycin and ATP were investigated. To demonstrate rational control over the signaling properties of the heterogeneous sensors, multiple parent:Mut ratios, including 75:25, 50:50, and 25:75 were tested. As a baseline measurement, sensors fabricated with a homogeneous surface comprising only the parent aminoglycoside aptamer exhibited a high dissociation constant ($K_d = 23 \pm 4 \mu\text{M}$). Conversely, sensors comprising only the Mut aptamer exhibited a low dissociation constant ($K_d = 0.045 \pm 0.003 \mu\text{M}$) (Fig. 26). As expected, skewing the ratio in favor of the parent aptamer on the sensor surface resulted in a signal that more closely resembled sensors employing the parent aptamer. For example, sensors fabricated with the parent aptamer displayed a $12 \pm 1 \mu\text{A}/\text{cm}^2$ signal change at $0.5 \mu\text{M}$ tobramycin, while, if 75% of the surface is modified with the parent aptamer, $33 \pm 8 \mu\text{A}/\text{cm}^2$ current density at the same concentration was observed. Thus, the heterogeneous sensor responses followed the predicted bi-Langmuir isotherm described previously.

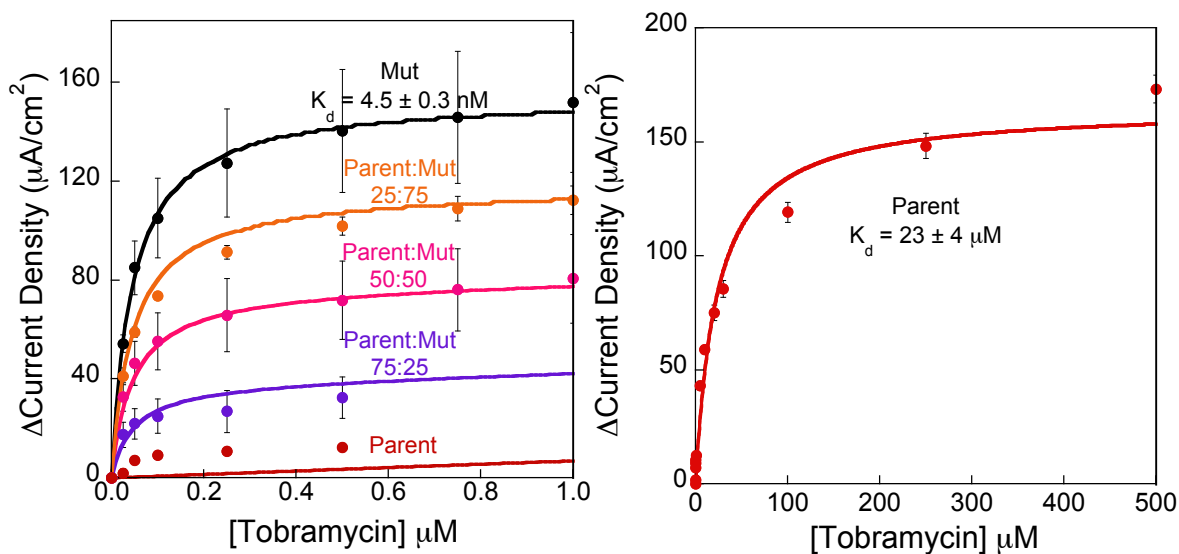


Figure 26. Heterogeneous sensor surfaces exhibited predictable bi-Langmuir binding properties. (a) When mixed in varying ratios on the electrode surface, the sensors performed as a weighted sum of the performance of the individual aptamer architectures. The lines are calculated with the derived combined binding isotherm using the dissociation constant values (K_d) and current densities at saturating concentrations. (b) Sensors built with the parent aptamer show minimal change at low concentrations, thus a titration curve using higher concentrations was used to calculate the dissociation constant. All data points and error bars represented the mean and standard deviation of at least 3 independently fabricated sensors.

Heterogeneous sensor responses fabricated with the parent and Mut ATP aptamer-based sensors followed the same trend as the aminoglycoside sensors and the bi-Langmuir isotherm (Fig. 27). For example, the Mut ATP aptamer sensors displayed a current density of $27 \pm 2 \mu\text{A}/\text{cm}^2$ at 2.5 mM ATP, where the sensors fabricated with 75% Mut aptamer exhibited $21 \pm 4 \mu\text{A}/\text{cm}^2$ (Fig. 27). The sensors employing parent aptamers showed a current density of $7.1 \pm 0.3 \mu\text{A}/\text{cm}^2$ at 2.5 mM, and when the sensors were modified with 75% parent the signal was $12 \pm 1 \mu\text{A}/\text{cm}^2$. When the sensors were employing 50% of each aptamer, the sensor response was $17 \pm 3 \mu\text{A}/\text{cm}^2$ at 2.5 mM ATP, which was in the middle of the sensor responses of Mut and parent. The strategy of

heterogeneous sensor surfaces is generally applicable to DNA and RNA aptamer-based sensing elements.

Table 6. K_m Values for Heterogeneous Sensor Surfaces

DNA-ATP (Parent:Mut)	μM^*	RNA-Tob (Parent:Mut)	μM^\dagger
100:0	134	100:0	23
75:25	148	75:25	0.052
50:50	162	50:50	0.045
25:75	171	25:75	0.042
0:100	206	0:100	0.045

*The estimated concentration of the signal at half-maximum for sensor responses assuming the maximum occurs at 2500 μM ATP.

† The estimated concentration of the signal at half-maximum for sensor responses assuming the maximum response occurs at 1 μM tobramycin, with the exception of 100% parent aptamer (assumed maximum at 500 μM tobramycin).

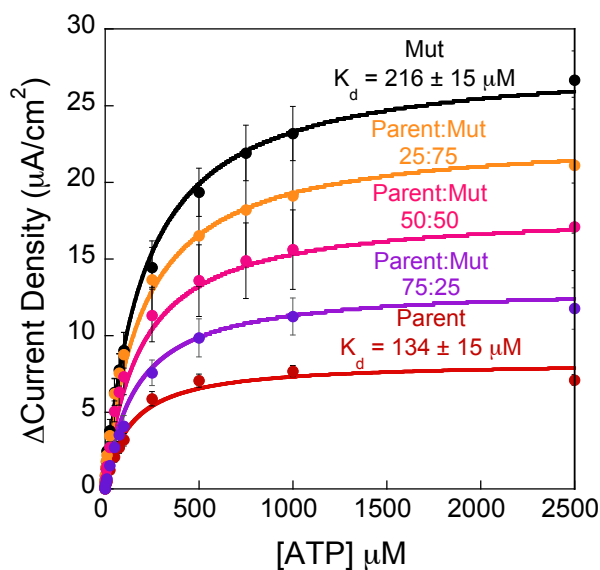


Figure 27. Heterogeneous sensors fabricated with two variations of the ATP aptamer exhibited predictable sensor performance based on the ratio of the two aptamers on the sensor surface. Much like the tobramycin sensors, the ATP sensors are fabricated with a high gain (Mut) and low gain (Parent) sequence. The sensor performance followed the bi-Langmuir isotherm described here as indicated by the solid lines. All data points and error bars represented the mean and standard deviation of at least 3 independently fabricated sensors.

Tuning Affinity, Sensitivity, and Dynamic Range of Electrochemical Sensors by Using Mixed Ratio of Aptamers

Sensors fabricated with mixed ATP DNA and aminoglycoside RNA aptamers had tunable affinities determined by the ratio of the parent and mutated aptamers employed on the sensor surface. Affinity is defined here as the concentration at which 50% of the signal is reached. To quantify heterogeneous sensor performance, the binding affinities for the parent and Mut DNA-based sensors are 134 and 216 μM , respectively were used. The maximum current density difference was assumed to be at 2.5 mM ATP for all of the heterogeneously coated sensors. Thus, the values of K_m for sensors comprising mixtures of 75:25, 50:50, and 25:75 (parent:Mut) fell between these boundaries, which are 148, 162, and 171 μM , respectively (Table 6). Conversely, the K_m values for the heterogeneous aminoglycoside sensors were very similar to the dissociation constant of the sensors fabricated with 100% Mut aptamer ($\sim 0.045 \mu\text{M}$). The K_m values were similar as a result of the mismatch in the magnitude of signal change at low tobramycin concentrations between the Mut and parent sequences²⁸. As such, the presence of Mut aptamer presumably dominated the signaling at low concentrations $< 1 \mu\text{M}$. The fact that the Mut aptamer contributes significantly to signaling at low concentrations indicated a quantitative limit to the tunability of sensor performance based on mutant sequences.

In addition to tunable affinities, the heterogeneous aptamer-based sensors had tunable dynamic ranges and sensitivities, which were dictated by the ratio of the two aptamers employed on the sensor surface. The dynamic range for each sensor was calculated using the limit of detection and the limit of linearity. While the limits of

detection calculated for the ATP sensors were all $\sim 2 \mu\text{M}$ (Table 7), the limit of linearity's followed the expected trend based on the ratio of the aptamers used. The same is true for the sensitivities, which is defined as the slope of the linear portion of the calibration curve. Specifically, sensors fabricated with the parent aptamer had the narrowest dynamic range, with an upper limit of $82 \mu\text{M}$ and a sensitivity of $0.0427 \mu\text{A}\mu\text{M}/\text{cm}^2$. Sensors fabricated with the Mut ATP aptamer displayed a limit of linearity of $123 \mu\text{M}$ and the best sensitivity of $0.0948 \mu\text{A}\mu\text{M}/\text{cm}^2$. Heterogeneous sensors fell between these limits of linearity and sensitivities according to the ratio of parent:Mut (Table 7). Conversely, the RNA aminoglycoside parent and Mut sensors had large disparity between their signaling, where their limits of detection varied by a factor of ~ 650 (260 nM and 0.395 nM , respectively) ⁴⁹. The heterogeneously coated RNA sensors had limits of detection (LOD) that trended similarly with mixes of the two aptamers, but weighted toward the mutant sensor properties, as did the limits of linearity. The sensitivities also exhibited a trend similar to the mutant being the most sensitive ($2381 \mu\text{A}\mu\text{M}/\text{cm}^2$) and the parent being the least sensitive ($5 \mu\text{A}\mu\text{M}/\text{cm}^2$) and the mixes fell between, which were weighted by the ratio of the aptamer sequences employed (Table 7).

The ability to quantitatively tune the analytical figures of merit based on mixtures of aptamers with different affinities to the same target was achieved via quantitative control over the ratio of the aptamers attached to the electrode surface. The magnitude of tunability of each figure of merit depends on the signaling of the individual aptamer components. Specifically, the difference between the magnitude of the signal change observed ($S_{\text{max}} - S_{\text{min}}$) with each aptamer and the dissociation constants (K_d) can bias, or weight, the performance favoring one aptamer over the other, which was seen in the

RNA-based aminoglycoside sensors. Nonetheless, the ability to quantitatively control sensor performance is general.

Table 7. The Dynamic Ranges and Sensitivities of Heterogeneous Sensors

DNA (Parent:Mut)	Dynamic Range* (μM)	Sensitivity [†] ($\mu\text{A}\mu\text{M}/\text{cm}^2$)	RNA (Parent:Mut)	Dynamic Range* (μM)	Sensitivity [†] ($\mu\text{A}\mu\text{M}/\text{cm}^2$)
100:0	3 _{.1} -82	0.0427	100:0	0.26-13	5
75:25	2 _{.1} -98	0.0555	75:25	0.0040-0.027 ₆	579
50:50	1 _{.0} -111	0.0681	50:50	0.0014-0.027 ₂	1192
25:75	2 _{.4} -118	0.0814	25:75	0.0010-0.027 ₁	1788
0:100	2 _{.1} -123	0.0948	0:100	0.00039 ₅ -0.027 ₁	2381

*The lower limits here represent limit of detection calculations and the upper limits (limit of linearity's) are within 10% deviation of the linear fit.

[†]The sensitivities are the slopes of the linear fits of the dynamic ranges.

Conclusion

In this work, for the first time, the use of a family of rationally designed aptamer sequences with different affinities for the same target were combined on a single sensor surface in order to quantitatively and predictably control sensor performance. Specifically, the ability to control the sensitivity, dynamic range, and dissociation constant of the resulting sensors by varying the ratio of a high- and low-affinity aptamer for the same target on a single sensor surface was demonstrated. To establish the generality of this approach, tunable sensors using several DNA aptamers for ATP detection and RNA aptamers for tobramycin detection were successfully developed. In addition a quantitative binding isotherm was presented that takes into account the absolute signaling of each aptamer sequence in both the target-free and target-bound states. The isotherm accurately predicted the experimental observations of heterogeneously coated sensors. A caveat to this method was the algebraic weighting of sensor signaling in favor of one mutant over the other. The magnitude of signal change

$(S_{\max} - S_{\min})$ and the difference in the dissociation constants limited the tunability of the sensor analytical figures of merit. Nonetheless, this variability is quantitatively predicted using the bi-Langmuir isotherm.

The parameters outlined here to tune the sensitivity, dynamic range, and dissociation constants for electrochemical aptamer-based sensors should be applicable to optimize the performance of any E-AB sensor using relatively simple sequence modifications. Furthermore, while the feasibility of this approach toward the development of electrochemical-based sensors, the approach is broadly applicable to structure-switching, aptamer-based sensors, regardless of the signal transduction mechanism.

Chapter 5: Biocompatible Hydrogel Membranes for the Protection of RNA Aptamer-Based Electrochemical Sensors

Introduction

Real-time molecular information in a healthcare setting could greatly enhance the caregiver's ability to efficiently administer treatment and improve patient outcome. For example, the ability to rapidly diagnose biomarker levels for time-sensitive critical care issues, such as infectious diseases¹²⁷ or sepsis¹²⁸ could provide accurate and actionable information to a clinician for immediate action and treatment.¹²⁷⁻¹³¹ In addition, the real-time monitoring of the pharmacokinetics of chemotherapeutics, particularly those with narrow therapeutic windows, could provide individualized treatment with improved patient outcome. The current methods for real-time therapeutic drug monitoring involves the monitoring of patient symptoms during treatment.¹³¹ Unfortunately, the quantitative information, which can take days to report, is verbally discussed with the patient and clinician and is open to interpretation.

Electrochemical, aptamer-based (E-AB) sensors represent a promising platform to achieve real-time detection of relevant biomarkers as a result of their specificity, selectivity and sensitivity.^{4,76} These sensors comprise single-stranded DNA or RNA aptamers that are attached to a sensing electrode surface and modified at the distal end with a redox active marker.^{2,7,14,50} The aptamer is selected to bind a specific target,¹³² and upon target-binding the aptamer undergoes a conformation change.² The aptamer conformation changes the accessibility of the redox marker to the sensing electrode surface. The efficiency of electron transfer is dependent on the distance and collisional

frequency of the redox marker, thus the conformation change is readily measured electrochemically.^{4,7,14,16,29,50,71,92} As a result, E-AB sensors are specific (aptamer binding is specific) and selective (there are relatively few electroactive interferents), and thus DNA-based sensors can achieve detection directly in untreated serum.^{4,16} On the other hand, serum need to be significantly pretreated in order for RNA-based sensors to achieve detection in this complex sample matrix.^{7,29} Specifically, to date all E-AB sensors employing RNA aptamers require filtered serum prior to use to remove any harmful nucleases or serum treated with an RNase inhibitor.^{7,16,29} Sample pretreatment is not amenable for providing rapid, real-time diagnostic and treatment information.

While, most E-AB sensors described are DNA-based as a result of the inherent stability of the biomolecule, some RNA aptamers have been demonstrated to exhibit better specificity and sensitivity. For example, the RNA theophylline aptamer binds theophylline but not caffeine, which only differs by a single methyl group.¹⁶ RNA aptamers can even exhibit enantioselectivity.¹³³ Furthermore, there are only ~20 DNA aptamers reported in comparison to ~90 RNA aptamers.¹³⁴ Presumably, the ability of RNA to adopt more complex tertiary structure leads to better aptamer binding abilities. The lack of employment of RNA aptamers for detection in complex media, such as serum thus motivated the work within. Here a biocompatible hydrogel membrane was formed on the E-AB sensor surface, which blocked access of harmful nucleases to the sensor surface and thus allowed for RNA sensor function for at least 3 hours, while still allowing for specific detection of analyte target. The findings suggest that this strategy has the potential to generate a general sensor platform, which mitigates sensor degradation to enable long-term, real-time detection directly in biological environments.

Materials and Methods

Materials

6-mercapto-1-hexanol (97%) and tobramycin (Sigma Aldrich) were used as received. Sodium chloride, Trizma base, and magnesium chloride (Sigma Aldrich), were used to make a Tris buffer solution at concentrations of 100mM, 20mM, and 5mM respectively. These salts were diluted with ultrapure water (Mili-Q Ultrapure Water Purification, Milipore, Billerica, MA) and used in electrochemical measurements unless otherwise noted. The 5'-thiol, 3'-methylene blue modified DNA and RNA aptamers (HPLC-purified, Biosearch Technologies, Inc. Novato, CA) were used as received. The DNA sequence used was 5'HS(CH₂)₆-GGG ACT TGG TTT AGG TAA TGA GTC CC-Methylene blue 3'[8]. The RNA aptamer sequence used was 5'HS(CH₂)₆-GGG ACU UGG UUU AGG UAA UGA GUC CC-Methylene blue 3'. Of note the RNA sequence displayed here is the same sequence as the Parent sequence mentioned in Chapters 2 & 4. The aptamer probes were stored in a 0.01M EDTA aqueous solution, pH 8.0 (Sigma Aldrich), when not in use, which was autoclaved for the RNA. Tris-2-carboxyethyl-phosphine (TCEP) (Sigma Aldrich) was used to reduce the disulfide bond of the aptamers 5' end prior to immobilization on the gold electrode surface. Acrylamide (40%w/v) (BioRad), bis-acrylamide (2%w/v) (BioRad), TEMED (N,N,N,N-tetramethylethylenediamine) (Sigma Aldrich), and ammonium persulfate (Sigma Aldrich) were used in the synthesis of the polyacrylamide hydrogel. Fetal bovine serum (Thermo Scientific) served as a serum proxy.

Electrochemical Aptamer Sensor Fabrication

E-AB sensors were fabricated on 2 mm diameter polycrystalline gold electrodes

(CH Instruments, Austin, TX). Electrode modification was performed using a previously described method [8]. In short, the electrodes were mechanically polished in a circular fashion on microcloth (Buehler) with a 1 μm diamond suspension (Buehler) followed by an alumina oxide slurry (Buehler). The electrodes were rinsed and sonicated for 5 min between mechanical polishing steps. Following the mechanical polishing, electrodes were cleaned electrochemically through a variety of voltammetric scans in dilute sodium hydroxide and sulfuric acid solutions. The electrochemical cleaning consisted of cycling 500 times between -0.4 V and -1.35 V vs. Ag/AgCl in 0.5 M NaOH, cycling 10 times at scan rates varying from 4 V/s to 0.1 V/s at potentials from -0.35 V to 1.5 V vs. Ag/AgCl in 0.5 M H₂SO₄, by cycling 10 times from 0.2 V to 1.5 V vs. Ag/AgCl in 0.1 M H₂SO₄ and 0.01 M KCl, and cycling 10 times from -0.35 V to 1.5 V vs. Ag/AgCl in 0.05 M H₂SO₄. After cleaning, each electrode was incubated in a solution containing 200 nM DNA in Tris buffer for 1h. These electrodes were then rinsed with water and incubated in 3 mM 6-mercapto-1-hexanol for 1 h, which was diluted with buffer [8]. Rinsed electrodes were stored in a solution of Tris buffer prior to use.

Electrochemical Measurements

All electrochemical measurements were performed using a CH Instruments 620D Electrochemical Work Station (CH Instruments, Austin, TX). All measurements were performed in a three-electrode cell utilizing an Ag/AgCl reference electrode and a platinum wire counter electrode. Square wave voltammetry parameters were as follows: a pulse amplitude of 25 mV, frequency of 60 Hz and step width of 1 mV or 4 mV. All measurements were performed in a glass cell with 3mL of Tris buffer or 3mL of fetal bovine serum.

Hydrogel Membrane Polymerization and Utilization

Encapsulation of the sensor surface with a protecting hydrogel was performed after sensor calibration with a tobramycin titration. The titration ensured that the sensors quantitatively responded to the presence of target analyte (tobramycin). A polyacrylamide solution was prepared to contain 2 mL of acrylamide solution (35.3%), 0.2 mL of the bis-acrylamide solution (0.2%), 15 μ L of (0.7%) TEMED, and 50 μ L of a 5 mM ammonium persulfate solution. The solution was inverted gently to mix the reactants. The freshly prepared pre-polymerized solution was then dispensed in \sim 10 μ L aliquots onto each electrode surface. Sensors were left in a humidity chamber until the solution polymerized (\sim 60 min).

Results and Discussion

Performance of Bare Sensors in Buffer

As a representative test-bed sensor platform, E-AB sensors were fabricated for the sensitive detection of the aminoglycoside antibiotic, tobramycin.⁷ The target was chosen because both RNA and DNA sequences that bind to tobramycin, as demonstrated by Rowe *et al.*⁷ exist. In the same report, several strategies were employed to protect RNA from degradation by nucleases, including methylation of the 2'-hydroxyl groups and conversion of the sequence to a DNA strand. While the DNA version maintained tobramycin-sensing ability, it did so with a lower affinity. Ultimately, the investigators had to resort to ultracentrifugation of the serum to allow RNA sensor use.

RNA and DNA aptamer-based sensors utilizing anti-aminoglycoside aptamer rapidly and reversibly responded to the presence of the aminoglycoside antibiotic, tobramycin (Fig. 28). As shown in Figure 28, the presence of tobramycin caused a

decrease in measured squarewave peak current for RNA and DNA-based sensors similar to previous reports.⁷ With a simple 5-second water rinse the signal was regenerated to within at least 95% of its original value.

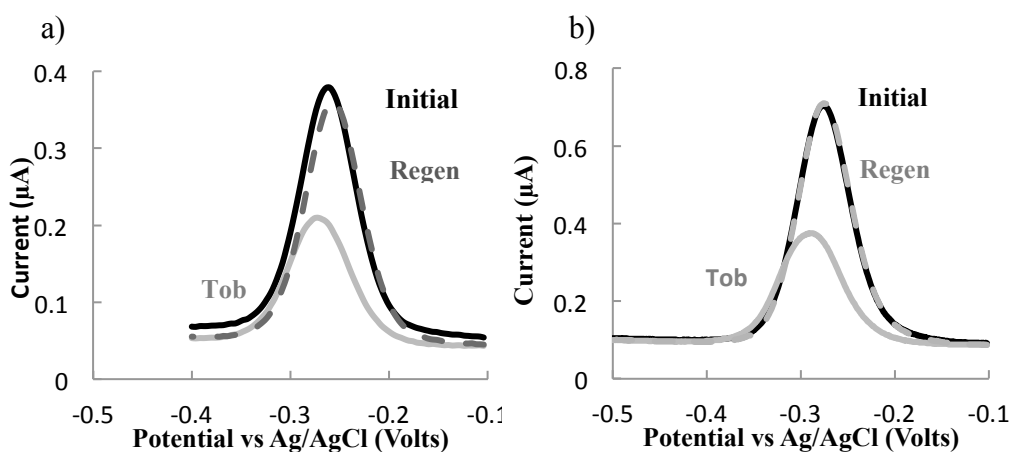


Figure 28. E-AB aminoglycoside sensors are rapid and reusable. RNA- (a) and DNA-based (b) sensors exhibited a decrease in peak current upon the addition of saturating levels of tobramycin (Tob - 2 mM). However in simply rinsing the electrode surface with water the initial signal was regenerated (regen). The sensor response occurred rapidly, and was equilibrated within the several seconds it takes between each voltammetric scan.

The sensors responded quantitatively to the presence of tobramycin (Fig. 29). The percent decrease in signal (signal suppression) provides indication of the amount of tobramycin that was present in solution. The data was fit to a Langmuir adsorption isotherm describing non-competing binding to a finite number of binding sites.^{2,50} Unlike previous reports, the DNA aptamer sensor out-performed the RNA sensor displaying a 45% signal change at saturating target concentration (2 mM) with a $160 \pm 22 \mu\text{M}$ dissociation constant. The RNA sensor displayed a 35% maximum signal change with a $306 \pm 70 \mu\text{M}$ dissociation constant (Fig. 29).⁷ The discrepancy in which the DNA sequence displays better affinity for tobramycin could be a result of unoptimized surface conditions. That is, observed binding affinity is sensitive to the packing density of the

probe aptamers on the electrode surface,⁵⁰ and sensors employed here were not optimized in terms of packing density.

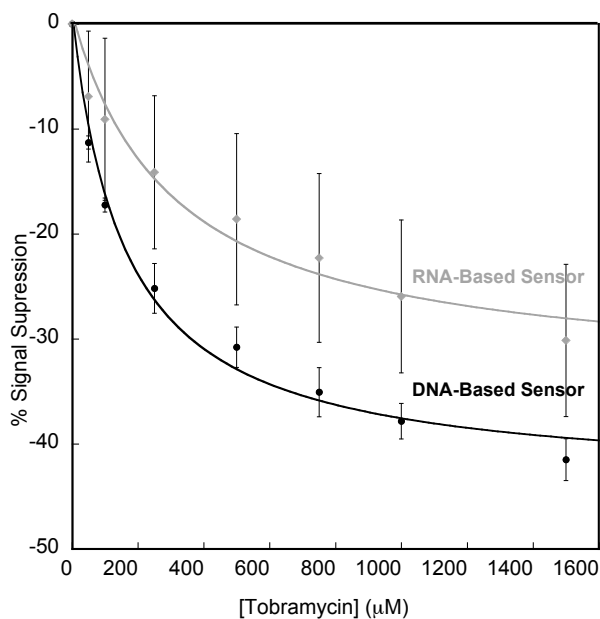


Figure 29. E-AB sensors responded quantitatively to the presence of target analyte. An increase in tobramycin concentration caused larger decrease in peak current (expressed as percent signal suppression) for both the DNA and RNA aptamer-based sensors. They exhibited a $160 \pm 22 \mu\text{M}$ and $306 \pm 70 \mu\text{M}$ observed binding affinity, respectively, when fit to a Langmuir isotherm. Signal suppression displayed was the average percent signal suppression for three DNA-based and three RNA-based sensors.

Performance of Bare Sensors in Serum

Anti-aminoglycoside E-AB sensors utilizing the DNA aptamer were selective, and capable of tobramycin detection directly in undiluted serum. Specifically, when challenged with saturating target concentrations in serum, E-AB sensors with DNA aptamers exhibited ~60% signal suppression (data not shown). Conversely, RNA-based sensors did not perform when challenged in undiluted serum, presumably as a result of degradation of the RNA aptamer. To further characterize the origin of RNA sensor failure, each sensor (RNA and DNA) was subjected to repeated scans in serum while monitoring peak current as a function of time (Fig. 30). E-AB sensors fabricated with

RNA aptamer sensing elements exhibited a rapid decrease in peak current, leveling off at ~70% signal loss after 120 min. Alternatively, DNA-based sensor's responses remained constant, within error, over the same 180 minutes. Any decreases in peak current are expected to have resulted from either physical steric blocking of access to the electrode surface (*e.g.*, the nonspecific adsorption of serum proteins) or loss of the redox molecule (*e.g.*, desorption of thiol or degradation of the sensing element). DNA-based sensors showed no decrease in measured peak current, thus non-specific adsorption as the cause of sensor failure was ruled out. Alternatively, the data presented here and literature reported that RNA degradation by RNase activity was the major cause of sensor failure.^{16,29}

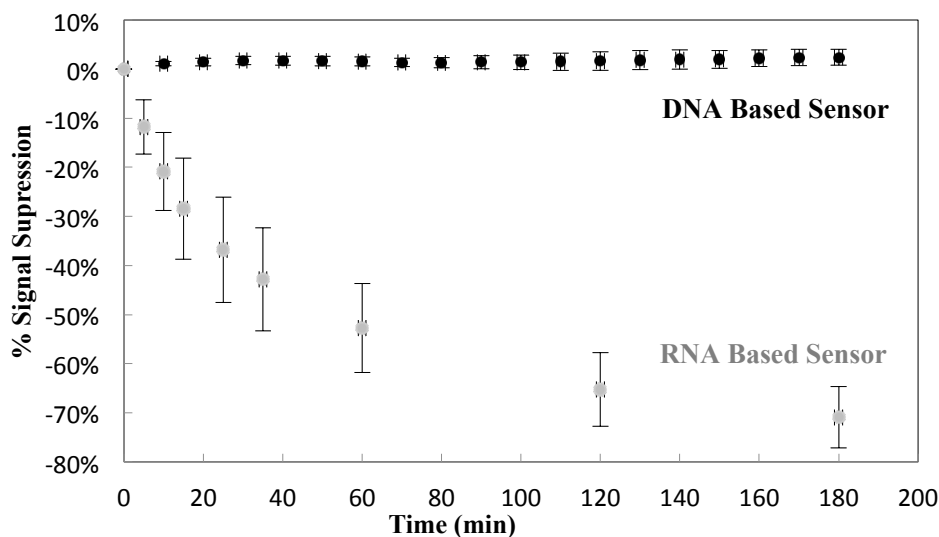


Figure 30. When employed in undiluted blood serum, RNA aptamer sensors exhibited rapid degradation in comparison to DNA aptamer-based sensors. Monitoring peak current as a function of time deployed in serum provided a qualitative picture of both the accessibility of the electrode surface to redox marker (which can change as a result of nonspecific adsorption of serum proteins) and the total amount of redox marker tethered to the surface (which can change if the aptamer degraded thus liberating the redox probe). Over the same 180-minute experiment, the DNA-based sensor responses remained virtually unchanged, while the RNA-based sensor rapidly lost ~70% of its signal. The DNA surface showed no susceptibility to nonspecific adsorption of protein, thus the loss in signal for the RNA surface was presumed to be a result of enzymatic/chemical

degradation of the RNA sensing element.

Performance of Hydrogel Coated Sensors in Buffer and Serum

Previous research reports demonstrated that RNA-based E-AB sensors will function in serum after significant pretreatment to eliminate the presence of nucleases. Specifically, Rowe *et al.* and Ferapontova *et al.* reported filtering the serum via ultracentrifugation with ~3000 Da molecular weight cutoff filters to remove serum proteins and utilizing the filtrate.^{7,16,29} Alternatively Ferapontova demonstrated that treating serum biochemically to inhibit nuclease dramatically improved RNA-based E-AB sensor performance in serum.

The approach here was to encapsulate the RNA-based sensor with a biocompatible membrane to prevent nucleases from reaching the sensor surface thus protecting the surface attached RNA. A polyacrylamide membrane was deposited onto the modified-electrode surface because of nuclease degradation. Upon polymerization the hydrogel membrane was characterized by its mesh (or pore) size. Mesh size was controlled via the concentration of the monomer (acrylamide) and crosslinker (bis-acrylamide) that were employed during hydrogel polymerization. Given the polymerization protocol (35.3% acrylamide and 0.2% bis-acrylamide), the mesh size was estimated using Flory-Rehner theory and equilibrium swelling measurements to be ~40 nm.^{135,136}

E-AB sensors encapsulated with a protecting hydrogel membrane supported sufficient E-AB sensor function. After the hydrogel membranes were allowed to polymerize, the encapsulated sensors were tested in buffer for their ability to bind tobramycin (Fig. 31). When challenged with tobramycin, the sensor yielded a 61% and

60% signal change for the DNA and RNA-based sensors, respectively (compared to the 45% and 35% observed from uncoated sensors). It is important to note that, upon submersing the sensor into Tris buffer, the peak current increased until reaching equilibrium after ~20 min. Similarly, after the addition of 2 mM tobramycin, the sensor signaling equilibrated after ~20 min. The equilibration time was a result of the solution inside the hydrogel equilibrating with the external solution. While ~20 min equilibration time was undesirable for rapid, real-time detection, the membranes used within this document are not yet optimized in terms of both membrane thickness and mesh size. Fabricating thinner membranes with an optimized mesh size are expected to improve the response time of the sensors and this is currently under investigation. Finally, after a ~90 min submersion in buffer without target, the sensors regenerated to ~60-70% of their original signal (Fig. 31). The origin of the less than optimal regeneration is presumed to be a function of the physical properties of the membrane-coated sensor, which is actively under investigation.

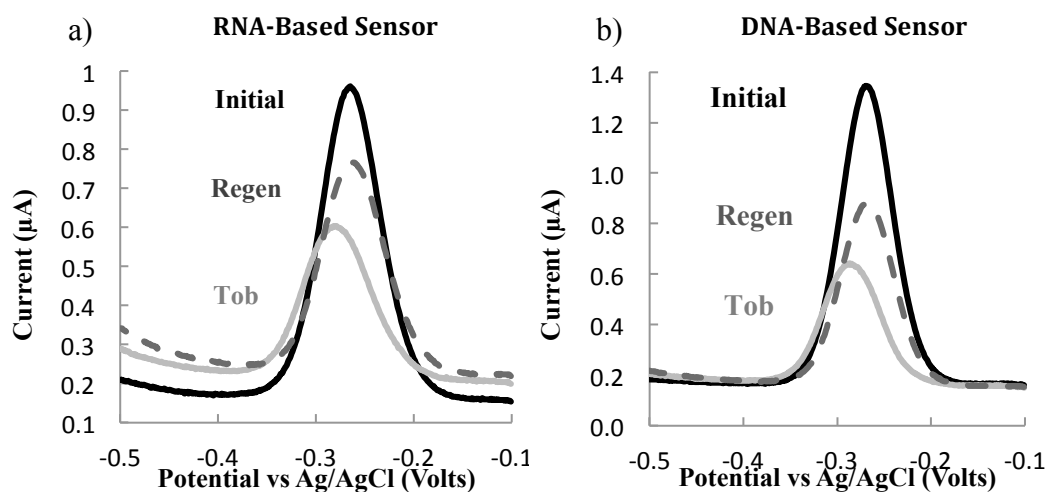


Figure 31. Hydrogel-protected RNA (a) and DNA (b) aptamer-based sensors responded effectively to the presence of target. Both polyacrylamide membrane coated sensors exhibited a decrease in peak current upon the addition of 2 mM tobramycin after equilibrating for ~20 min. In rinsing the electrode surface with water the initial signal was regenerated to within ~60-70%.

To test the protection abilities of the polyacrylamide membrane the RNA-based E-AB sensors were immersed directly in undiluted serum with and without a polyacrylamide membrane (Fig. 32). As described above, squarewave voltammetric peak current was monitored as a function of time to qualitatively test the integrity of the sensing monolayer. As such, the sensors were placed in fetal bovine serum and were tested every 10 minutes for 3 consecutive hours. The percent change was calculated with respect to the initial squarewave voltammogram in serum (Fig. 32). After a ~50 min equilibration period (where buffer is exchanged for serum in the membrane), RNA E-AB sensors show almost no degradation for 3h, in comparison to an uncoated sensor, which decays by 70% within the first hour (Fig. 30 and Fig. 32).

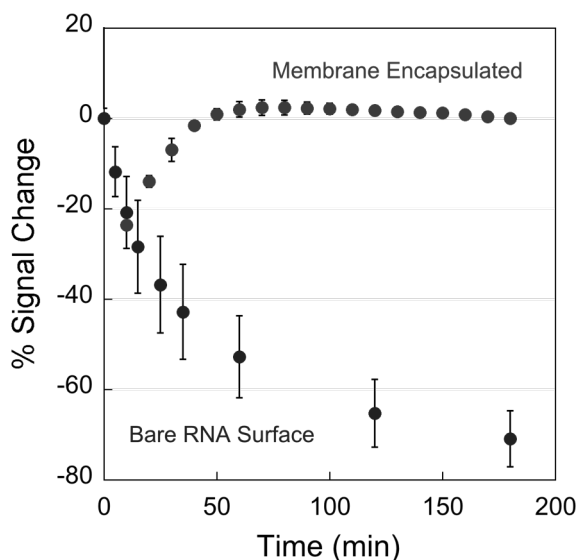


Figure 32. Incorporation of a protecting hydrogel layer dramatically improved the stability of an RNA-based E-AB sensor in serum. The graph shows the peak current percent signal change with respect to the initial peak current measured in fetal bovine serum over time. The graph displays RNA sensor signals' stability (with membrane) and degradation (without membrane) for 200 minutes.

Conclusions

Electrochemical aptamer-based sensors that employed RNA sensing elements suffer from sensor failure upon employment in a complex sample matrix, such as blood serum. The failure mode appears to be a product of enzymatic degradation of the actual sensing element (RNA) as opposed to nonspecific adsorption of serum proteins onto the sensor surface. Nuclease degradation is supported by the observation that E-AB sensors fabricated with DNA aptamers are relatively robust on long time scales (~hours) when employed in undiluted serum. Several literature reports attempt to overcome degradation by significant sample pretreatment either through ultracentrifugation,⁷ biochemical treatment to inhibit nuclease activity,^{7,29} or RNA 2' hydroxyl modification via attempting to protect the hydroxyl or replacing it with a fluorine.^{7,137}

Here, the encapsulation of the sensor surface with a protecting, biocompatible polyacrylamide hydrogel membrane allowed RNA-based sensor function directly in serum. The unoptimized hydrogel membrane dramatically improved the stability of the RNA-based sensors when employed in serum. In addition to protecting the RNA sensing element for at least ~3h, the new hybrid membrane/sensor interface supported efficient sensor signaling. The encapsulated sensors still recognized and responded to the addition of the tobramycin target, albeit with a diminished temporal response. Optimization of the physical parameters of the membrane, which allow for rapid diffusion of the analyte, while still inhibiting the enzymatic attack of the RNA aptamers, is still needed and is under investigation. Nonetheless, these preliminary findings suggest that the method of hydrogel encapsulation of sensor surface will enable the use of RNA based E-AB sensors directly in complex media rendering them suitable for rapid diagnostics.

Chapter 6: Conclusions and Future Directions

Quantitative Sensor Performance Conclusions and Future Directions

The work presented in this dissertation provides a better fundamental understanding of sensor performance and signaling to bridge the gap between laboratory devices and practical real-world devices. Specifically, rational aptamer sequence modifications have profound effects on analytical sensor performance. For example, designing aptamers to undergo larger conformational changes upon target binding or that exhibit alternative folds prior to target binding results in tunable E-AB sensor signaling in terms of sensitivity and observed binding affinity. However, care must be taken in the choice of mutations to the oligonucleotide sequence, as altering a single nucleotide in the binding site of the aptamer-target complex can result in complete disruption of target binding. Lastly, employing two aptamers of different affinities for the same target on one sensor surface enables tunable sensor performance based on the ratio of the aptamers utilized. All of the aforementioned techniques that alter E-AB sensor signaling, provide valuable information about sensor function, and enable steps towards the widespread use of E-AB sensors.

While aptamer sequence and sensor surface modifications enabled tunable sensor performance, there are still several unknowns about sensor performance. This dissertation demonstrates a link between the sensitivity and the binding affinity, but the quantitative relationship is unclear. The relationship between the observed binding affinity and maximum percent signal needs to be analyzed and is under investigation. The maximum percent signal change is controlled by the squarewave interrogation frequency. It is hypothesized that changing the squarewave interrogation frequency will alter the

observed binding affinity because the current measured in the target-unbound state will arise from redox-labeled aptamers of different secondary structures depending on the time the current is sampled (*i.e.* frequency). For example, at a frequency of 5 Hz the contribution to the current measured may arise from redox-modified aptamers that are flexible and are not forming distinct secondary structures. On the other hand, at a frequency of 100 Hz the current measured could come from redox-modified aptamers in a stem-loop structure. Therefore, at different frequencies the various binding affinities measured may arise from a comparison between two different unbound states and one bound state.

Membrane Coated Sensor Conclusions and Future Directions

Electrochemical aptamer-based sensors have been utilized in a variety of real world applications, but are limited from long-term use as a result of degradation of the biorecognition element or non-specific absorption of proteins to the sensor surface. A biocompatible, hydrogel coating for E-AB sensors developed in this dissertation enabled RNA sensor function in undiluted serum. The RNA E-AB sensors were stable for up to 3h in serum and the hydrogel negligibly affected E-AB sensor function as measured by the maximum signal change and observed binding affinity. Coating aminoglycoside E-AB sensors with a hydrogel enables sensor stability for up to 3h without inhibiting sensor performance, which should be applicable to any small molecule aptamer-based sensor.

Further studies need to be conducted in enabling long-term sensor function and rapid response times to target concentrations. Specifically, hydrogel crosslinker and monomer percentages/ratios, or mesh size, needs to be optimized to ensure RNase enzymes cannot penetrate the membrane, while still allowing for small molecule

diffusion. Hydrogel membranes utilized did not enable rapid target diffusion, which was due to the thickness of the hydrogel deposited on the sensor surfaces (~1-5 mm). Thus, attenuated hydrogels are currently being investigated and should be further investigated to enable rapid response times for real-time target detection. Upon hydrogel optimization the protected sensors will be tested further in a microfluidic device with serum/blood to simulate blood flow. In conclusion, this dissertation delivers an understanding of E-AB sensor function in order to converge laboratory technology and real-world applications.

References

- (1) Lai, R. Y.; Plaxco, K. W.; Heeger, A. J. *Anal. Chem.* **2007**, *79* (1), 229–233.
- (2) White, R. J.; Phares, N.; Lubin, A. A.; Xiao, Y.; Plaxco, K. W. *Langmuir* **2008**, *24* (18), 10513–10518.
- (3) Schoukroun-Barnes, L.; White, R. *Sensors* **2015**, *15* (4), 7754–7767.
- (4) Swensen, J. S.; Xiao, Y.; Ferguson, B. S.; Lubin, A. A.; Lai, R. Y.; Heeger, A. J.; Plaxco, K. W.; Soh, H. T. *J. Am. Chem. Soc.* **2009**, *131* (12), 4262–4266.
- (5) Liu, J.; Wagan, S.; Davila Morris, M.; Taylor, J.; White, R. J. *Anal. Chem.* **2014**, *86* (22), 11417–11424.
- (6) Porchetta, A.; Vallée-Bélisle, A.; Plaxco, K. W.; Ricci, F. *J. Am. Chem. Soc.* **2012**, *134* (51), 20601–20604.
- (7) Rowe, A. A.; Miller, E. A.; Plaxco, K. W. *Anal. Chem.* **2010**, *82* (17), 7090–7095.
- (8) Liu, Y.; Zhou, Q.; Revzin, A. *Analyst* **2013**, *138* (15), 4321–4326.
- (9) Kang, D.; Zuo, X.; Yang, R.; Xia, F.; Plaxco, K. W.; White, R. J. *Anal. Chem.* **2009**, *81* (21), 9109–9113.
- (10) Ferapontova, E. E.; Gothelf, K. V. *Langmuir* **2009**, *25* (8), 4279–4283.
- (11) Willner, I.; Zayats, M. *Angew. Chemie - Int. Ed.* **2007**, *46* (34), 6408–6418.
- (12) Song, S.; Wang, L.; Li, J.; Fan, C.; Zhao, J. *Trends Anal. Chem.* **2008**, *27* (2), 108–117.
- (13) Liu, J.; Morris, M. D.; Macazo, F. C.; Schoukroun-Barnes, L. R.; White, R. J. *J. Electrochem. Soc.* **2014**, *161* (5), H301–H313.
- (14) Xiao, Y.; Lubin, A. A.; Heeger, A. J.; Plaxco, K. W. *Angew. Chem. Int. Ed. Engl.*

2005, 44 (34), 5456–5459.

- (15) Rajendran, M.; Ellington, A. D. *Nucleic Acids Res.* **2003**, 31 (19), 5700–5713.
- (16) Ferapontova, E. E.; Olsen, E. M.; Gothelf, K. V. *J. Am. Chem. Soc.* **2008**, 130 (13), 4256–4258.
- (17) Ferguson, B. S.; Hoggarth, D. A.; Maliniak, D.; Ploense, K.; White, R. J.; Woodward, N.; Hsieh, K.; Bonham, A. J.; Eisenstein, M.; Kippin, T. E.; Plaxco, K. W.; Soh, H. T. *Sci. Transl. Med.* **2013**, 5 (213), 213ra165.
- (18) Baker, B. R.; Lai, R. Y.; Wood, M. S.; Doctor, E. H.; Heeger, A. J.; Plaxco, K. W. *J. Am. Chem. Soc.* **2006**, 128 (10), 3138–3139.
- (19) Levicky, R.; Herne, T. M.; Tarlov, M. J.; Satija, S. K. *J. Am. Chem. Soc.* **1998**, 120 (38), 9787–9792.
- (20) Josephs, E. A.; Ye, T. *ACS Nano* **2013**, 7 (4), 3653–3660.
- (21) Macazo, F. C.; Karpel, R. L.; White, R. J. *Langmuir* **2015**, 31 (2), 868–875.
- (22) Lai, R. Y.; Seferos, D. S.; Heeger, A. J.; Bazan, G. C.; Plaxco, K. W. *Langmuir* **2006**, 22 (22), 10796–10800.
- (23) Ulman, A. *Chem. Rev.* **1996**, 96 (4), 1533–1554.
- (24) Ricci, F.; Zari, N.; Caprio, F.; Recine, S.; Amine, A.; Moscone, D.; Palleschi, G.; Plaxco, K. W. *Bioelectrochemistry* **2009**, 76 (1-2), 208–213.
- (25) Ricci, F.; Lai, R. Y.; Heeger, A. J.; Plaxco, K. W.; Sumner, J. J. *Langmuir* **2007**, 23 (12), 6827–6834.
- (26) Steel, A. B.; Levicky, R. L.; Herne, T. M.; Tarlov, M. J. *Biophys. J.* **2000**, 79 (2), 975–981.
- (27) Xiao, Y.; Lai, R. Y.; Plaxco, K. W. *Nat. Protoc.* **2007**, 2 (11), 2875–2880.

- (28) Schoukroun-Barnes, L. R.; Wagan, S.; White, R. J. *Anal. Chem.* **2014**, *86* (10), 1131–1137.
- (29) Ferapontova, E. E.; Gothelf, K. V. *Electroanalysis* **2009**, *21* (11), 1261–1266.
- (30) Prins, R.; Korswagen, A. R.; Kortbeek, A. G. T. G. *J. Organomet. Chem.* **1972**, *39* (2), 335–344.
- (31) Han, S. W.; Se, H.; Chung, K.; Kim, K. *Langmuir* **2000**, *16*, 9493–9500.
- (32) Zhang, S.; Zhou, G.; Xu, X.; Cao, L.; Liang, G.; Chen, H.; Liu, B.; Kong, J. *Electrochem. commun.* **2011**, *13* (9), 928–931.
- (33) Chang, A. L.; McKeague, M.; Liang, J. C.; Smolke, C. D. *Anal. Chem.* **2014**, *86* (7), 3273–3278.
- (34) Latham, M. P.; Zimmermann, G. R.; Pardi, A. *J. Am. Chem. Soc. Commun.* **2009**, *131* (14), 5052–5053.
- (35) Liu, Y.; Liu, Y.; Matharu, Z.; Rahimian, A.; Revzin, A. *Biosens. Bioelectron.* **2015**, *64*, 43–50.
- (36) Pheaney, C. G.; Barton, J. K. *Langmuir* **2012**, *28* (17), 7063–7070.
- (37) Uzawa, T.; Cheng, R. R.; White, R. J.; Makarov, D. E.; Plaxco, K. W. *J. Am. Chem. Soc.* **2010**, *132* (45), 16120–16126.
- (38) Huang, K.; White, R. J. *J. Am. Chem. Soc.* **2013**, *135* (34), 12808–12817.
- (39) Farjami, E.; Campos, R.; Ferapontova, E. E. *Langmuir* **2012**, *28* (46), 16218–16226.
- (40) Anne, A.; Bouchardon, A.; Moiroux, J. *J. Am. Chem. Soc.* **2003**, *125* (5), 1112–1113.
- (41) Anne, A.; Demaille, C. *J. Am. Chem. Soc.* **2006**, *128* (2), 542–557.

- (42) Steel, A. B.; Herne, T. M.; Tarlov, M. J. *Anal. Chem.* **1998**, *70* (22), 4670–4677.
- (43) Esteban, B.; Watkins, H. M.; Pingarro, J. M.; Plaxco, K. W.; Palleschi, G.; Ricci, F. *Anal. Chem.* **2013**, *85* (14), 6593–6597.
- (44) Schoukroun-Barnes, L. R.; Glaser, E. P.; White, R. J. *Langmuir* **2015**, *31* (23), 6563–6569.
- (45) White, R. J.; Plaxco, K. W. *Anal. Chem.* **2010**, *82* (1), 73–76.
- (46) Ricci, F.; Lai, R. Y.; Plaxco, K. W. *Chem. Commun.* **2007**, No. 36, 3768–3770.
- (47) Zuker, M.; Jacobson, A. B. *RNA* **1998**, *4* (6), 669–679.
- (48) Zuker, M. *Nucleic Acids Res.* **2003**, *31* (13), 3406–3415.
- (49) White, R. J.; Rowe, A. A.; Plaxco, K. W. *Analyst* **2010**, *135* (3), 589–594.
- (50) White, R. J.; Plaxco, K. W. *Proc Soc Photo Opt Instrum Eng* **2009**, *7321*, 732105–732116.
- (51) Catherine, A. T.; Shishido, S. N.; Robbins-welty, G. A.; Diegelman-parente, A. *FEBS Open Bio* **2014**, *4*, 788–795.
- (52) Fetter, L.; Richards, J.; Daniel, J.; Roon, L.; Rowland, T. J.; Bonham, A. J. *Chem. Commun.* **2015**, Just Accepted for Publication.
- (53) Jiang, L.; Patel, D. *Nat. Struct. Biol.* **1998**, *5* (9), 769–774.
- (54) Wang, Y.; Rando, R. R. *Chem. Biol.* **1995**, *2* (5), 281–290.
- (55) Lubin, A. A.; Lai, R. Y.; Baker, B. R.; Heeger, A. J.; Plaxco, K. W. *Anal. Chem.* **2006**, *78* (16), 5671–5677.
- (56) Radi, A.-E.; O’Sullivan, C. K. *Chem. Commun.* **2006**, No. 32, 3432–3434.

- (57) Blouin, S.; Lafontaine, D. A. *RNA* **2007**, *13* (8), 1256–1267.
- (58) Zayats, M.; Huang, Y.; Gill, R.; Ma, C. A.; Willner, I. *J. Am. Chem. Soc.* **2006**, *128* (42), 13666–13667.
- (59) Wu, Z.-S.; Guo, M.-M.; Zhang, S.-B.; Chen, C.-R.; Jiang, J.-H.; Shen, G.-L.; Yu, R.-Q. *Anal. Chem.* **2007**, *79* (7), 2933–2939.
- (60) Zhang, S.; Xia, J.; Li, X. *Anal. Chem.* **2008**, *80* (22), 8382–8388.
- (61) Liu, Y.; Tuleouva, N.; Ramanculov, E.; Revzin, A. *Anal. Chem.* **2010**, *82* (19), 8131–8136.
- (62) Liu, Y.; Kwa, T.; Revzin, A. *Biomaterials* **2012**, *33* (30), 7347–7355.
- (63) Matharu, Z.; Patel, D.; Gao, Y.; Haque, A.; Zhou, Q.; Revzin, A. *Anal. Chem.* **2014**, *86* (17), 8865–8872.
- (64) Bayley, H.; Cremer, P. S. *Nature* **2001**, *413*, 226–230.
- (65) Bayley, H.; Martin, C. R. *Chem. Rev.* **2000**, *100*, 2575–2594.
- (66) Macazo, F. C.; White, R. J. *Anal. Chem.* **2014**, *86* (11), 5519–5525.
- (67) Rotem, D.; Jayasinghe, L.; Salichou, M.; Bayley, H. *J. Am. Chem. Soc.* **2012**, *134* (5), 2781–2787.
- (68) Li, T.; Liu, L.; Li, Y.; Xie, J.; Wu, H.-C. *Angew. Chemie Int. Ed.* **2015**, *54* (26), 7568–7571.
- (69) Zhang, L.; Zhang, K.; Liu, G.; Liu, M.; Liu, Y.; Li, J. *Anal. Chem.* **2015**, *87* (11), 5677–5682.
- (70) Cho, E. J.; Lee, J.-W.; Ellington, A. D. *Annu. Rev. Anal. Chem.* **2009**, *2*, 241–264.
- (71) Xiao, Y.; Uzawa, T.; White, R. J.; DeMartini, D.; Plaxco, K. W. *Electroanalysis* **2009**, *21* (11), 1267–1271.

- (72) Mao, Y.; Luo, C.; Ouyang, Q. *Nucleic Acids Res.* **2003**, *31* (18), e108.
- (73) Hianik, T.; Ostatná, V.; Sonlajtnerova, M.; Grman, I. *Bioelectrochemistry* **2007**, *70* (1), 127–133.
- (74) Stojanovic, M. N.; de Prada, P.; Landry, D. W.; Prada, P. De; Landry, D. W. *J. Am. Chem. Soc.* **2001**, *123* (21), 4928–4931.
- (75) Zuo, X.; Xiao, Y.; Plaxco, K. W. *J. Am. Chem. Soc.* **2009**, *131* (20), 6944–6945.
- (76) Zuo, X.; Song, S.; Zhang, J.; Pan, D.; Wang, L.; Fan, C. *J. Am. Chem. Soc.* **2007**, *129* (5), 1042–1043.
- (77) Ikebukuro, K.; Kiyohara, C.; Sode, K. *Biosens. Bioelectron.* **2005**, *20* (10), 2168–2172.
- (78) Miao, P.; Tang, Y.; Wang, B.; Han, K.; Chen, X.; Sun, H. *Analyst* **2014**, *139* (22), 5695–5699.
- (79) Cox, J. T.; Zhang, B. *Annu. Rev. Anal. Chem.* **2012**, *5* (1), 253–272.
- (80) Wang, T.; Viennois, E.; Merlin, D.; Wang, G. *Anal. Chem.* **2015**, *87* (16), 8173–8180.
- (81) Hu, K.; Gao, Y.; Wang, Y.; Yu, Y.; Zhao, X.; Rotenberg, S. A.; Gökmeşe, E.; Mirkin, M. V.; Friedman, G.; Gogotsi, Y. *J. Solid State Electrochem.* **2013**, *17* (12), 2971–2977.
- (82) Wang, K. Y.; McCurdy, S.; Shea, R. G.; Swaminathan, S.; Bolton, P. H. *Biochemistry* **1993**, *32* (8), 1899–1904.
- (83) Li, Y.; Guo, L.; Zhang, F.; Zhang, Z.; Tang, J.; Xie, J. *Electrophoresis* **2008**, *29* (12), 2570–2577.
- (84) Paborsky, L. R.; McCurdy, S. N.; Griffin, L. C.; Toole, J. J.; Leung, L. L. *J. Biol. Chem.* **1993**, *268* (28), 20808–20811.

- (85) Zhou, C.; Jiang, Y.; Hou, S.; Ma, B.; Fang, X.; Li, M. *Anal. Bioanal. Chem.* **2006**, *384* (5), 1175–1180.
- (86) Cruz-Aguado, J. A.; Penner, G. *J. Agric. Food Chem.* **2008**, *56* (22), 10456–10461.
- (87) Hamula, C. L. A.; Zhang, H.; Guan, L. L.; Li, X.-F.; Le, X. C. *Anal. Chem.* **2008**, *80* (20), 7812–7819.
- (88) Berezovski, M. V.; Lechmann, M.; Musheev, M. U.; Mak, T. W.; Krylov, S. N. *J. Am. Chem. Soc.* **2008**, *130* (28), 9137–9143.
- (89) Mairal, T.; Ozalp, V. C.; Lozano Sánchez, P.; Mir, M.; Katakis, I.; O’Sullivan, C. K. *Anal. Bioanal. Chem.* **2008**, *390* (4), 989–1007.
- (90) Jhaveri, S.; Rajendran, M.; Ellington, A. D. *Nat. Biotechnol.* **2000**, *18*, 1293–1297.
- (91) Wang, Y.; Killian, J.; Hamasaki, K.; Rando, R. R. *Biochemistry* **1996**, *35* (38), 12338–12346.
- (92) Jiang, L.; Patel, D. *Nat. Struct. Biol.* **1998**, *5* (9), 769–774.
- (93) Shen, H.; Mark, J. E.; Seliskar, C. J.; Mark, H. B.; Heineman, W. R. *J Solid State Electrochem* **1997**, *1*, 148–154.
- (94) Balamurugan, S.; Obubuafo, A.; Soper, S. A.; Spivak, D. A. *Anal. Bioanal. Chem.* **2008**, *390* (4), 1009–1021.
- (95) O’Mullane, A. P.; Ippolito, S. J.; Sabri, Y. M.; Bansal, V.; Bhargava, S. K. *Langmuir ACS J. Surfaces Colloids* **2009**, *25*, 3845–3852.
- (96) Laviron, E. *J. Electroanal. Chem. Interfacial Electrochem.* **1979**, *101* (1), 19–28.
- (97) Mirceski, V.; Laborda, E.; Guziejewski, D.; Compton, R. G. *Anal. Chem.* **2013**, *85* (11), 5586–5594.

- (98) Laborda, E.; Molina, A.; Li, Q.; Batchelor-McAuley, C.; Compton, R. G. *Phys. Chem. Chem. Phys.* **2012**, *14* (23), 8319.
- (99) Jeuken, L. J. C.; McEvoy, J. P.; Armstrong, F. A. *J. Phys. Chem. B* **2002**, *106* (9), 2304–2313.
- (100) Komorsky-Lovric, S.; Lovric, M. *Amal. Chim. Acta.* **1995**, *305*, 248–255.
- (101) Setia, U.; Gross, P. A. *J. Infect. Dis.* **1976**, *134*, S125–S129.
- (102) Skoog, D. A.; Holler, F. J.; Crouch, S. R. *Instrumental Analysis*, 6th ed.; Brooks/Cole: India, 2007.
- (103) Wilson, G. S.; Yibai, H. *Chem. Rev.* **2000**, No. 100, 2693–2704.
- (104) Ronkainen, N. J.; Halsall, H. B.; Heineman, W. R. *Chem. Soc. Rev.* **2010**, *39* (5), 1747–1763.
- (105) Yang, H. *Curr. Opin. Chem. Biol.* **2012**, *16* (3-4), 422–428.
- (106) Kimmel, D. W.; Leblanc, G.; Meschievitz, M. E.; Cliffel, D. E. *Anal. Chem.* **2012**, No. 84, 685–707.
- (107) Zhu, L.; Anslyn, E. V. *Angew. Chemie - Int. Ed.* **2006**, No. 45, 1190–1196.
- (108) Lei, Y.; Yan, X.; Zhao, J.; Liu, X.; Song, Y.; Luo, N.; Zhang, Y. *Colloids Surf. B. Biointerfaces* **2011**, *82* (1), 168–172.
- (109) Shi, J.; Claussen, J. C.; McLamore, E. S.; ul Haque, A.; Jaroch, D.; Diggs, A. R.; Calvo-Marzal, P.; Rickus, J. L.; Porterfield, D. M. *Nanotechnology* **2011**, *22* (35), 355502.
- (110) Mayhew, M. P.; Reipa, V.; Holden, M. J.; Vilker, V. L. *Biotechnol. Prog.* **2000**, No. 16, 610–616.
- (111) Zhong, Z.; Li, X.; Zhao, Y. *J. Am. Chem. Soc.* **2011**, No. 133, 8862–8865.

- (112) Schlehuber, S.; Skerra, A. **2002**, *96*, 213–228.
- (113) Houk, K. N.; Leach, A. G.; Kim, S. P.; Zhang, X. *Angew. Chem. Int. Ed. Engl.* **2003**, *42* (40), 4872–4897.
- (114) Hernandez, K.; Fernandez-Lafuente, R. *Enzyme Microb. Technol.* **2011**, *48* (2), 107–122.
- (115) Vallée-bélisle, A.; Ricci, F.; Plaxco, K. W. *J. Am. Chem. Soc.* **2012**, *20* (6), 2876–2879.
- (116) Kang, D.; Vallée-Bélisle, A.; Porchetta, A.; Plaxco, K. W.; Ricci, F. *Angew. Chem. Int. Ed. Engl.* **2012**, *51* (27), 6717–6721.
- (117) Jarczewska, M.; Kékedy-Nagy, L.; Nielsen, J. S.; Campos, R.; Kjems, J.; Malinowska, E.; Ferapontova, E. E. *Analyst* **2015**, No. 140, 3794–3802.
- (118) Farjami, E.; Campos, R.; Nielsen, J. S.; Gothelf, K. V.; Kjems, J.; Ferapontova, E. E. *Anal. Chem.* **2013**, *85* (1), 121–128.
- (119) Dill, K. A.; Bromberg, S. *Molecular Driving Forces: Statistical Thermodynamics in Biology, Chemistry, Physics, and Nanoscience, 2nd Edition*; 2010.
- (120) Cheng, A. K. H.; Sen, D.; Yu, H.-Z. *Bioelectrochemistry* **2009**, *77* (1), 1–12.
- (121) Wang, Y.; Bao, L.; Liu, Z.; Pang, D.-W. *Anal. Chem.* **2011**, *83* (21), 8130–8137.
- (122) Huizenga, D. E.; Szostak, J. W. *Biochemistry* **1995**, *34* (2), 656–665.
- (123) Hermann, T.; Patel, D. J. *Science* **2000**, *287* (5454), 820–825.
- (124) Yoshizumi, J.; Kumamoto, S.; Nakamura, M.; Yamana, K. *Analyst* **2008**, *133* (3), 323–325.
- (125) Yu, Z.; Lai, R. Y. *Anal. Chem.* **2013**, *85* (6), 3340–3346.
- (126) Umpleby, R. J.; Baxter, S. C.; Rampey, A. M.; Rushton, G. T.; Chen, Y.; Shimizu,

- K. D. *J. Chromatogr. B. Analyt. Technol. Biomed. Life Sci.* **2004**, 804 (1), 141–149.
- (127) Shu, C.-C.; Wu, M.-F.; Hsu, C.-L.; Huang, C.-T.; Wang, J.-Y.; Hsieh, S.-L.; Yu, C.-J.; Lee, L.-N.; Yang, P.-C. *BMC Infect. Dis.* **2013**, 13, 45.
- (128) Santini, J.; Milano, G.; Thyss, a; Renee, N.; Viens, P.; Ayela, P.; Schneider, M.; Demard, F. *Br. J. Cancer* **1989**, 59 (2), 287–290.
- (129) Kibe, S.; Adams, K.; Barlow, G. *J. Antimicrob. Chemother.* **2011**, 66 (Suppl 2), 33–40.
- (130) Pascual, A.; Calandra, T.; Bolay, S.; Buclin, T.; Bille, J.; Marchetti, O. *Clin. Infect. Dis.* **2008**, 46 (2), 201–211.
- (131) Basch, E.; Artz, D.; Dulko, D.; Scher, K.; Sabbatini, P.; Hensley, M.; Mitra, N.; Speakman, J.; McCabe, M.; Schrag, D. *J. Clin. Oncol.* **2005**, 23 (15), 3552–3561.
- (132) Iliuk, A. B.; Hu, L.; Tao, W. A. *Anal. Chem.* **2011**, 83 (12), 4440–4452.
- (133) Geiger, T.; Cox, J.; Mann, M. *PLoS Genet.* **2010**, 6 (9), e1001090, 1–11.
- (134) Carrasquilla, C.; Lau, P. S.; Li, Y.; Brennan, J. D. *J. Am. Chem. Soc.* **2012**, 134 (26), 10998–11005.
- (135) Leach, J. B.; Bivens, K. a.; Patrick, C. W.; Schmidt, C. E. *Biotechnol. Bioeng.* **2003**, 82 (5), 578–589.
- (136) Wu, C.; Quesada, M. A.; Schneider, D. K.; Farinato, R.; Studier, F. W.; Chu, B. *Electrophoresis* **1996**, 17 (6), 1103–1109.
- (137) Ulrich, H.; Martins, A. H. B.; Pesquero, J. B. *Curr. Protoc. Cytom.* **2005**, Chapter 7 (May), Unit 7.28.

